Helsinki University of Technology Publications in Materials Science and Metallurgy
Teknillisen korkeakoulun materiaalitekniikan ja metallurgian julkaisuja
Espoo 2004 TKK-MK-160

HIGH TEMPERATURE OXIDATION OF METAL, ALLOY AND CERMET POWDERS IN HVOF SPRAYING PROCESS

Doctoral Thesis

Kari Korpiola

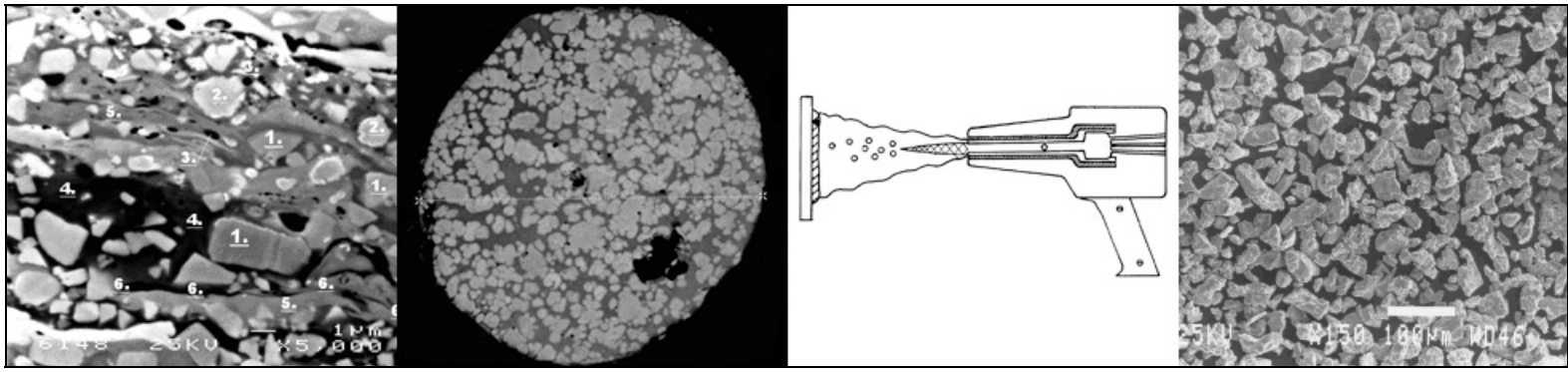

TEKNILLINEN KORKEAKOULU
TEKNISKA HÖGSKOLAN
HELSINKI UNIVERSITY OF TECHNOLOGY
TECHNISCHE UNIVERSITÄT HELSINKI
UNIVERSITE DE TECHNOLOGIE D'HELSINKI

Helsinki University of Technology Publications in Materials Science and Metallurgy

Teknillisen korkeakoulun materiaalitekniikan ja metallurgian julkaisuja

Espoo 2004 TKK-MK-160

HIGH TEMPERATURE OXIDATION OF METAL, ALLOY AND CERMET POWDERS IN HVOF SPRAYING PROCESS

Kari Korpiola

Dissertation for the degree of Doctor of Science in Technology to be presented with due permission of the Department of Materials Science and Rock Engineering for public examination and debate in Auditorium V 1 at Helsinki University of Technology (Espoo, Finland) on the 3rd of December, 2004, at 12 o'clock noon.

Helsinki University of Technology

Department of Materials Science and Rock Engineering

Laboratory of Metallurgy

Teknillinen korkeakoulu

Materiaali- ja kalliotekniikan osasto

Metallurgian laboratorio

Helsinki University of Technology
Laboratory of Metallurgy
P.O. Box 6200
FIN-02015 TKK, Finland

Available in pdf-format at http://lib.hut.fi/Diss/

Cover: HVOF spray process from powder to coating

ISBN 951-22-7312-8
ISBN 951-22-7328-4 (electronic)
ISSN 1455-2329

Edita Prima Oy
Helsinki 2004

ABSTRACT

In thermal spraying, the coatings, alloys and metals oxidise during the spraying process. Oxidation often results in a decrease in the mechanical and corrosion properties of the coating. In this study, oxidation of HVOF coatings is examined.

In the beginning of the study, the HVOF spraying process is analysed, including the combustion process, gas temperature, oxygen concentration, gas velocity, and gas momentum. Temperature and velocity of the spray particles are measured. Thermodynamic and kinetic equations of metal oxidation are introduced. In the experimental part of the work, calculations and coating experiments were carried out. Thermodynamic calculations of metal oxidation were done in the HVOF spray gun environment using different fuel/oxygen ratios, fuel quality and metals. The metal oxidation calculations were performed with HSC thermodynamic software.

The thermodynamic calculations showed that Ni and Co can be sprayed without any oxidation in the HVOF gun nozzle whereas Cr, Ti, Al and Mg are always oxidised. No significant differences were found in the oxidizing potential of fuels such as H_2 and kerosene.

In the spraying experiments, oxidation of WC-Co17 and NiCr80/20 coatings was studied. It was shown experimentally that the short process dwell time does not enable coatings to oxidise completely. It was also found that spray powder oxidation occurs in three steps. First, primarily in the HVOF gun nozzle, second, to a small extent in the plume and third, hardly at all on the surface being coated.

The thermodynamic calculations, reaction kinetics and experimental work showed that oxidation of spray powder is a complex phenomenon involving selective and volatile oxidation, and formation of solid oxide. Oxidation of the coating is strongly related to the temperature of the particles and combustion gas. Oxidation of the spray powder can take place in solid or molten state.

Experimental work showed that the oxidation processes in the HVOF spray process can not be completely prevented, but can be controlled. The degree of oxidation is reduced by lowering the temperature of the flame, by using a higher gas velocity and density, and employing effective substrate cooling.

Keywords: WC-Co17 coating, NiCr80/20 coating, oxidation, HVOF spraying, thermal spraying, oxidation kinetics, high temperature oxidation, coating oxidation, decarburization of WC-Co17.

PREFACE

The work described in this thesis was carried out at the Technical Research Centre of Finland (VTT) in connection with several national research projects in which the use of HVOF spray gun has been studied.

Financial support from TEKES and VTT is gratefully acknowledged. This work was supervised by Professor Lauri Holappa from Helsinki University of Technology, to whom I wish to express my sincere gratitude for advice and encouragement.

One central theme of the work was to develop a general view of spray powder oxidation in thermal spraying. The resulting view is based on a valuable series of lectures by Professor Heikki Jalkanen from the Helsinki University of Technology, as well as subsequent discussions. His ideas about high temperature chemistry and thermodynamics, formed the basis for this work.

I am deeply indebted to my friends Professor Petri Vuoristo, Tommi Varis, Petri Jokinen and Timo Kinos for many valuable discussions and ideas about the planning of experimental work and the testing of coating and spray processes.

My thanks also go to Professor Juha-Pekka Hirvonen, former leader of the Surface Technology Group in VTT Manufacturing Technology and Professor Simo-Pekka Hannula, who made the decision to invest in thermal spraying at VTT.

I would like to extend special thanks to the following members of staff at VTT Manufacturing Technology: Seija Kivi, Markku Lindberg, Marketta Ryhänen, Vesa Suomela, Pirkko Thurman, Annika Mäklin and Anja Knorring. From TKK, I want to thank Into Rämä and Ahti Turpela.

I would also like to thank my friends from the Lepakko Society, Heikki, Igor, Timppa, Teemu, Keppa and Harri, with whom I had hundreds of critical and encouraging discussions about how to find fresh ideas for this work.

Finally, I want to thank my parents, for their continuous support and encouragement through the years spent on this work, my partner Tiina, and my children Roope, Sampo and Ina for their patience.

Espoo, 4th November, 2004

Kari Korpiola

CONTENTS

LIST OF SYMBOLS AND ACRONYMS

A	Area
p	Pressure
c_p	Specific heat
F/O	Fuel to oxygen ratio
F	Force accelerating a particle
$\Delta G°$	Standard free energy
HVOF	High Velocity Oxygen Fuel
$h°$	Combustion enthalpy
v	Gas velocity
k	Aerodynamic constant/coefficient
K	Equilibrium constant
m	Mass
$\underline{m}$	Mass flow/s
M	Mach number
Me	Metal
M	Momentum flux
$p°$	Combustion chambre pressure
p	Ambient pressure
Q	Activation energy
p_{O2}	Partial pressure of oxygen
1/n	Pressure factor
R	Universal gas constant
slm	Standard Litre Per Minute
σ	surface energy of liquid metal
t	Time
T_1	New gas temperature
$T°$	Adiabatic or static flame temperature
T	Temperature
T part	Particle temperature
t cooling	Cooling time
t dwell	Fly time in spray process
v part	Particle velocity
Δv	Convection velocity
γ	Ratio of specific heats
ρ	Gas density
ρ air	Air density
ρ flow	Flame density
$\Delta_R G°$	Gibbs energy
SEM	Scanning electron microscope
SEI	Secondary electron image
BEI	Back scattering image
OM	Optical microscope
XRD	x-ray diffraction
EDS	Energy dispersive spectrum
[ ]	dissolved element in liquid metal.

ORIGINAL FEATURES

The following features of this thesis are believed to be original.

Oxidation always occurs in the HVOF spraying of alloys, cermets and metals. Thermodynamic calculations show that oxidation cannot be avoided by altering the fuel or metal quality. It was shown experimentally that the short process dwell time does not allow metals and alloys to oxidise completely.

New proposals resulting from this work are that spray powders oxidise:

- primarily in the HVOF gun nozzle,
- only to a small extent in the plume,
- hardly at all on the surface being coated if the surface is cold and the work speed is sufficiently high.

The thermodynamic calculations, reaction kinetics and experimental work showed that spray powder oxidation is a complex phenomenon involving the following processes:

- selective oxidation, with some elements oxidising more rapidly than others,
- formation of both volatile and solid oxides, some elements forming gaseous oxides and others forming solid oxides. Oxidation mechanisms are strongly related to gas and particle temperatures.

Estimations, which were subsequently proved by experimental work, showed that the oxidation reactions in the HVOF spray process cannot be completely prevented, but can be controlled in the following way:

- by reducing the flame temperature, controlling F/O ratio, i.e. lowering the spray particle temperature,
- by using a higher gas velocity and density, i.e. lowering the particle dwell time in the spray process and lowering the spray particle temperature,
- by employing effective substrate cooling, an adequate work distance and a sufficiently rapid work speed.

Microstructural findings show that formation CO gas occurs in WC-Co coatings. The phenomena are comparable with the decarburization process in steel making. A new mechanism for solid and molten state oxidation of WC-Co is proposed.

1. INTRODUCTION

The High Velocity Oxygen Fuel (HVOF) spray process consists of a water-cooled or air-cooled spray gun, in which combustion occurs at high pressure in the combustion chamber. The resulting hot gas flows out of the combustion chamber and through the nozzle at supersonic speed. At the nozzle exit, there are shock diamonds, and the flow transforms to a plume. This plume is a mixture of the surrounding air and hot combustion gas. The object to be coated is typically at a work distance (stand-off distance) of 150 to 400 mm from the nozzle exit. The spray powder coating is injected either axially into the combustion chamber or radially into the hot gas stream. The spray powder is heated and accelerated by the hot gas stream and projected onto the surface to be coated. On a cool or warm surface less than 200°C, the high temperature droplets of the spray powder solidify and form a solid coating. Figure 1 is a schematic diagram of the HVOF coating process.

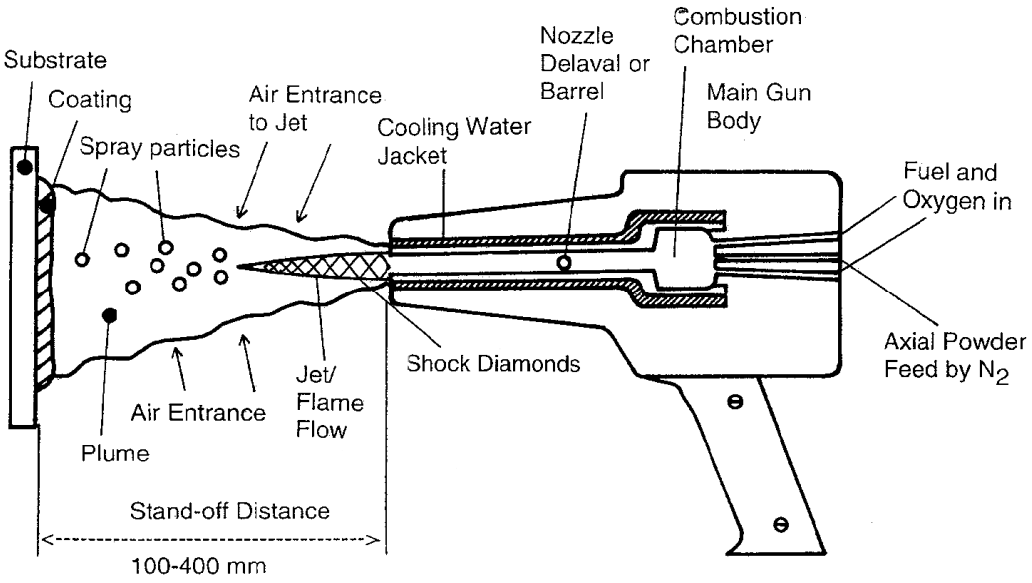

Figure 1. *Schematic diagram of the HVOF coating process and key parameters relating to the HVOF coating process.*

The thermal spray process has several advantages which make it useful for industrial purposes. Nearly all materials which can be melted, such as metals, cermets, ceramics and even plastics, can be sprayed and used to coat solid materials. The temperature of the piece being coated remains typically below 150°C. Therefore, it is possible to coat thin-walled components and thermally sensitive materials, such as plastics or wood. Coating can also provide properties which are difficult to obtain in the bulk material. On the other hand, the thermal spray process has some disadvantages, such as oxidation of the molten metal to be sprayed. The physical properties of thermally sprayed alloys are impaired by oxidation.

In atmospheric conditions, thermally sprayed alloys always oxidise. The process of oxidation is controlled by chemical reactions occurring at elevated temperatures. It is therefore influenced by the choice of spraying consumables and spraying parameters.

1.1 Why to control the degree of oxidation?

Oxide and carbon content are important in coatings, since they usually control the operational properties of the materials. Oxidation of alloys reduces ductility, tensile strength, corrosion properties, erosion, corrosion resistance etc. of the coatings, compared to the bulk materials. Depending on the quality of carbides, such as WC-Co17 and Cr_3C_2-NiCr80/20 and 75/25, bond strength with the substrate and ductility (cracks in the coating), are reduced during decarburization.

Mechanical properties of the coating decrease compared to the bulk material. Young's modulus (E) can decrease by 40 to 200 %, e.g. E of WC-Co17 decreases from 500 GPa to approximately 150 GPa. Tensile strength of the oxidised coating is anisotropic. The bond strength of NiCr80/20 coating parallel to the surface is reduced to 50 Mpa, and uniaxial tensile strength of the coating is reduced to 300 Mpa, compared to the tensile strength of the bulk material tensile strength which is 1000 MPa. Reduced mechanical properties make it impossible to manufacture functional freestanding bodies (tubes, impellers, etc). Composite structures are also impossible, e.g. fibre-reinforced machine parts relying on load carrying properties of the coating of the carbon fibre/WC-Co17 roll, where WC-Co17 coating carries surface loads, tensile and shear stresses (1, 2).

Residual stresses are a difficult problem in oxidised coatings, because the fracture strength and ductility of the coatings have decreased. Thermal and electrical conductivity in oxidised bulk materials decrease as well, and therefore it is expected that oxidised coatings will not be an exception (2). High temperature corrosion and oxidation properties decrease in MCrAlY coatings. When a MCrAlY coating loses aluminium, its lifetime is reduced. Corrosion properties of coatings decrease when alloys lose their original chemistry, including oxides of important elements, Cr and Ni (3, 4). Optical and magnetic properties are strongly related to the original structure and chemistry of the material. Oxidation of the coating changes the material's original structure and chemistry. The manufacturing process of the coating changes the transport properties of materials, sprayed metals or alloys, that are no longer fully dense. The corrosion medium can penetrate through the porous coatings on the base material, and corrode the substrate material. It is impossible to manufacture waterproof thermally sprayed coatings on mild steel to protect the base material. Oxidised Ti, Inconel or AISI 316 do not offer corrosion protection of the base material (5, 6).

The oxidation of coatings is not always harmful, e.g. when oxidation of WC-Co17 coatings is quite mild, the coating hardness increases 60-75 % (from 850 to 1500 $HV_{0.3}$), compared to the sintered WC-Co17 material. Wear resistance of the sprayed coating can increase up to 250% compared to sintered material. In HVOF sprayed Stellite 6 material, the high temperature coefficient of friction decreases 40-60% compared to welded Stellite 6 coatings, due to oxidation of the coating. It is equally important to control and understand the different aspects of oxidation of coatings in a positive way. Positive operational features due to oxidation of the coating, are balanced by those that cause decreased corrosion properties and reduced adhesion to the substrate. Therefore, it is important to find an optimum level for oxidation of coatings (16, 7, 2).

There is very little information on how oxidation of coatings improves manufacturing processes such as grinding, milling, welding, etc. Oxidation of coatings usually makes machining more difficult due to increased hardness of the coating.

In contrast to the standard high-temperature metallurgical process, i.e. ladle refining of metals, in which the chemical reactions occur under approximately isothermal conditions, and in relatively large volumes and extended times, the characteristic features of the thermal spraying process are different. The chemical reactions which occur between a spray particle and the surroundings, take place in less than 1 ms. Furthermore, the volume where the reactions take place, is often extremely small (spray particle size <50 µm). The spray particle temperature gradients are of the order of <10000 °C/mm, i.e. a hot surface and a cold nucleus, with the quenching rate of spray particles being very high $>10^7$ °C/s (8). There is no oxidation model for molten metal or alloy. One consequence of this situation is that the calculation of the degree of oxidation of spray powder in the thermal spray process, is difficult.

The problem of coating oxidation is significant, because most thermal spraying is performed in ambient conditions, where the hot molten metal is able to react with oxygen. This is the situation in all atmospheric thermal spraying processes in which metals and alloys are sprayed, i.e. flame, plasma, wire arc and HVOF spraying processes.

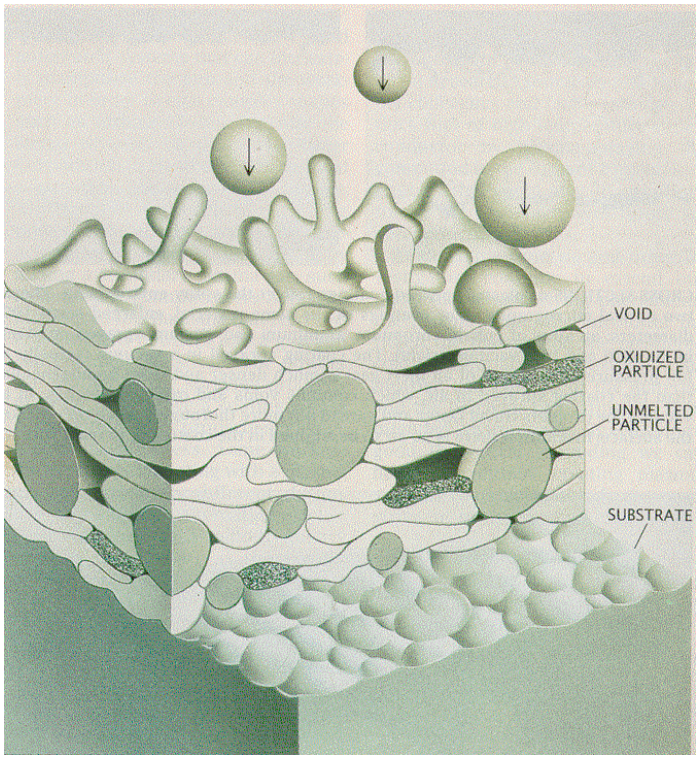

Figure 2. *Coating deposition and the oxidation process (9).*

The process of oxidation during thermal spraying in Figure 2 is different from that in bulk material oxidation, which starts from the surface of the material and propagates to the inner volume. Compared to ordinary high temperature steady state oxidation, the oxidation time during thermal spray coating is short, typically less than 0.01 s, and can occur in either the solid or molten state. Thermal spray coating oxidation is not a surface phenomenon. The coating is oxidised in a relatively homogeneous manner from the surface to the coating substrate interface. The shape of oxide inclusions vary from spherical oxide cores to flat pancakes, and sometimes consist of layer oxidation caused by individual gun passes. The microstructure of the coating can be a combination of all possible variations of oxidation. In

spite of intensive research work and the examination of the microstructures of coating cross-sections, the causes of the oxidation morphology have not yet been established.

The results of spray powder oxidation are important, since oxidation changes the properties of the original spray material. Typically, the bulk material has better mechanical and corrosion properties than the same material when sprayed. There are some consequences of coating oxidation, such as coating porosity and low bond strength of the coating with the substrate. Alloy hardness increases due to hard oxide particle dispersion in the coatings, which can lose their good corrosion resistance properties (10). The wear resistance properties of plasma or HVOF sprayed WC-Co17 coatings, can be higher than those of the sintered materials. In sprayed alloys, a decrease in coating ductility occurs and high levels of residual stresses are present, because there is no capacity for plastic deformation, which could release the residual stresses (11).

Studies of oxidation in plasma and HVOF coatings are limited. Existing studies are mainly concerned with the tungsten carbide cobalt system, WC-Co17, which is a special case in metal oxidation. It is a decarburizing (i.e. carbon consuming) process, which does not produce solid oxide layers. Kreyer, who reports on the effect of fuel gases on the phase contents of the coating and its structural changes, points out that spraying with high flame temperature burning acetylene, produces coatings with higher carbon loss, than when spraying at a lower temperature with hydrogen and propane (12). However, the report does not explain the reason for the high carbon loss of coating in terms of thermodynamics. Krayer completed his studies by pointing out that high particle and gas velocities decrease the oxidation of carbide coatings (13).

Hackett has carried out interesting work on the HVOF oxidation process (14). He proposed a three-step oxidation process with oxidation occurring firstly in the HVOF gun nozzle, secondly in air (plume), and thirdly, on the substrate. He concluded that primary oxidation occurs on the substrate due to the hot HVOF plume, with the fuel/oxygen ratio (F/O ratio) causing the oxidation and the substrate temperature controlling the degree of oxidation. More detailed analysis of where the coating oxidation actually takes place is necessary, because in Hackett's work, substrate temperatures were uncommonly high (>300°C), and the coating dwell times under the hot plume were several seconds. The dwell times were very long compared to the ordinary spray process, in which coating dwell time under the hot plume is less than 0.1 s. The work speed of the sprayed item has therefore been extremely slow, and this may be the reason for the high degree of oxidation.

Hackett has carried out work on an HVOF shrouding system with a Tafa gun in an inert gas chamber. He pointed out that changing the atmosphere around the HVOF gun plume, to nitrogen, reduces coating oxidation. He concluded that the main source of oxidation is the surrounding atmosphere, which mixes with the hot supersonic jet. However, he did not clearly show how the addition of the shrouding gas to the hot jet, decreases problems with cooling and quenching of the coating on the substrate. Substrate cooling rate is an important parameter in the oxidation rate of the coating, as will be shown later.

Earlier studies have concentrated more on answering questions about what happens to the microstructure and wear properties of the coating, than on consideration of how the oxidation process occurs, and whether it can be controlled (15, 16, 17, 18, 19, 20, 21, 22, 23, 24, 25, 26, 27, 28, 29, 30, 31). Alloy or metal oxidation has seldom been studied in systems other than WC-Co17 (14, 32).

On the other hand, much fundamental research work has been carried out which makes it possible to try to form a “new view” of the metal/alloy oxidation in the HVOF process. Such studies have considered particle velocity and temperature measurements (33, 34, 35, 36), models of HVOF fluid dynamics including gas velocity, and density and gas chemical composition in the thermal spraying process (37, 38, 39, 40). These theories and experimental results describe the HVOF spraying conditions. There are also fundamental studies of the chemical thermodynamics of metal and alloy oxidation, which are now well established. There are also theories of solid oxidation kinetics, but unfortunately, there is no good theory of liquid metal oxidation kinetics, which would be useful, because the spray particle is often in a molten state during the spray process.

2. METAL OXIDATION

Oxidation of metals in thermal spraying cannot be studied without employing thermodynamic and kinetic bases of the reactions as well as oxidation models. It is possible to carry out experimental work analysing the oxygen contents of coatings, but it is difficult to explain the results obtained. Thermodynamics and kinetics provide a good background for the prediction and explanation of the oxidation results of thermal spraying.

2.1 Thermodynamic considerations

Thermodynamics is an important tool for use in predicting which species tend to oxidise in the thermal spraying process. It defines the conditions for a metal to oxidise in thermal spraying. Thermal spraying is a very rapid process (<2 ms). The rate of reactions can not be determined by thermodynamics alone. Therefore, chemical kinetics is employed to explain the degree of oxidation reaction, which is dependent on time, area, mass transfer, temperature, etc. Metals and alloys form an oxide scale on the metal/alloy surface. In alloys, the scale is typically a compound of oxygen and metal, for example Cr_2O_3, Al_2O_3, NiO, CoO, WO_3, MoO_3 and FeO. However, oxides can be also combinations of two metals, such as Cr and Ni and O_2, when they form a mixed oxide of spinel $NiCr_2O_4$, which is the case when NiCr alloy is oxidised. Typically, these are solid oxides, which can be found in the material after the thermal spraying process. On the other hand, the formation of solid oxides is not the only oxidation process in thermal spraying. Decarburization of WC-Co17 is an important oxidation process in thermal spraying, because carbon of WC is removed by gaseous CO(g) at high temperatures. The oxidation of a metal, Me, may be represented as follows (41, 42, 43, 44):

$$Me(s) + 1/2O_2\,(g) = MO(s). \qquad (1)$$

The standard free energy, $\Delta G°$, available for the formation of an oxide may be written as:

$$\Delta_R G°\,(1) = -\,RT \ln K\,(1) \qquad (2)$$

Here, R is the universal gas constant and T is the temperature in Kelvin degrees. K is the equilibrium constant for any reversible reaction at equilibrium and is the ratio of the activities of the products to reactants. In the specific case of a reaction (1):

$$K(1) = a_{MeO} * a_M^{-1} * a_{O2}^{-½} = a_{MeO} * a_{Me}^{-1} * (p_{O2}/p_O)^{-½} \qquad (3)$$

Here a_{MO}, a_M^{-1},a_M and a_{O2} are activities of the components in the reaction. Since the metal and its oxides are solid and in their standard states at atmospheric pressure, their activities can be assumed to be unity. In addition, the activity level for oxygen can be replaced by its partial pressure, since it will behave as an ideal gas. Hence, Equation (3) can be simplified to:

$$K(1) = 1/\,p_{O2}^{1/2} \qquad (4)$$

Here, p_{O2} is the partial pressure of oxygen at which the reaction represented by Equation (4), is in

equilibrium, $\Delta G° = 0$.
Table ***1*** shows some common dissociation pressures of some oxides, p_{O2} (41). The dissociation pressures of metal oxide, p_{O2} at 1200°C are very low. A low dissociation pressure means that the presence of a low amount of oxygen will oxidise the pure metal.

Table 1. *Dissociation pressures of some metal oxides, pO_2 at 1200°C.*

Cr_2O_3	FeO	NiO
$1.57*10^{-18}$ atm	$1.28*10^{-12}$ atm	$1.0*10^{-8}$ atm

In the HVOF combustion process, hot combustion gas contains large quantities of H_2O, CO_2 and CO (>20 %) and relatively small quantities of free O_2 (>0.01 %), as can be seen in Table 2 and Table 3. Metals and alloys also oxidise by these species as shown by the following reactions:

$$Me(s)+ H_2O(g) = MeO(s)+ H_2(g) \quad (5)$$

$$Me(s)+ CO_2(g) = MeO(s) + CO(g) \quad (6)$$

The standard free energy for a reaction is the difference in the free energies for the formation of reactants:

$$\Delta_R G°(5)=\Delta_f G°(MeO)-\Delta_f G°(H_2O) \quad (7)$$

and $$\Delta_R G(6) = \Delta_f G°(MeO) + \Delta_f G°(CO)-\Delta_f G°(CO_2) \quad (8)$$

The standard free energy for reaction is:

$$\Delta_R G° = - RT \ln K, \quad (9)$$

where the equilibrium constant for the reaction (5) can be written as:

$$K(5) = a\,(MeO) * p\,(H_2) / (a\,Me * p\,(H_2O)) \quad (10)$$

$$K(5) = p\,(H_2) / p\,(H_2O) \quad (11)$$

and therefore,

$$\Delta_R G°(5) = -RT \ln [pH_2 / pH_2O]. \quad (12)$$

Similar free energy calculations can be made for metal oxidation by carbon dioxide shown in reaction (6).

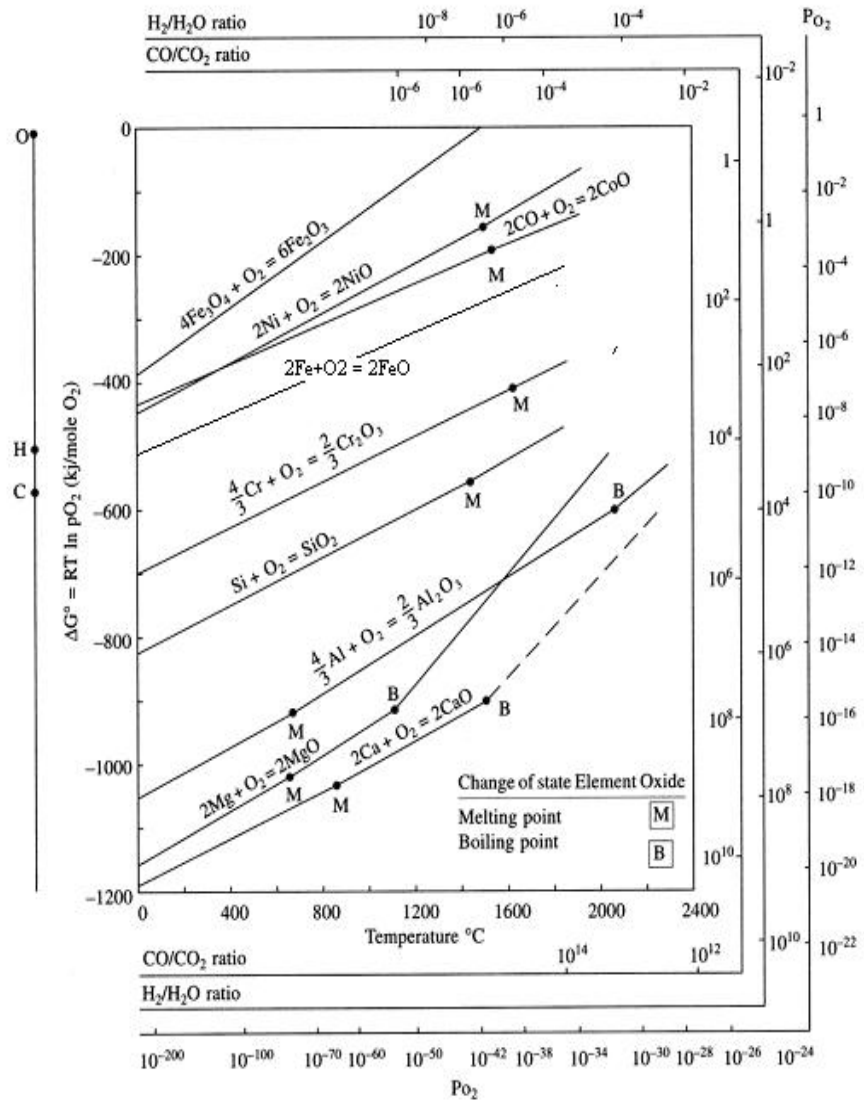

Figure 3. *Ellingham diagram for metallurgically important oxides (47).*

The variation of the standard free energy change with absolute temperature, for a number of metal oxides, is shown in Figure 3, Ellingham diagram. The noble metals, which are easily reduced, occur at the top of the diagram, while the more reactive metals are at the bottom. However, some of the metals at the bottom of the diagram (Al, Ti, Zr), resist oxidation at room temperature, due to the impermeability of the coherent oxide film which forms first.

At high temperature close to their melting point, metals dissolve gases. Metals dissolve oxygen, solubility increasing when metals melt and with increasing temperature. [ ] denotes dissolved element in liquid metal. In the presence of carbon, oxygen tends to react with carbon

$$[C] + [O] = CO(g) \qquad (13)$$

Equilibrium pressure of carbon monoxide is dependent on the activities of carbon and oxygen in the solution

$$K(13) = (p_{CO}/p^{o}) / (a_C * a_O) \quad (14)$$

If standard states for carbon is pure carbon (graphite) and for oxygen and carbon monoxide pure gases at atmospheric pressure

$$K(13) = \exp [(-\Delta_f G°(CO) /RT] \quad (15)$$

Some metals, such as Cr, W, Mo, Si and C, form oxides which are volatile at high temperatures. This means that in high-temperature processes, metal oxides can evaporate as soon they are formed, and metals or alloys lose their protective oxide layer. This is important in the case of many engineering alloys, which rely on the formation of a protective oxide layer. For example, chromium can evaporate as $CrO_3(g)$ in high-temperature oxidation, particularly at high gas flow rates which cause chromium depletion in the alloy. $WO_3(g)$ is volatile above 725°C and CO(g) is gaseous at room temperature. W and C are important compounds in tungsten-containing alloys e.g. WC-Co17 (44, 45, 46, 47, 50). In thermal spraying, formation of protective oxides is important, because these oxides protect the spray particles during the spraying process. On the other hand, properties of the coatings, such as wear and corrosion resistance, are adversely affected by oxidation.

Alloys also have volatile elements, which may cause the alloy composition to change during the thermal spraying process, as in the case of $WO_3(g)$, $CrO_3(g)$, $MoO_3(g)$ and CO(g) (57, 48). Volatile elements cause selective oxide layer formation during the thermal spraying process. Volatility of oxides may lead to chromium depletion occurring around the spray particles, as Siitonen and Magrome have pointed out in the case of plasma spraying (49, 10). When the oxide layer thickness is reduced, oxidation starts to accelerate, as the mass transfer of oxygen is easier through a thinner protective oxide layer. Oxide volatility can probably also produce improved coating properties, e.g. better cohesion between spray particles may be caused by the absence of a solid oxide layer between WC-Co17 lamellas in the coating.

Most of the oxides forming during spraying are solid and visible, under an optical microscope. Solid metal oxides can be seen in a polished coating, as grey or black lamellas, which have formed between the round or flat spray particles forming the actual coating. Typical oxides in metals are Al_2O_3, NiO, Cr_2O_3, SiO_2, MgO, FeO, WO_3 and CoO. In alloys, oxides are often more complex, e.g. in the case of NiCr80/20 alloy, spinels of $NiO*Cr_2O_3$ are formed (50, 51).

Selective oxidation means that some alloying elements (Cr, Ti, Al, C etc.) of an alloy or composite, have a higher affinity for oxygen than other alloying elements (Ni, Fe, Co, Cu etc.), and consequently, oxidise earlier and more rapidly. The selective oxidation phenomenon is based on the higher negative free energy, ΔG, in forming metal oxides. For example, Cr has a stronger tendency to form an oxide than Ni or Co. This means that in an oxide layer, there is more Cr_2O_3 than NiO, of an alloy being oxidised. Kinetic factors additionally control the oxidation process. The affinity of a metal for oxygen can be seen from the Ellingham diagram, Figure 3 (41). The higher the negative ΔG, the higher the tendency of a metal to form an oxide in an alloy. However, the affinity of the element for oxygen does not predict the rate of oxidation.

Composites play an important role in thermal spraying. Spray powders, WC-Co17 and Cr_3C_2-NiCr80/20, contain significant quantities of carbon, which has a high affinity for oxygen. If

the carbon of the composite is lost, many important mechanical properties are reduced. For this reason, the selective oxidation of carbon is also an important aspect of the HVOF coating process.

2.2 Kinetics of oxidation

Thermodynamics allows prediction of the final equilibrium state for a reaction, but gives no information about the reaction rate. Kinetics expresses the speed of the oxidation process. Reaction rates, and corresponding rate equations for the oxidation of a metal, depend on a number of factors, such as temperature, oxygen pressure, dwell time of reaction, surface area, surface pre-treatment, etc. Rate equations can be in principle derived from reaction mechanism. If the reaction mechanism and rate determine steps of the overall oxidation reaction could be established, a lot of experimental data is needed to predict the actual oxidation rate even in the case of ordinary high temperature oxidation process of thermal spraying.

The rate equations developed for steel melts are insufficient for explaining the oxidation mechanism. Rate equations may be used to classify the oxidation behaviour of metal, but not to predict the real reaction rates. Oxidation processes of thermal spraying are more complex than the ordinary high temperature oxidation, because no process variables are steady. There is no constant spray temperature, time or oxygen partial pressure. Furthermore, spray material oxidation properties vary more than those of pure metals. In thermal spraying, spray powders are alloys, and are often above the molten state, or close to melting point. This raises the question of whether use can be made of previous studies, because most of the oxidation studies of metals, as well as the studies of alloys, have been performed in the solid state far below melting point, and have been often of pure metals.

2.2.1 Heterogeneous oxidation

Metal oxidation is a typical example of a heterogeneous reaction. These reactions involve two or more phases (gas and solid/liquid), and occur at the interface between a fluid and a solid. In HVOF spraying, oxidation occurs between the combustion gas and spray particles. These can be either in solid or molten state, and thus oxygen mass transfer can occur by diffusion or, in the molten state, by fluid convection. A remarkable fact is that oxygen diffusion rates in liquid metals are many times higher than those in solids (46). This has a significant effect on the oxidation reaction rate.

2.2.2 Solid oxidation

Empirical reaction rate models are available, which describe the growth rate of oxides on pure metals. For solid metal oxidation there are four oxide layer growth rate models: parabolic, logarithmic, cubic and linear. The parabolic oxidation law is employed in this work because spray materials are usually sprayed close to, or below, their melting point. In 1933, Wagner showed that ideal ionic diffusion-controlled oxidation of pure metals, follows a parabolic oxidation rate law (44, 52):

$$(m/A)^2 = k\,t, \qquad (16)$$

where A is the area on which the reaction occurs, m is mass, k is the reaction rate constant (g^2 cm^{-4} s^{-1}) and t is time. Equation (16) can be rewritten:

$$m/A = (k\,t)^{1/2}. \quad (17)$$

Equation (17) indicates that the reaction rate is strongly affected by the surface area of the reacting powder. This is important in the case of thermal spraying since the specific surface area of the spray powder is 300 to 500 times greater than the surface area of the bulk material and this large surface area will increase the oxidation rate. For example, one cm^3 of spherical spray powder particles (30 μm) has a specific surface area of 0.2 -0.4 m^2. If the spray particle size is reduced by half, the surface area available for the chemical reaction doubles. The reaction rate constant k can be written:

$$k = \text{const}\, p_{O2}^{\,1/n} \exp^{(-Q/RT)}, \quad (18)$$

where p is partial pressure of the reacting gas, oxygen. The pressure factor is relatively weak because in the exponent 1/n, n can vary from 3.5 to 6. This explains why the concentrations of oxygen, water vapour or carbon dioxide do not have a significant effect on the reaction rate. The p_{O2} level in HVOF, varies from relatively low values of p_{O2} 10^{-16} bar, to a high value of p_{O2}, 0.21 bar. The exp (-Q/RT) term in Equation (18) is the Arrhenius law parameter, which shows that chemical reaction rates are temperature-dependent (44, 46, 47). Oxidation reactions are very temperature-sensitive. The parabolic oxidation law suggests that particle and gas temperatures are the most important factors affecting spray powder oxidation. Time, t, in the reaction process is a function of the distance that the particles travel, and their velocity. In HVOF spraying, typical process times for spray particles are <1 ms in the nozzle, <1 ms in air and for coating, 10-100 ms under the hot plume on the substrate (14). Spray particle oxidation time, T_{dwell}, in the HVOF gun nozzle and in the plume, is quite fixed. The dwell time of spray particles in the nozzle and plume are both controlled by gas velocity and density, and dwell time does not vary by more than a factor of two. The coating oxidation time in the plume and on the substrate can vary by more than a factor of ten.

2.2.3 Effect of alloying elements on oxidation rate

Formation of a protective oxide layer at high temperatures on alloys, is widely utilized to decrease their oxidation rate. In high-temperature alloys, Cr, Al and Si form stable oxides with low diffusion coefficients for oxygen. In spite of Cr, Al and Si having a high affinity for oxygen, when formed, the thin oxide layer resists oxygen diffusion and limits further oxidation of the alloy. This phenomenon is useful in thermal spraying, where the spray particles are in the solid state. Figure 4 shows the kinetic constants for pure metals in the air, which are the most important components of high-temperature alloys, and reveals the low parabolic oxidation rate of Cr, Si and Al (53, 54) in air.

Some metals, such as Fe, Cu, Ni, Co, W and Mo, do not form protective oxide layers. Ti has a high affinity for oxygen and oxygen is highly soluble in Ti, thus the rate of oxidation is not limited. W, Cr, Mo, C can form volatile oxides which may accelerate the rate of oxidation due to the absence of a protective oxide layer. The metal can then lose weight when it oxidises (44).

Some elements such as Li, accelerate the rate of oxidation even though they are present in an alloy in only small amounts. Other elements such as niobium, form highly stabilising protective oxide scales when oxidising in high-temperature atmospheres (55, 53).

Many of the alloys used at high temperatures contain elements which form these volatile oxides, which survive in high-temperature environments. Questions related to oxidation rates of metal alloys are therefore complex, and outside the scope of this study.

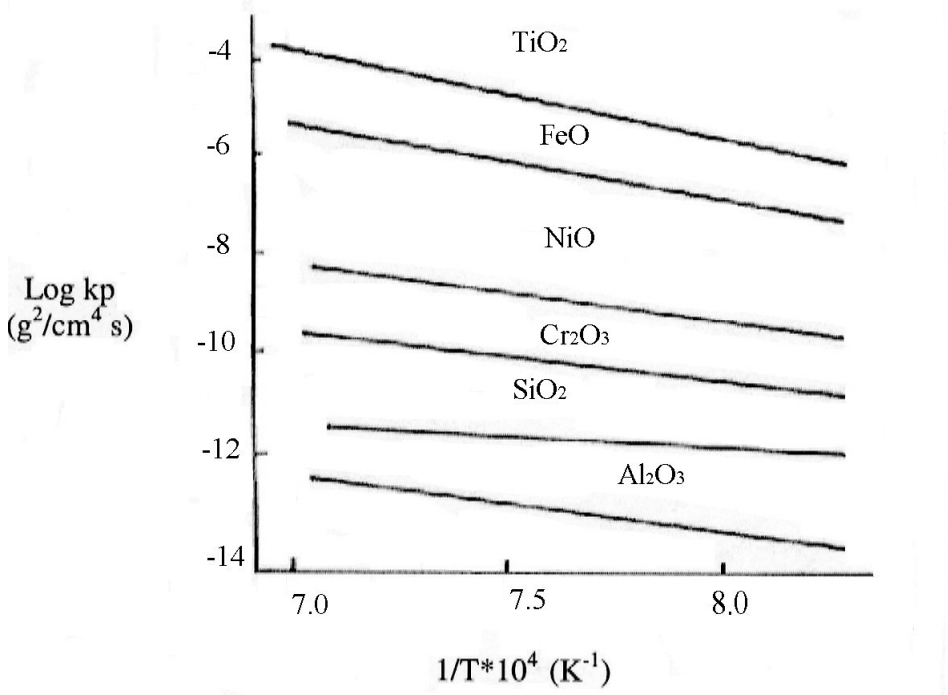

Figure 4. *Rate constants for the parabolic growth of various oxides in air. In pure metals oxide growth rates vary according to the metal and the temperature. High temperature increases the oxidation rate (53).*

2.2.4 Liquid oxidation

Oxidation processes in liquid particles are important processes in thermal spraying. The temperature of spray particles is often over 1700°C which can be above the melting point of the alloy and oxides formed, In molten state oxidation does not follow the same mechanisms proposed by Wagner for solid state oxidation (50).

Chemical equilibria of solid/liquid oxides and dissolved gases form a basis for understanding of oxidation phenomena in liquid phases. Liquid metal can contain oxygen dissolved in metal in much higher amounts than in the corresponding solid phase. When oxygen saturation is attained oxide phase is nucleated and forms a separate phase. Due to the high solubility of gases to liquid metal and favourable kinetic factors, chemical reactions can take place in and on the liquid metal. Chemical reaction can form gaseous, liquid or solid oxides. If gases are formed they generate bubbles in liquid metal.

Although the data of oxygen solubility, diffusion rates and oxidation rates in liquid alloys are quite scanty the knowledge available can be applied to understand oxidation phenomena in spraying process. Oxygen solubility in liquid metal increases when temperature and partial pressure increase. For example oxygen solubility can be 0.23 wt% in liquid steel at 1700 °C. When the solubility limit has been reached iron starts to oxidize and form iron oxide, wustite "FeO". When oxygen is blown into a steel melt in BOF process for decarburization, wustite formation starts at remarkably lower average oxygen content of the bulk melt. The reason is that oxygen saturation is reached locally at the impact area of the oxygen jet and iron oxidation can occur in the surface region. At the same time the "principal" reaction of carbon oxidation takes place in the same region. Although diffusion rates of elements like carbon in liquid metal are 100-1000 times (46) higher than in solids the huge surplus of oxygen at the reaction zone results in deviations from the thermodynamic oxidation order defined by the Gibbs energy of formation of oxides.(54)

Refining of steel is an example of liquid decarburization process, which can be compared with the decarburization process in WC-Co spray powder system, where carbon is lost from the liquid metal. In the steel making process oxygen is introduced into the liquid iron-based hot metal which contains about 4.5 w-% carbon dissolved into the iron in blast furnace process (19). In liquid iron, carbon and oxygen react and form carbon monoxide as shown in Equations 19, 20 and 21.

$$C = [C]_{Fe} \quad (19)$$

$$O_2 = 2[O]_{Fe} \quad (20)$$

$$[C]_{Fe} + [O]_{Fe} = (CO)(g) \quad (21)$$

Here $[x]_{Fe}$ denotes dissolved element in molten iron. Similar reactions can be expected to occur in molten spray powders, dissolving different elements of spray powder in molten metal. Solubility of oxygen in molten spray powder and chemical reactions forming oxides can be assumed comparable to the steel refining process (41, 54). The topic is further discussed in the section 6.3.

3. AIM OF THE PRESENT WORK

The main objectives of this thesis are to present the theoretical and experimental studies on the oxidation of powders in the HVOF spraying process. The study concentrates on demonstrating the general features of the oxidation processes, rather than the details. Initially, the HVOF spraying process is reviewed as it relates to the combustion process, including studies of flame temperature, oxygen partial pressure, gas velocity and density. Spray process, spray particle temperature and velocity history are analysed and measured in the plume and on the substrate. These features were considered important for understanding the spray particle oxidation behaviour in high velocity and temperature processes.

In the experimental part of this thesis, oxidation behaviour of the spray particles is calculated for different HVOF fuels and metal combinations, to understand the tendency of spray particles to oxidise. In the coating experiments with HVOF spraying, different oxidation processes, such as selective oxidation and oxide volatility of the alloys and carbides, are demonstrated. The degree of oxidation of the alloys and carbides are studied in the HVOF gun nozzle, in the plume and on the substrate. Finally, microstructures of the alloys and carbides are evaluated to classify the effects of spray parameters on oxidation morphology and degree.

4. CHARACTERISTICS OF THE HVOF PROCESS

This section summarises gas and particle behaviour in the HVOF spray process: i.e. spray parameters such as spray gas temperature, gas velocity, spray particle and gas convection velocity, gas density and chemical composition of the combustion gas. Spray particle properties are also discussed, including temperature, surface area, and dwell time in the spray process. This is necessary because of the importance of understanding the actual coating process, before discussing the high temperature oxidation of metals or alloys. There is no review available, regarding the manner in which spray process input parameters, such as fuel flow, combustion chamber pressure and fuel/oxygen ratio, affect the properties of gas and spray particles in the HVOF spray process.

4.1 Combustion reaction equations and chemical species

In the HVOF combustion process, there are two main chemical reactions; the combustion of hydrogen H_2 and carbon C with oxygen O_2. The hydrogen and oxygen flame system is one of the most extensively studied. Combustion of hydrogen occurs according to reactions (22) and (23). A detailed description of this topic can be found in (1, 38, 39, 56, 57**,** 58).

$$H_2(g) + 1/2O_2(g) <=> H_2O(g) \quad (22)$$

$$H_2(g) + O_2(g) <=> 2HO(g) \quad (23)$$

Combustion of carbon involves two main steps:

$$C + 1/2O_2(g) <=> CO(g) \quad (24)$$

$$CO(g) + 1/2O_2(g) <=> CO_2(g) \quad (25)$$

Combustion of C_xH_y by reaction Eq. (26) involves reactions (22), (23), (24) and (25).

$$aC_xH_y + bO_2 = cH_2O + dCO + eCO_2 + fO_2 + gO + hOH \quad (26)$$

In high-temperature flames, oxidation is not complete, i.e. the fuel is not combusted completely to H_2O and CO_2. Typically, a high temperature flame of 1000 to 3000 K contains the following combustion products: water vapour, H_2O, carbon monoxide, CO, carbon dioxide, CO_2 and oxygen, O, O_2 and OH. The combustion reaction is considered to be completed once the flame or jet temperature has cooled to room temperature and all the flame species have been combusted to water vapour and carbon dioxide.

Flame equilibrium chemical compositions can be calculated using computer programs, e.g. HSC-Chemistry and Gordon & McBridge (57, 59). In Table 2 and Table 3, it can be seen that the calculated (HSC) flame composition changes as a function of flame temperature. An increase in temperature reduces combustion products and a decrease in temperature increases combustion products. It is important to note that the amount of free oxygen (O_2) is relatively small at low temperatures compared to the other species (H_2O and CO_2), but it increases when temperature is above 1500°C.

***Table 2**. The combustion products of O_2 and $C_{10}H_{20}$ as mole percents (%) in the HVOF gun. F/O ratio, is stoichiometric.*

Temperature (°C)	**600**	**1040**	**1480**	**2030**	**2470**	**2800**
CO_2(g)	50	50	49.75	44.94	30.7	16.77
H_2O(g)	50	50	49.87	47.52	39.33	27.86
CO(g)	2.98E-07	0.002371	0.1869	3.773	13.93	22.5
O_2(g)	5.327E-07	0.001752	0.1104	1.986	6.834	10.24
HO(g)	1.992E-08	0.000270	0.03185	0.9167	4.407	8.766
H_2(g)	7.796E-07	0.001277	0.05042	0.6941	2.548	4.821
O(g)	1.393E-14	9.362E-08	0.000256	0.07121	1.128	4.623
H(g)	4.183E-13	4.911E-07	0.000542	0.08284	1.077	4.369
OH(g)	4.497E-09	0.000021	0.001051	0.01246	0.0328	0.04351
HO_2(g)	6.122E-14	1.082E-08	4.871E-06	0.000356	0.002466	0.005231
C_2H_4(g)	<< 1E-34	< 1E-34	5.097E-29	1.915E-23	1.078E-20	2.607E-19

***Table 3**. The combustion products of O_2 and H_2 as mole percents (%) in the HVOF gun. Fuel oxygen ratio, F/O, is stoichiometric.*

Temperature °C	**600**	**1040**	**1480**	**2030**	**2470**	**2800**
H_2O(g)	99.99	99.99	99.75	95.74	81.21	58.88
H_2(g)	1.379E-06	0.002904	0.1379	2.164	8.104	14.65
HO(g)	2.995E-08	0.0003575	0.03853	1.046	5.103	10.63
H(g)	5.564E-13	7.405E-07	0.0008969	0.1462	1.921	7.616
O_2(g)	6.805E-07	0.001356	0.0591	0.83	2.88	4.95
O(g)	1.574E-14	8.236E-08	0.0001875	0.04603	0.7326	3.215
OH(g)	6.761E-09	0.0000279	0.001271	0.01422	0.03797	0.05274
HO_2(g)	1.04E-13	1.263E-08	4.311E-06	0.0002627	0.001853	0.004409

4.2 Flame temperature and its control in the combustion chamber

The HVOF flame temperature can be controlled in three ways; by selecting the fuel quality, by adjusting the fuel to oxygen ratio (F/O ratio), and by altering the combustion pressure. The highest flame temperature obtainable is called the adiabatic flame maximum temperature ($T°$), and is reached by combusting fuel with pure oxygen, close to the stoichiometric ratio. Flame temperature can be altered by the fuel quality, e.g. acetylene (C_2H_2) produces a flame temperature of 3250°C, and hydrogen and kerosene both produce a flame temperature of 2750°C (60).

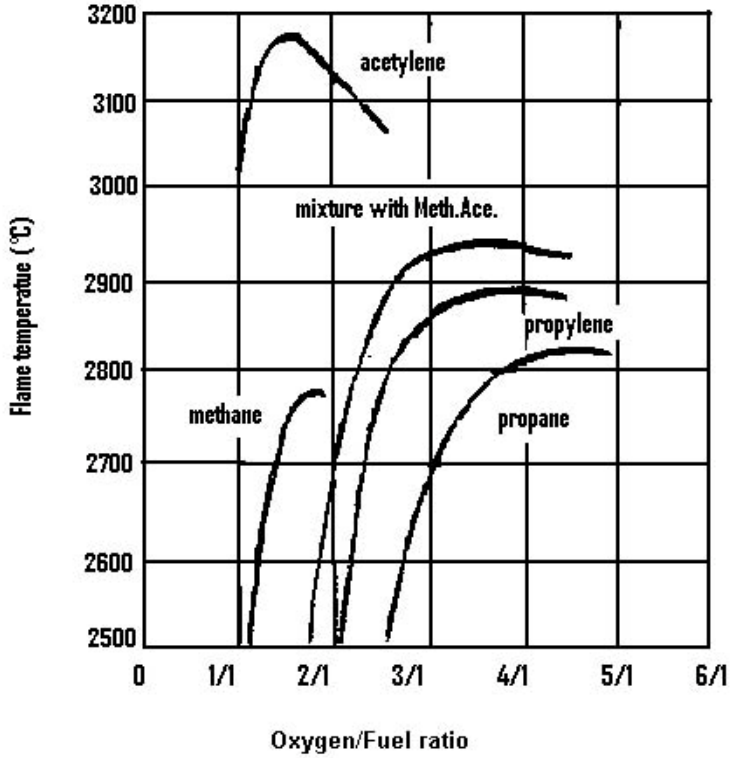

Figure 5. *Schematic diagram of flame temperatures of different fuels. The temperature of the flame varies with mixture composition (F/O ratio) of different combustion gases; acetylene, propylene, methane and propane.*

Fuel quality is not the only way of controlling flame temperature. Adjusting the F/O ratio can also control it. The F/O ratio is defined as the mixing ratio of oxygen (O) and fuel to be combusted. Fuel can be H_2, hydrocarbons, acetylene, propane, kerosene, etc. The maximum flame temperature will be obtained by using F/O ratios close to those presented in Figure 5. If the F/O ratio is either lean or rich, flame temperature will be lower than the adiabatic temperature (16, 32). Figure 5 shows calculated maximum adiabatic flame temperatures for different combustion gases, and the effect of the F/O ratio on them. The maximum flame temperatures, i.e. adiabatic temperatures, are reached using close to stoichiometric F/O ratios (61).

Combustion pressure increases flame temperature. In the HVOF spray gun, combustion occurs at elevated pressures, typically 1.5 to 15 bar. A higher combustion pressure than ambient (1 bar), increases the adiabatic temperature, $T°$, and the combustion chamber temperature. The increase in combustion chamber temperature can be estimated from the isentropic Equation (27), which is for a calorically perfect gas. In the real combustion process, chemical equilibrium lowers the temperature (40).

$$T°/T_1 = (p_o/p)^{-((\gamma-1)/\gamma)}, \qquad (27)$$

where T^o is the adiabatic flame temperature at 1 bar pressure, T_1 is the elevated temperature, γ is the ratio of specific heats (Cp/Cv), p_o is the combustion chamber pressure and p is ambient pressure. For example, the increase in combustion chamber temperature for chamber

pressures of 2, 5 and 10 bar, is 12%, 30% and 46%, respectively. In a real spray process, gas temperature is lower than the calculated temperature. The lower temperature of the process gas is due to the chemical equilibrium of the gas. Figure 6 shows the effect of the combustion pressure on the temperature of the gas. The lower curve shows the effect of the chemical equilibrium on gas temperature. The upper curve shows the temperature of the perfect gas, according to Equation (27) (39).

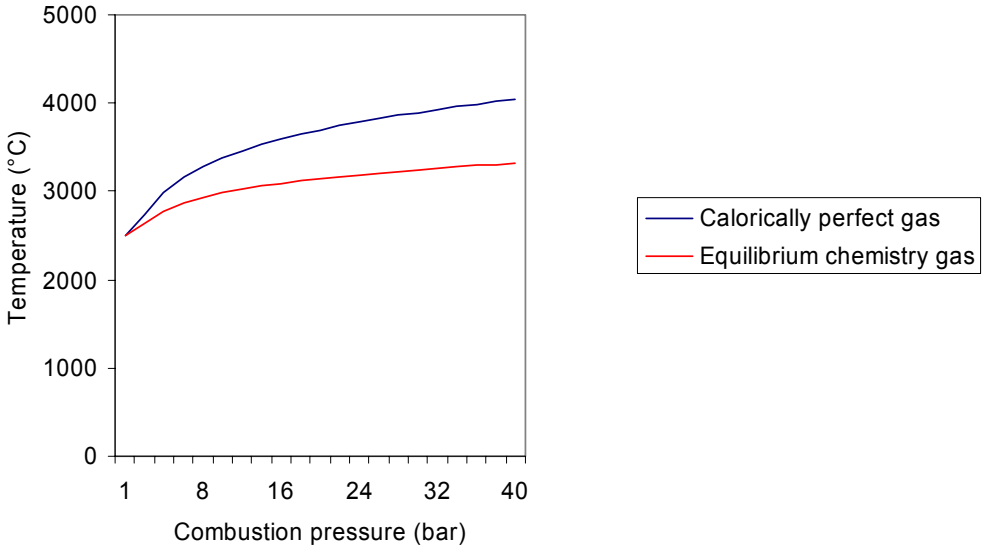

***Figure 6**. Schematic diagram of the effect of the combustion pressure on the flame temperature. Combustion pressure increases gas temperature. Calorically perfect gas has a higher temperature than gas with equilibrium chemistry (39).*

Some fuels have technical or safety considerations, which limit the increase in the combustion chamber pressure. For example, with acetylene (C_2H_2), an increase in combustion pressure is impossible; safety considerations rule out an operating pressure higher than 1.5 bar, as it spontaneously ignites at elevated pressures (62). Other gases, such as H_2, $C_{10}H_{20}$, propane and MAPP (liquefied petroleum gas with Methylacetylene-Propadiene), can be used at elevated combustion chamber pressures. For example, hydrogen and oxygen have a calculated combustion temperature of 3387°C at a pressure of 22 bar (39). Gas density affects heat transfer to the spray particles and the gas/spray particle velocity. Gas density is related to the flow velocity, gas temperature, the combustion chamber pressure and fuel quality. As the spray gun nozzle diameter is fixed in the HVOF spraying process, gas density increases when the gas flow rate in the combustion chamber is increased, while the gas velocity remains constant in the nozzle, as explained in the theory of the super sonic nozzles. Gas density is also affected by fuel quality, being higher when combusting hydrocarbons, than hydrogen. When combusting hydrogen, the average exit gas molecular weight is between 12 and 16 g/mole, while when combusting hydrocarbons, the average is in the range of 25 to 28 g/mole. Gas density has an effect on the spray particle velocity (73, 16), increasing it as can be seen from Equation (30). Gas density is also proportionally related to combustion chamber pressure.

4.3 Gas velocity in the combustion chamber

Combustion gas velocity is slower in the combustion chamber than in the nozzle, because the combustion chamber cross-sectional area is ≈ 10 to 25 times greater than the cross-sectional area of the nozzle ($A_{combustion\ chamber}/A_{nozzle}$). The large difference in cross-sectional area keeps the gas velocity lower in the combustion chamber compared to that in the gun nozzle. The estimated gas velocity is approximately 50 -100 m/s, and depends on the size of the combustion chamber, quality, temperature and flow rate of the gas (38, 39, 63). In most HVOF guns, the combustion chamber is short compared to the nozzle section (Miller HV-2000 and Sulzer Metco DJ Hybrid). The typical length of the combustion chamber in HVOF guns is 15 to 25 mm, while the nozzle length is from 60 to 150 mm. In kerosene fuelled HVOF guns, such as the Tafa Hobart JP-5000 and the OSY CJS, spray particles are fed axially after the combustion chamber so that the combustion chamber gas velocity does not affect spray particle velocity. It appears that gas velocity in the combustion chamber does not have a great effect on spray particle gas velocity, because it is 10 times smaller than the gas velocity at the nozzle exit.

4.4 Effect of HVOF process on spray particle

In the HVOF process, gas temperature, velocity and composition vary along the nozzle and in the combustion chamber. There are two main factors which reduce gas temperature in the nozzle from that in the combustion chamber; the conversion of the heat into the kinetic energy, and the heat transfer from the hot gas to the wall of the combustion chamber and the nozzle. Calculated heat transfer to the spray particles is negligible, being only <1 % of the total combustion energy (Table 5). The heat formation in the combustion process can be expressed as shown in Equation (28):

$$h^\circ = c_p\, T^\circ, \tag{28}$$

where h° is the combustion enthalpy, heat released during combustion, c_p is the specific heat of the combustion gas per mol and T° is the adiabatic temperature of the combustion gas. It is called stagnation temperature while the gas has no kinetic energy, and is in a state of rest. In the combustion chamber, the transformation of heat and pressure to kinetic energy starts. This causes the combustion gas temperature to fall and the level of kinetic energy to rise, while the total energy remains constant according to the law of conservation of energy. The new lower gas temperature can be obtained from Equation (29):

$$h^\circ = c_p\, T_1 + 0.5\, \mathrm{m}\, v^2, \tag{29}$$

where T_1 is the new lower gas temperature and the last term is the thermal energy transferred to the kinetic energy; v is velocity of the gas and m is the molar mass flow of the gas. The gas temperature reduction varies according to the Mach number of the HVOF gun nozzle (M). M is local velocity of sound. Typical values for HVOF gun nozzles are from 1 to 2 M, while typical values for ratio of specific heats, γ, are from 1.15 to 1.2. This results in a 13-45 % reduction in T°. T_1 is the new gas temperature available to heat the spray particles in the

supersonic jet. Figure 7 shows a schematic temperature distribution through a converging-diverging nozzle with supersonic flow. Gas temperature falls from that in the combustion chamber, as the Mach number (M) increases, i.e. the gas velocity rises (16, 37, 38, 39).

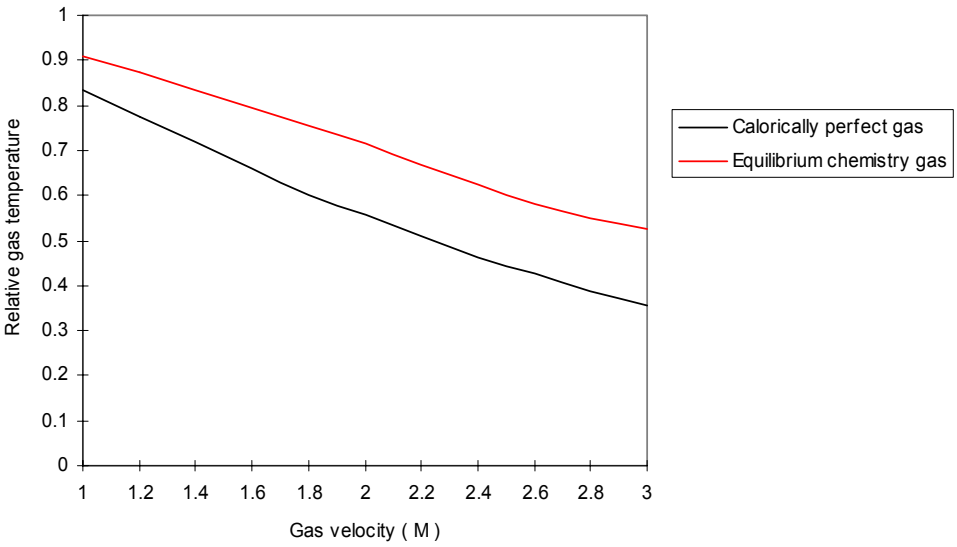

***Figure** 7. Relative decrease of the gas temperature in a supersonic nozzle compared to the temperature of the combustion chamber. Figure shows the temperature distribution through a converging-diverging nozzle (de Laval nozzle) with supersonic flow equilibrium and a calorically perfect gas (39).*

The second important aspect of the combustion process, is heat transfer from the hot gases to the cooling water. If the combusting gas heat transfer rate is high, flame temperature will be reduced, resulting in a significant lowering of the spray particle temperature. Low flame temperatures are easily visible in the coating microstructure, resulting in many unmelted round metal particles in the coating, with consequent high porosity. This is a feature of HVOF guns with large combustion chamber surface areas and long nozzles, and is an HVOF gun design factor which cannot be greatly influenced by adjusting gas parameters.

Nearly all HVOF spray guns are water-cooled. This is necessary because the high heat transfer rate melts uncooled copper components, the nozzle and the combustion chamber. The heat transfer to HVOF gun cooling water, varies from 25 to 45% of the combustion power (energy balance) in the Miller Thermal HV-2000, and Jet-Kote guns, respectively. The heat transfer rate depends on the construction of the HVOF gun, i.e. the length of the nozzle and the size of the combustion chamber (64). High cooling rates lower gas and particle temperatures (64, 65**,** 66). In the HVOF gun, water-cooling can be combined with a gas cooling system, which reduces heat loss in the combustion chamber and the nozzle. This is a feature of the Sulzer Metco DJ-Hybrid and OSY CJS HVOF spray guns.

In the combined water/gas cooling system, cool gas flows along the wall of the combustion chamber and nozzle. The boundary layer of the cool gas reduces the heat transfer from the hot combustion gas to the cooling water. Heat losses to the cooling water have been reported to reduce to 10% of the combustion power (67). Low heat losses keep temperatures of the

combustion gas high. High gas temperature increases the degree of melting of the spray powder.

In the HVOF spraying gun nozzle, gas velocity can remain constant or increase. In a barrel nozzle design, gas velocity remains constant while in the de Laval nozzle, velocity will increase. After leaving the combustion chamber, the gas velocity reaches the speed of sound in the nozzle throat. At a combustion temperature of 2500°C, the velocity of sound is between 1000 and 1500 m/s. In a barrel nozzle, the gas velocity remains constant, but in the de Laval nozzle, gas velocity increases to between 1800 to 2100 m/s. A more detailed description is provided by Korpiola (68). During this part of the process, the gas temperature falls according to Equation (29).

High gas velocity is obtained by using hot gas at high pressure. Pressure energy is converted to kinetic energy in the nozzle of the HVOF gun. A simple barrel nozzle of HVOF gun produces gas velocities of Mach 1. Increasing the pressure of the combustion chamber does not increase the exit velocity at the nozzle of the HVOF gun, but does increase the density of the gas. Jet-Kote, Top-Gun and Diamond Jet Standard are Mach 1 HVOF guns.

If a further increase in HVOF gas velocity is required, the combustion chamber pressure must be increased from 2 to 4-15 bar and the nozzle of the HVOF gun must be of the type of the converging-diverging nozzle called a converging-diverging Laval nozzle, or de Laval nozzle. The de Laval nozzle can be found, for example, in the Sulzer Metco DJ-Hybrid 2600, OSY CJS, and Hobart Tafa JP-5000 HVOF guns. Experimental, non-commercial models of HVOF guns, which utilise a de Laval nozzle, also exist, namely, the VTT Miller Thermal HV-2000 and Browning's "High impact HVOF" (68, 69). Schematic representation of the de Laval and the barrel nozzle are presented in Figure 8.

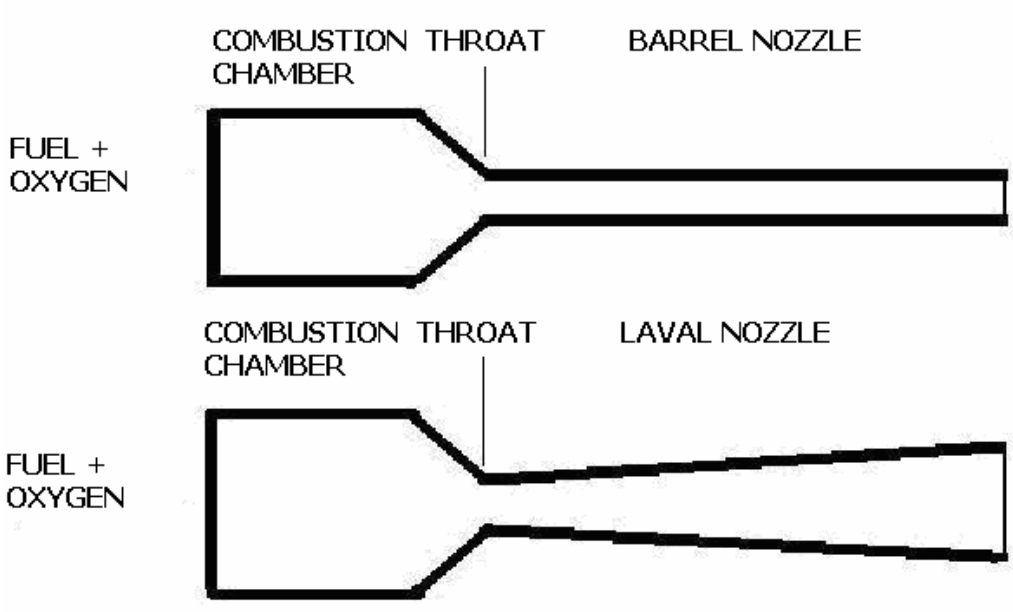

Figure 8. *Schematic diagram of two commonly used nozzles including combustion chamber, a barrel nozzle on the top and a converging-diverging de Laval nozzle on the bottom.*

The effect of fuel quality on gas velocity has not been clearly shown, but it is clear from propulsion technology, that hydrogen and oxygen produce the highest gas velocities (39). This fact has not been utilised in HVOF technology in the form of a high-pressure hydrogen

HVOF gun. So far, high-pressure HVOF guns have been based on the combustion of kerosene and oxygen. Combusting hydrocarbons produces lower theoretical gas velocities, because the exit gas has a higher density compared to hydrogen-oxygen combustion.

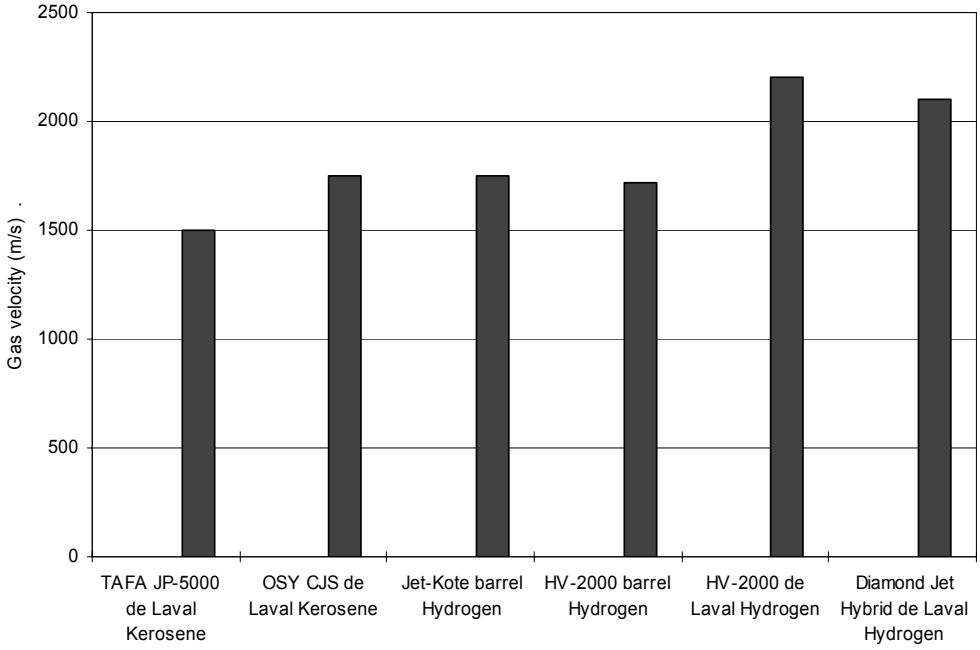

Figure 9. *Gas velocity comparison of commercial hydrogen and kerosene combusted HVOF guns. Hydrogen combusted HVOF guns have the highest gas velocity (64, 68).*

Figure 9 shows the gas velocities of commercial HVOF guns. The first generation HVOF gun employing a barrel nozzle, produces a gas velocity of 1700 m/s with hydrogen (Jet-Kote, Top-Gun, HV-2000 Miller Thermal), while a second generation modified HV-2000 VTT gun with a de Laval nozzle produces a gas velocity of 2200 m/s (64). The OSY CJS kerosene gun produces a gas velocity of 1750 m/s (70), while the Sulzer Metco DJ-Hybrid has been reported as producing a gas velocity of 2100 m/s. The Tafa JP-5000 has been reported as producing a gas velocity of 1500 m/s, which is lower than velocities produced by hydrogen-combusting HVOF. Both the Tafa JP-5000 and OSY CJS HVOF guns combust kerosene, and the exit gas has a higher density than the hydrogen-combusting HVOF guns. Therefore, the Tafa JP-5000 and OSY CJS HVOF guns produce equal particle velocities to the Sulzer Metco DJ-Hybrid gun (13).

Browning has reported the use of an HVOF gun to produce a gas velocity higher than 2900 m/s, when operating with high pressure liquid oxygen and kerosene (71). Figure 9 shows that hydrogen combusting guns have higher maximum gas velocities than kerosene combusting HVOF guns (72).

Figure 10 shows the effect of the F/O ratio on gas velocity, in the Jet-Kote and Miller Thermal HV-2000 guns with a barrel nozzle, and the Miller Thermal HV-2000 HVOF spray gun with a de Laval nozzle (72). Increasing the level of hydrogen in the combustion process increases gas velocity. This is due to the lower density of combustion gas, since the combusting gas contains more light hydrogen than heavy oxygen. The effect of high pressure in the combustion chamber of the HVOF gun, has been widely discussed, but to utilise the advantages of the high-pressure effect, the nozzle of the gun must be designed accordingly. It

must correspond to a de Laval nozzle, with the design procedure following the well-established theoretical laws of compressible flow. A good description can be found in several textbooks on fluid mechanics (37, 38, 39, 40).

Little experimental work of the effect of nozzle length on particle velocity has been reported, but much modelling work has been done. A long nozzle length is expected to increase the velocity of the spray particles (85). HVOF gun manufacturers produce nozzles with a variety of lengths, from 20 to 200 mm (OSY, Tafa, and Top-Gun).

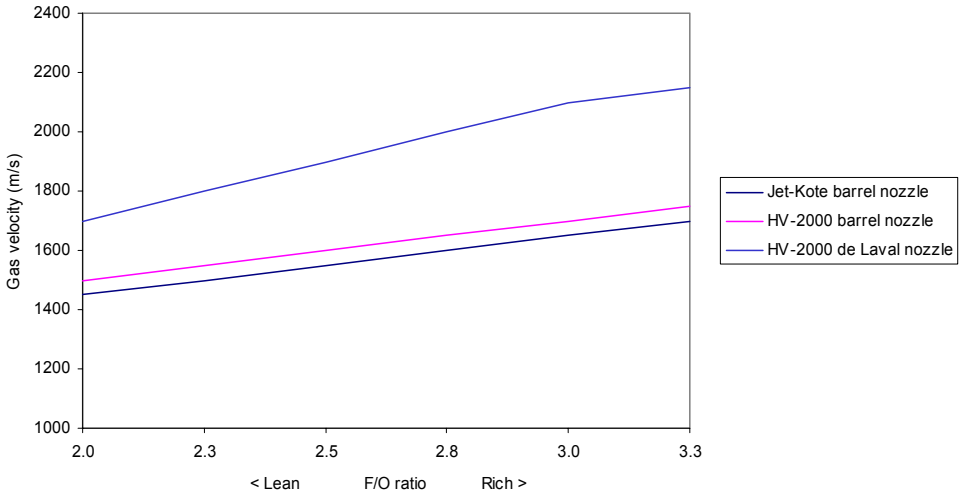

Figure 10. *Effect of F/O ratio and nozzle type on gas velocity with hydrogen and oxygen. Gas velocity increases when combusting more hydrogen than oxygen and using a de Laval nozzle instead of a barrel nozzle (64).*

4.4.1 Effect of gas velocity on spray particle

The HVOF spraying gas velocity acts on spray particles in two ways. Firstly, acceleration of the spray particles to a high velocity affects the dwell time of the particles in the spray process, i.e. the oxidation time. Secondly, gas velocity has an effect on the convection velocity of the spray particles. Convection velocity controls particle oxidation rate, i.e. mass transfer of oxidising combustion gas to the hot surface of the particle. The effect of HVOF gas velocity on a spray particle is related to Equation (30) (73, 88):

$$F = k\rho v^2, \tag{30}$$

where F is the force accelerating a particle to a high velocity, k is the aerodynamic constant/coefficient, which is related to shape, etc., ρ is the gas density, which is related to combustion chamber pressure and gas velocity in a nozzle, and v is the gas velocity in an HVOF gun nozzle. As can be seen in Equation (30), the most powerful factor is gas velocity, if the lowest possible oxidation time and high gas density in the spray process, are desired. It is therefore useful to utilise gas velocity, rather than gas density, to obtain high particle velocities and consequently low oxidation times. In addition, if high particle velocities are obtained, these produce high solid impact fusion, which, as Dvorak has pointed out, produces lower oxide content of coatings (74).

The convection velocity is the velocity difference of the gas and the spray particles in the HVOF process. The influence of convection velocity on the chemistry of spray particle oxidation is apparently very poorly understood. However, this is an important factor because convection velocity controls the rate of the chemical reaction of the spray particle, both in the nozzle and in the plume. Chemical reactions occur on the surfaces of spray particles with a gas convection velocity between 1000 and 1500 m/s, falling when the spray particle gains momentum in a manner that depends on the gun type. The estimate of gas convection velocity is based on measurement of the particle and gas velocity. It is affected by the drag force, Equation (30), and the density of the particle.
The momentum flux of the HVOF gun, *M,* is the main factor accelerating spray particles to a high velocity. It can be defined as shown in Equation (31):

$$M = \rho v^2 \tag{31}$$

If the momentum flux of the HVOF gun is high, high spray particle velocities can be obtained. HVOF guns employ many kinds of fuel: hydrogen, acetylene, natural gas, propane and kerosene. Hydrogen produces higher gas velocities than kerosene, but kerosene guns operate with 4 to 10 times higher combustion chamber pressures than hydrogen guns. Kerosene guns produce higher gas densities (ρ) than hydrogen combusted guns. The momentum flux of the HVOF gun, is the combination of high gas velocity and density, as in Equation (31). It is therefore, more reasonable to compare the momentum flux of HVOF guns, than gas velocity. Measurements and calculations for a variety of HVOF guns determined the following momentum flux at the exit of the spray gun nozzle, as shown in Figure 11. Momentum flux has been calculated in two ways; (1) from results of recoil and gas velocity measurement of the HVOF guns, HV-2000, Osy and Jet-Kote (68, 72, 67), and (2) published data from the JP-5000 and DJ-Hybrid (34, 35, 36, 38, 66, 75, 77, 78, 87, 100).

- $M = F_{\text{recoil of HVOF gun}} / A_{\text{exit of HVOF nozzle}}$
- $M = v_{\text{gas}} * \underline{m} / A_{\text{exit of HVOF nozzle}}$

The results of the calculation and measurement show that the guns employing kerosene (OSY CJS and JP-5000), have a momentum flux advantage over hydrogen combusting HVOF guns. This is due to the increased density of the gas, i.e. molecular weight and pressure in the nozzle of the HVOF gun, which replaces the effect of lower gas velocity, when compared to hydrogen combusting HVOF guns. This can be compared with the results of the gas velocity measurements of HVOF guns in Figure 9. For this reason, high gas velocity is not the only important parameter of HVOF guns.

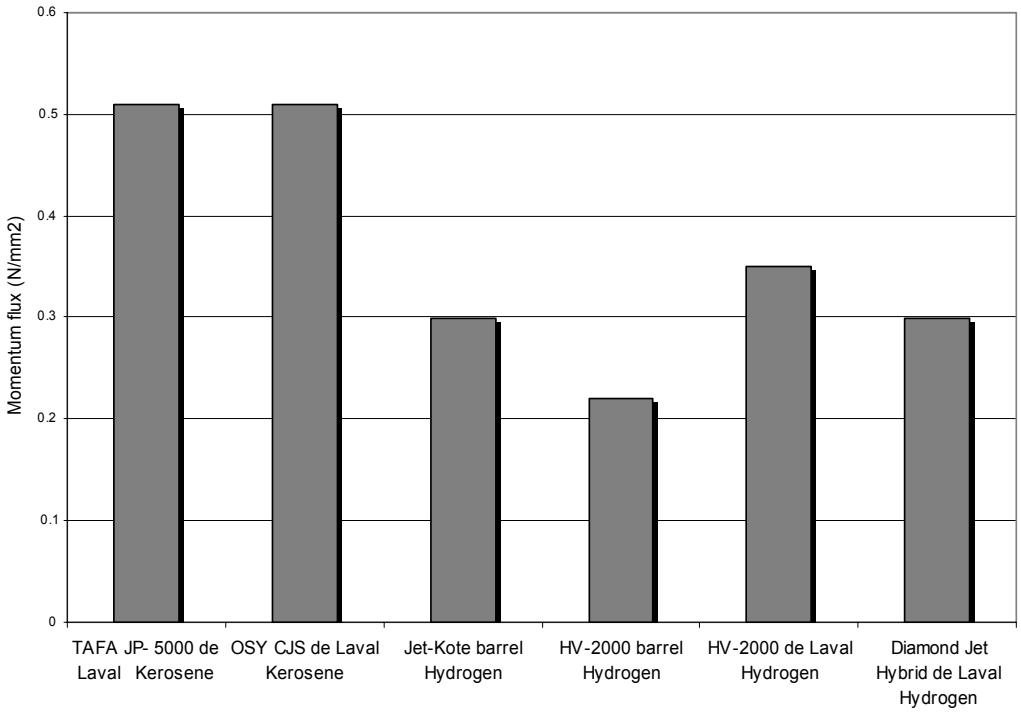

Figure 11. *Momentum flux of commercial HVOF guns. Kerosene combusting HVOF guns have higher momentum flux than hydrogen combusting HVOF guns.*

4.5 Flow properties in the plume and on the substrate

When the supersonic flow leaves the nozzle of HVOF gun and the shock diamonds, the properties of the flow change quickly. This is due to the flow system operating in open air, i.e. ambient air is mixed into the flame and the plume of the HVOF gun. Mixing happens because the density of the air is high compared to that of the hot flow ($\rho_{air} / \rho_{flow} \approx 7$) (75, 76, 77, 78). The mixing of the air causes several changes to properties of the flow: temperature, velocity, chemical composition and convection velocity of the spray particles.

The temperature of the flame and the plume falls because of the mixing with cold air. The fall in temperature of the plume is important because it makes it possible to keep temperatures of the substrate sufficiently low. The plume can contain 80-90% of cold air at level of the substrate, therefore the temperature of the plume has been fallen.

The temperature of the jet was calculated (HSC) as falling from 2000 to 500°C along the centre line of the flow onto the substrate. When the gas temperature is reduced, the flow no longer heats spray particles, and may cool them. The size of the drop in temperature of the gas depends on several factors: fuel combusted, spray distance, F/O ratio, amount of combustion gas and gas velocity. A cool plume allows the sprayed particles to cool rapidly on the surface of the substrate.

Gas velocity also falls in ambient air because of mixing with the cooler air. The air mixed into the high velocity flow has to be accelerated, and this consumes kinetic energy of the flow, although the momentum of the flow is conserved. According to the law of conservation of momentum, the reduction in the velocity of the flow can be calculated. When the degree of air

mixing is known (80-90 %), the new velocity of flow can be calculated. When the maximum velocity of the flow is 1500 m/s and the addition ratio of the cold air mass is 5 to 10 times the mass of the flow, gas velocity at the substrate is reduced to 150-300 m/s (79, 80). The low gas velocity in an orthogonal direction to the surface, allows free and stable formation of the coating.

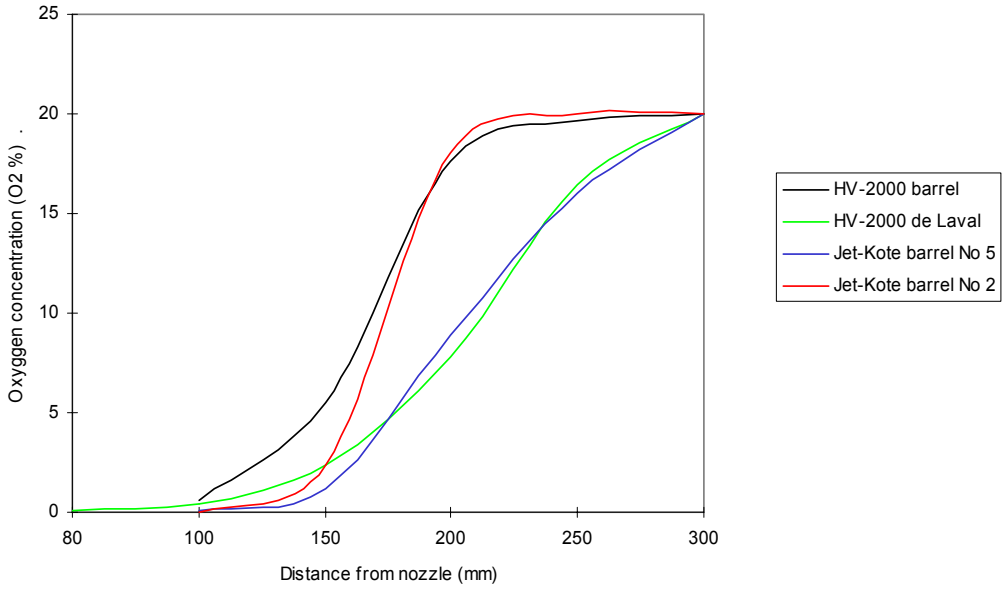

Figure 12. *Oxygen concentration in vol-%, in the plume along the jet axis for the Jet-Kote and Miller Thermal HV-2000 guns. The concentrations were measured with different nozzles (81).*

The chemical composition of the plume gas changes due to air mixing. Entrained air burns the unburned species in the flame, i.e. CO, OH and H_2, to water and carbon dioxide. The oxygen partial pressure of the flow increases from a level of 10^{-6} % to 2 - 20%. Nitrogen from the air acts only as an inert gas, which cools the hot flow. The concentrations of H_2O and CO_2 fall to below 10%. Figure 12 shows the oxygen (%) concentration for the Jet-Kote and Miller Thermal HV-2000 HVOF guns, along the jet axis from a work distance of 50-350 mm. The oxygen partial pressure has been measured with the solid electrolyte ZrO_2 cell (15). Hydrogen was employed as the combustion gas (15, 81). The convection velocities of the spray particle and gas, fall from 1000-2000 m/s to 1000-150 m/s, as a result of air mixing in the plume.

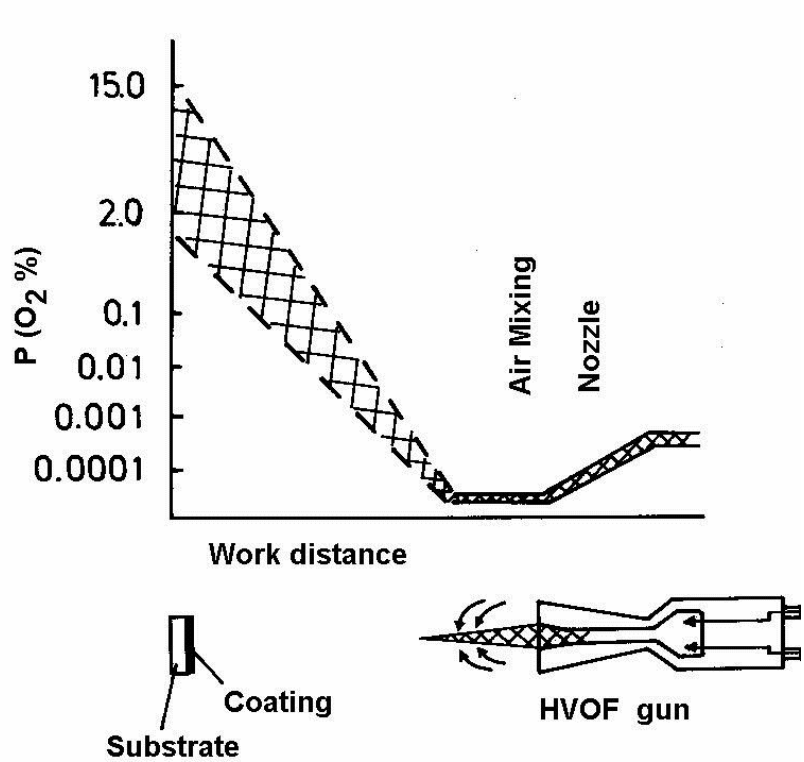

***Figure 13**. Schematic picture of oxygen partial pressure in the HVOF spray process. Oxygen partial pressure is shown from the combustion chamber to the substrate (15).*

The temperatures and velocities of the flow fall as a result of air mixing (80-90 %) with the jet (32). The temperature of the gas on the substrate can vary greatly, depending on the work distance, the type of HVOF gun and the F/O ratio, but typically it remains below 1000°C. The composition of the gas falling on the substrate is highly oxidising, containing N_2 50-60 vol. %, O_2 10-20 vol. % and H_2O and CO_2 <10 vol. % (14, 82). The calculated convection velocity falls to <200 m/s, and the area of the plume increases from the exit plane of the jet (0.5 cm^2) to several hundred square centimetres. The gas velocity orthogonal to the substrate surface is 150-300 m/s. Schematic picture of oxygen partial pressure in the HVOF spray process is presented in Figure 13. Oxygen partial pressure is shown from the combustion chamber to the substrate. The oxygen partial pressure of HVOF process is increases from low to high level.

4.6 Spray particle properties in the nozzle, in the plume and on the substrate

There are relatively few measurable properties of the flying spray particles which have a general effect on oxidation; particle velocity v, temperature T, flying time t and size d. However, there are specific properties, such as material manufacturing method, composition, density, diffusion rate of ions, cations and electrons in the oxide layer, viscosity of the molten oxide layer, etc., which affect the oxidation rate of the spray particles. The hot gas flow properties, gas velocity v_g, density ρ and heat transfer properties affect the spray particle variables T and v.

In this section, measurements of particle velocity and temperature are presented. The particle in-flight measurements were done with the DPV 2000™, Tecnar Ltd, Canada, and Oseir Ltd, SprayWatch™, Finland, instruments. The HVOF guns used in measurements were the Miller Thermal HV-2000 and Sulzer Metco DJ Hybrid. The particles used in the measurement were NiCr 80/20, with a size of +50-20µm and WC-CoCr with a size of +45-22µm. The results are not comparable, as measurements were done at different times, but results show the effect of the process parameters on temperature and velocity of the spray particles (81, 83, 93).

The nozzle of an HVOF gun has two tasks; (1) to accelerate particles to a high velocity, and (2) to heat them close to their melting point. Inside the nozzle, particles are heated by forced convection using hot gas, typically at a temperature of 1200-2200°C. As the spray particles have a wide size distribution (-50+5µm), spray particles do not reach a uniform temperature. Smaller particles are heated to higher temperatures than larger ones, with the results of the measurements shown in Figure 14 (83).

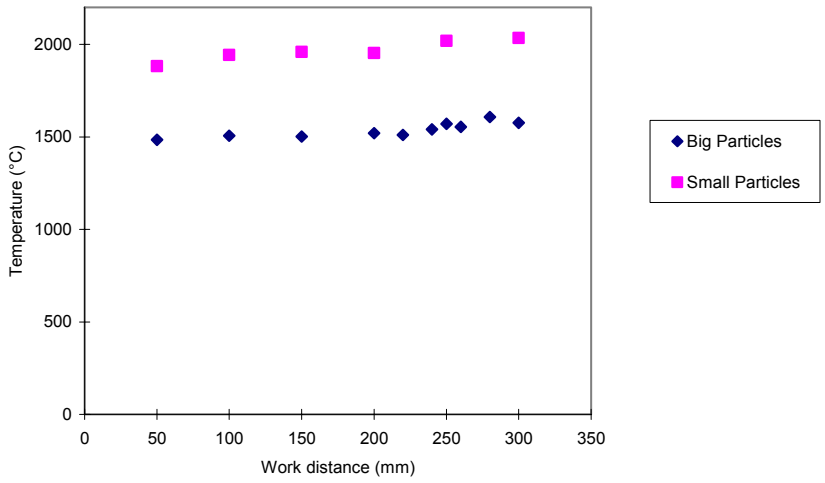

Figure 14. *Temperature of small and big NiCr80/20 spray particles. Temperature of the spray particles was measured as a function of work distance (DPV 2000™) (64).*

Most of the heat and acceleration is transferred to particles in the nozzle of the gun. The actual velocity of the particle is a function of gas velocity, gas density and the length of the nozzle (85). The drag force acting on the spray particles, Equation (30) and momentum flux Equation (31) shows that the velocity and density of the gas affect the particle velocity. Gas density can be controlled by adjusting the pressure of the combustion chamber. Gas density is increased only when the nozzle of HVOF is working in under-expanded mode (38, 39, 32, 84).

Particle temperature varies from 20 to 2200°C in the nozzle and shock diamonds (flame). The temperature of the spray particle is closely related to the type of HVOF gun, the fuel and the particle size used. Acetylene produces higher gas and particle temperatures, while kerosene produces the lowest. Properties of the spray particles such as their size, thermal conductivity, specific heat and porosity, all affect the temperature that is reached (38, 13, 88).

The specific surface area of the particle is considered to be an important parameter because the rate of oxidation is significantly affected by it. An increase in surface area accelerates the oxidation process. Fine spray powders have a high nominal surface area. Calculations using a particle size of 20-35 μm and a spray pass thickness of 0.05 mm, have shown that the HVOF sprayed powder has a surface area 500-600 times higher than a solid coating after a single spray pass.

The oxidation process is time-limited. The dwell time of a particle in the spray process affects the degree of oxidation. The dwell time of a spray particle in the nozzle of the gun is a function of several factors: gas velocity, density, length of the nozzle, and particle size and density. The typical dwell time for a spray particle with a mean velocity of 250 m/s in a 0.12 m long nozzle, has been estimated as <0.001 s (88, 85).

The effect of the length of the nozzle on particle temperature and gas velocity has not been the subject of much experimental work, but modelling has been carried out. A longer nozzle increases the velocity and temperature of the spray particle. This is due to particles dwelling longer in the hot flow (86, 87, 88, 89).

In the free air after the shock diamonds, the temperature of the particle remains relatively constant over a spray distance of 300 mm, but the flow properties change as air is mixed with the jet. When the spray particles leave the exit plane of the nozzle, the surface temperature of the spray particle remains nearly constant at 1200-2200°C and starts to fall only slowly. The temperature of the spray particle is related to size; the smaller the particle the hotter it is, while larger particles are cooler. Figure 14 shows the temperature change of the spray particle as a function of work distance, for small and large particles (72). The effect of the F/O ratio on the temperature of the spray particle is presented in Figure 17. The results show that the temperature of the particle increases when the F/O ratio is adjusted to the stoichiometric ratio (2.0). The experiment was done with hydrogen as the combustion gas. The results also show that the type of the nozzle (de Laval or barrel) has little effect on the temperature of the spray particles. This result will be used below, to explain the results of the degree of coating oxidation. Adjusting the F/O ratio to the stoichiometric ratio, increases the temperature of the flame and spray particles. The result of the increased process temperature will be acceleration of the oxidation rate.

Measurements have shown that there is no single particle temperature, but a temperature distribution among the spray particles (64, 90). The surface area of the spray powder remains

unchanged until the spray particles hit the surface which is to be coated. The dwell time in oxidising air is calculated as being less than 0.001 s. The velocity of the particle remains relatively constant at 400-700 m/s, when the work distance is 0.15-0.35 m (72).
The velocity of the spray particles is related to the size of the spray particles. Small particles reach higher velocities compared to larger ones. The results of the velocity measurements are presented in Figure 15 (81). Particle velocity and temperature are also related to the density of the particle. Particles which have a high nominal density (WC-Co17 14.5 g/cm^3), will exhibit higher velocities for longer, than particles which have a low nominal density (Al_2O_3 3.5 g/cm^3), although they will have lower maximum velocities than particles of low density.

When the spray particles hit the substrate, particle velocity decreases to zero and rapid quenching occurs below 300°C. When the spray particle stream solidifies and forms a coating, the calculated surface area of the spray particles, decreases to 300-500 th part of nominal surface area prior to spraying. The temperature of the spray particles has been reported to fall at a very high rate (10^7 C°/s). In most cases, the low temperature of the coating stops the oxidation process (91, 92). The build-up process of the coating slows the oxidation process, because the nominal surface area of the spray powder is reduced by a factor of 300-500 to 1. During the solidification of the spray particles, the hot tail flame of the HVOF gun still has an effect on the cooling rate of the spray particles. If the substrate speed (work speed) of the spray gun is low, the flame heats the surface and lowers the rate at which the coating cools. Calculations show that the dwell time of spray particles under the hot tail flame (<1000°C) ranges from 0.1 to 0.01 s, depending on the work speed.

The velocity of the particles does not increase greatly (10%), when the F/O ratio is adjusted to the stoichiometric ratio, as shown in Figure 16. The effect of the type of the nozzle is stronger; the de Laval nozzle produces 20% higher particle velocities than the barrel nozzle. The particle velocities follow the gas velocities, as presented in Figure 10.

The particles do not have a single velocity and the spray particles have a velocity distribution. Bigger particles fly slower than smaller ones. The velocity difference between “small” (30 µm) and “big” (45-30 µm) NiCr80/20 particles, sprayed with Jet-Kote is presented in Figure 15.

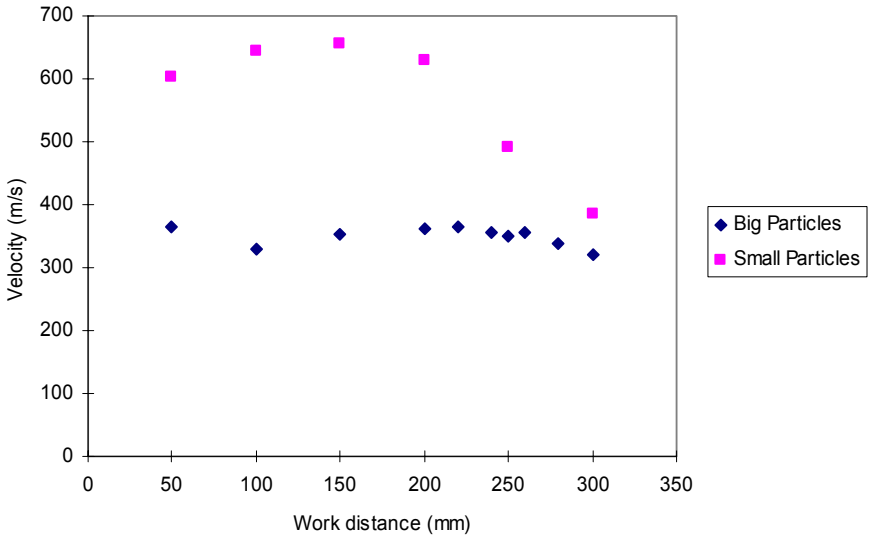

Figure 15. *Velocity of small and big NiCr80/20 spray particles. (DPV 2000™). The particle velocity was measured as a function of work distance (64).*

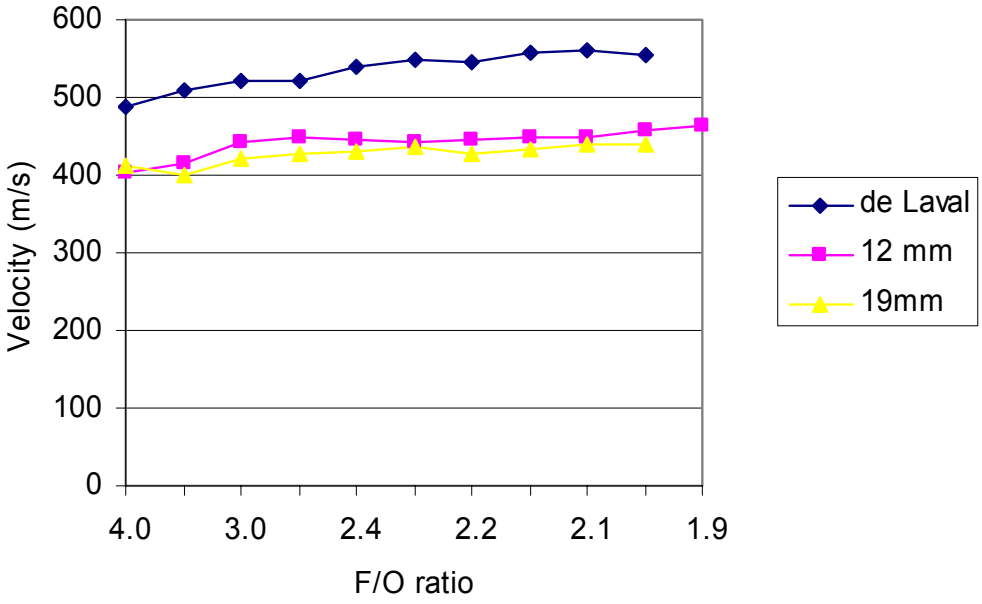

Figure 16. *Velocity profile of WC-CoCr particle as a function of F/O ratio and the type of the nozzle (SprayWatch™). The results of HV-2000 gun with the 12/19 mm barrel and de Laval nozzle (93).*

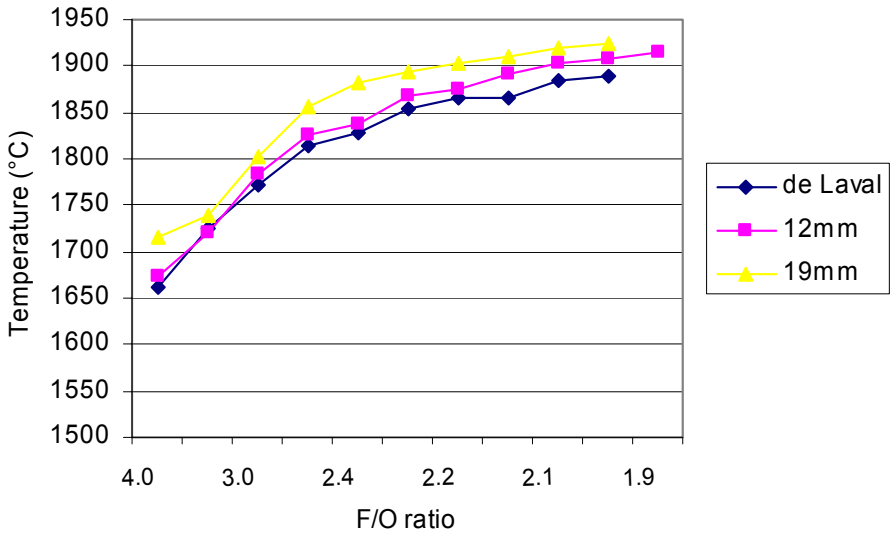

***Figure 17**. Temperature profile of WC–CoCr particles as a function of F/O ratio and the type of the nozzle (SprayWatch™). The result of HV-2000 gun with the 12/19 mm barrel and de Laval nozzle (93)*

4.7 Factors affecting gas and spray particle behaviour

In the previous section, the spray parameters of the HVOF gun were discussed in terms of physics and chemistry, gas temperature, density, velocity and gas concentration. In spraying job-shops, coating parameter tables, and in many scientific papers, the spray variables are discussed with respect to gas flow, feeding, or pressure of the hose in the HVOF spray system. The input variables, pressure and flow, are easier to measure than the physical properties of the hot process, such as gas temperature, gas velocity and oxygen partial pressure (94, 95, 96). In spite of spray parameters being easy to measure, these measurements do not allow us to understand and control what happens to the spray powder, i.e. degree of melting, oxidation, etc. This is because the spray parameters are not directly linked to the behaviour of the melting of the metal, or the gas temperature.

It is also difficult to compare the oxidation tendency of particles of different HVOF spray guns, such as the JP-5000, HV-2000, Sulzer Metco DJ-Hybrid, Jet-Kote and OSY CJS, because they all have different spray parameters.

Modelling the spray process itself, in order to predict the effect of each process parameter on the temperature and velocity of spray particles, is very complex. Prediction of the degree of oxidation of spray particles is even more difficult because it is the sum of temperature, environmental conditions, time and material factors. In spite of these difficulties, an understanding of the effects of parameter changes on temperature and time history of the spray particle, can help us to find ways of controlling the degree of oxidation. In Table 4, the summary of the properties of the flame and the spray particle in HVOF spraying is presented.

Table ***5*** shows the calculated and measured energy balance of an HVOF gun. The results are based on the gas and particle velocity and temperature measurements of the Miller HV-2000 and Jet-Kote HVOF guns (57, 64, 68, 72, 82). The HVOF gun combusts H_2 and O_2 at a power level of 107 kW. The feed rate of the spray powder is 60g/min of the Fe/Cr/Ni type of

powder. The table shows the energy distribution in the HVOF process. Only a small amount of thermal and kinetic energy (less than 1.5%) is transferred to the spray particles. This energy transferred, is divided into kinetic energy (< 0.3 %) and heat capacity (<1 %). Energy distribution of the gas and the spray particles varies according to the velocity of the gas and spray particles.

Table 4. *Summary of the properties of the flame and the spray particles in HVOF spraying.*

Process area	Flame temperature (°C)	Gas velocity (m/s)	Particle residence time (s)	Particle velocity (m/s)	Particle temperature (°C)	Oxygen partial pressure (O_2 bar)
HVOF gun	2000-3000	100-2500	0.001-0.002	0-750	0-2200	$10^{-20..-10}$
Plume	100-2500	300-2100	0.001-0.002	0-750	1200-2200	10^{-20}-0.2
Substrate	100-500	100-300	0.01-2	0	150-500	0.01-0.2

Table 5. *Energy balance of HVOF gun in hydrogen combustion with oxygen; percentual distribution*

Combustion energy (%)	100
Cooling water loss	10-45
Gas velocity (kinetic energy)	8-17
Kinetic energy of spray particles	0.1-0.3
Heat content of spray particles at T=1700 ºC	1
Heat content of gas	50-80

5. EXPERIMENTAL INVESTIGATIONS

The aim of the experimental study was to investigate the following aspects:

- Effect of spray parameters on the oxidation rate of the coating,
- Effect of spray parameters on microstructure changes,
- Features related to oxidation of the coating, selective oxidation, and formation of gaseous, liquid and solid oxides.

The spray parameters used in the experiments were:

- F/O ratio, F/O,
- Work speed, the surface velocity of the item to be coated,
- Work distance, distance between the gun and the item to be coated.

5.1 Experimental set-up

The Jet-Kote and Miller Thermal HV-2000 HVOF spray guns were used in the coating experiments (Appendix A). The combustion of fuel with oxygen took place in a separate water-cooled combustion chamber and the hot combustion gases were conducted into a water-cooled copper barrel type nozzle, with a diameter of 8 mm and length of 120 mm. The spray powder was injected axially into the barrel nozzle, where hot combustion gases heated the powder to high temperature and projected it at high velocity onto the substrate. The spray gun was attached to a manipulator, which enabled it to move in an vertical and horisontal direction. The powder hopper was a Miller Thermal model 1260, and operated on a volumetric feed principle.

The combustion gases used were hydrogen and oxygen. The hydrogen flow rate varied over the range of 500-700 slm (standard litters per minute) and the oxygen flow rate varied over the range of 150-400 slm, depending on the actual experiment being carried out. The F/O ratio volumetric ratio varied between 4:1 and 1.5:1. The stoichiometric ratio is defined as F/O = 2.0 with H_2/O_2. The gas used to feed the spray powder was argon. Work distance varied from 50 to 350 mm. Details of the Jet-Kote and HV-2000 variables can be found in Table 7 and Table 8.

The spray powders used in the experiments were gas-atomised Anval NiCr80/20, (Figure 18), sintered and crushed Alloys International AI-1173, WC-Co17, (Figure 20) and sintered and crushed Alloys International AI-1005 Cr_3C_2-NiCr75/25, (Figure 19). The powders were of typical commercial HVOF quality, with particle sizes in the range of +15- 45 μm. The details of the powders are shown in Table 6. The WC-Co17 and Cr_3C_2-NiCr75/25 powders were selected because they have been widely studied (17, 19, 20, 21, 22, 23, 24, 25, 26, 27), and therefore it was possible to compare the results obtained on carbon loss and powder oxidation. Furthermore, the NiCr80/20 alloy is widely used and obtaining information about its oxidation behaviour in coatings is important. Powders were sprayed onto mild steel coupons of 40x120x2 mm in size. The coupons were used in optical microscopy studies, and carbon and oxygen content analyses.

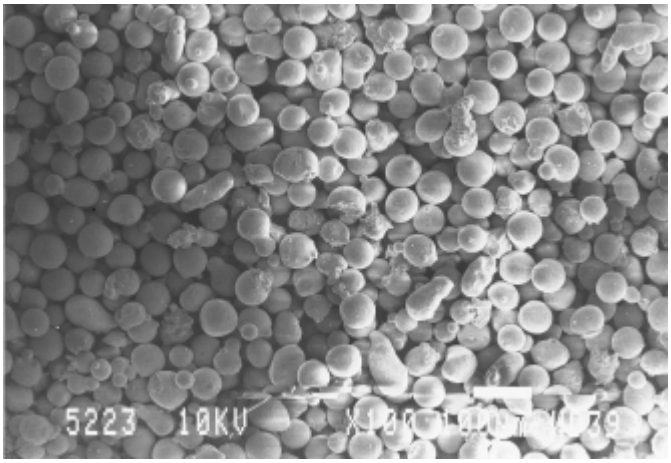

Figure 18. *SEM picture of gas atomised NiCr80/20 powder (100x).*

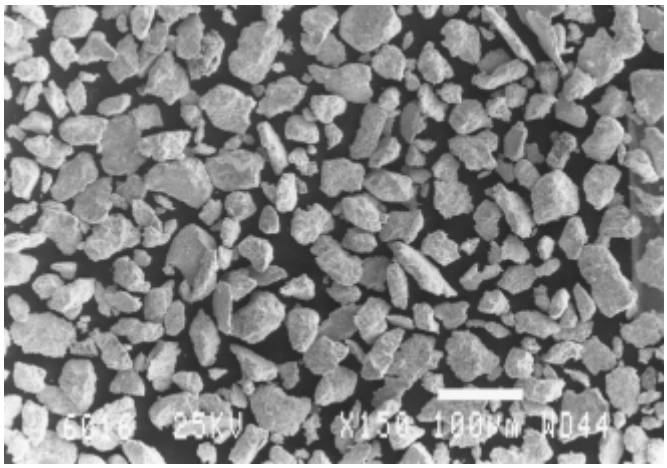

Figure 19. *SEM picture of sintered and crushed* Cr_3C_2*-NiCr75/25 powder (150 x).*

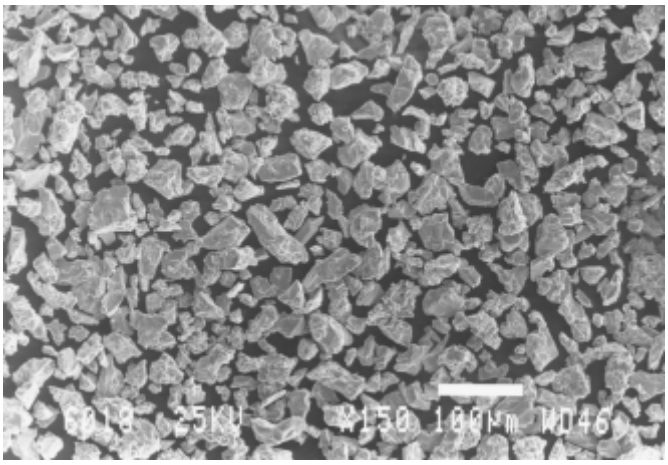

Figure 20. *SEM picture of sintered and crushed WC-Co17 powder (150x).*

***Table 6**. Spray powder characteristics.*

Material	Type	Size +/-µm	Composition wt%
WC-Co 17	Sintered and crushed Praxair AI-1173	+15- 45 µm	W 77.5, C 5.5, Co 17
NiCr 80/20	Gas atomized Anval NiCr80/20	+22- 45 µm	Ni80, Cr20
Cr_3C_2-NiCr75/25	Sintered and crushed PraxairAI-1005	+22 - 45 µm	Cr 70,C 10, Ni20

***Table 7**. Spray parameter variables of Jet-Kote HVOF gun.*

Gas flow rates for H_2, O_2 and Ar, slm	700/500-200/30
F/O ratio	1.5 to 4
Work distance, mm	50, 200, 350
Substrate work speed, m/s	0.03, 0.3, 3, 30
Powder feed, g/min	35
Coating surface temperature, °C	100-300
Coating thickness, µm	150-250

***Table 8**. Spray parameter variables of HV-2000 HVOF gun.*

Gas flow rates for H_2, O_2 and Ar, slm	600/300 -150/25
F/O ratio	2.0 to 4.13
Work distance, mm	250
Substrate work speed, m/s	0.3
Powder feed, g/min	30
Coating surface temperature, °C	100-300
Coating thickness, µm	150-250

The sprayed coatings were cross-sectioned, polished and examined using an optical microscope (OM) or scanning electron microscope (SEM) with a secondary electron image (SEI) and a back scattering image (BEI). The magnification used when examining the cross-sections varied from 200x to 1000x. Examination of the microstructure with the OM used a magnification of 200x. Cross-sectioned WC-Co17 coating samples were etched with Murakami's reagent (26) to show phase structure in the coating in the HV-2000 experiment.

The degree of oxidation, oxygen concentration (O_2 wt %) in NiCr80/20 coatings, was analysed with the combustion method, using the Leco TC-136 system. Carbon loss (C wt %) in WC-Co17 coatings was analysed with the combustion method using the Leco CS-44LS system. The coatings were peeled off the spray coupons, and then milled and analysed.

Changes in alloy composition were analysed using a Jeol JSM 6400 scanning electron microscope SEM, equipped with an energy dispersive X-ray spectrometer, EDS. The sample material analysed was micron-size spray dust (<1 µm) taken from around the sprayed sample. The composition of the micron-sized spray dust was compared to the powder prior to spraying. The powders analysed were WC-Co17, NiCr80/20 and Cr_3C_2-NiCr75/25.

X-ray diffraction (XRD) analysis was used to identify the phase structure in WC-Co17 coatings. Monochromatic CuK_α radiation was generated by a Siemens D-500 diffractometer with a nickel filter and a secondary crystal monochromator. The diffractometer was operated at 40 kV and 30 mA. In the WC-Co17 coatings, WC, W_2C, eta, nano or amorphous phases were identified and a rough estimate was obtained of the quantity of the phases present.

5.2 Experimental results

In this section, the experimental results are shown: concerning the changes of chemical composition of powders in the spraying process. The degree of oxidation of WC-Co17 and NiCr80/20 coatings, and microstructural changes of WC-Co17 and NiCr80/20 coatings as a function of F/O ratio, work speed and work distance.

5.2.1 Change of composition of powders in HVOF spraying

Generally the composition of powders changes during spraying due to oxidation. Particularly strong deviations are observed if volatile compounds, (oxides) are formed. Oxide volatility is possible with the WC-Co17, Cr_3C_2-NiCr75/25 and NiCr80/20 spray powders. The volatile oxides expected were WO_3(g) and CrO_3(g) at high temperatures (>800°C), while CO(g) is always in gaseous form. Oxide volatility was studied by determining the depletion of the alloying elements in the sprayed powder. The original concentration of the spray powder was compared to its concentration in the sprayed powder. The procedure used was as follows. If a metal oxide is volatile, gaseous oxide will evaporate from the spray powder during the spraying process, in the nozzle of HVOF gun and in the plume. The concentration of the volatile component in the sprayed powder will therefore decrease. The sample used to establish volatile oxidation was the spray dust around the sprayed coupons and on the coating. The spray dust, with a size of <1μm was generated from the original large spray powder (+22-45μm). The round dust was expected to form from molten spray particles. The high velocity difference between spray particles and gas stream cause fragmentised molten spray particles. As an oxidation sample, the spray dust was preferred to the coating sample because the spray dust was more reactive than the coating and the spray powder. Higher element concentration makes SEM-EDS analysis easier. In sprayed NiCr80/20 coatings, the oxidation level varied from 1 to 4 wt %. The loss of alloying elements in the coating due to oxide volatility would probably be less than in the oxidised spray dust. The high surface area of the spray dust and the small particle size, resulted in high temperature and a higher nominal surface area of the particle, with a consequent high reaction rate during the spraying process, accelerating the oxidation rate and the evaporation of volatile species from the spray powder. The small spray dust, therefore, exhibited more clearly the effects of volatility, than the sprayed coating. The high degree of oxidation of the spray dust makes SEM-EDS analyses easier, because the elemental composition changes are higher in the dust than in the coating.

Element changes in thermal spraying process in WC-Co17, Cr_3C_2-NiCr75/25 and NiCr80/20 spray powders were tested. Composition of the powder, before and after spraying, are shown in Table 9.

***Table 9**. SEM-EDS analyses of the spray powders before and after spraying (nano-sized dust), WC-Co17, Cr_3C_2-NiCr75/25 and NiCr80/20, N=100 particles. Carbon was analysed with Leco CS-444 LS.*

Spray material	Cr wt %	Ni wt %	C wt %
Cr_3C_2-NiCr75/25, before spraying >20 µm	71.0	19.3	9.7
Cr_3C_2-NiCr75/25 dust, after spraying 0.1µm	75.6↑	16.9↓	7 (approximated)
NiCr80/20, before spraying >20 µm	23.9	73.1	None Tot (97%)
NiCr80/20 dust, after spraying, <0.1 µm	26.6 ↑	70.6 ↓	None Tot (97.2%)
	W wt %	Co wt %	C wt %
WC-Co17 before spraying, >11 µm	84.6	14.1	4.3 (Leco) tot (103%)
WC-Co17 dust, after spraying <0.1 µm	84.3	14.3	3.5 (Leco) from coating; tot (103%)

Table 9 shows the chemical composition of Cr_3C_2-NiCr75/25 powder before and after spraying. The nano-scale spray dust collected on the substrate after spraying, contains more Cr (75.6 wt %) than the original spray powder (71.0 wt %). The change of chromium is Δ = +4.6 wt %. On the other hand, the Ni content decreased from 19.3 to 16.9 wt %. The change of nickel was Δ = -2.4 wt %. Carbon loss was not measured, but it was estimated to be 7 wt %.

In the case of the WC-Co17 coating system, the ratio of W to Co remains constant and this indicates that no volatilization of WO_3(g) occurs. Unfortunately, it proved to be impossible to analyse carbon depletion in the dust by EDS. Carbon loss of the spray dust was impossible to perform, because only 20 mg of the powder was able to be collected. Leco analysis needs at least 2 g of sample material. Carbon loss during the spraying process was 0.8 wt % in the coating (Leco analysis).

In the experiments of NiCr80/20 coating, chromium increased to 26.6 wt %. Chromium increased with Δ = +2.7 wt % and Ni decreased with Δ = -2.5 wt % showing that chromium was vaporised and enriched in the dust.

5.2.2 Effect of spray parameters on degree of decarburization and oxidation

Aim of this section was to study the effects of the spray parameters on:

- Degree of decarburization of WC-Co17 powder
- Changes of microstructure of WC-Co17 powder
- Degree of oxidation of NiCr 80/20 powder
- Changes of microstructure of NiCr 80/20 powder.

The spray parameter variables were F/O ratio, work distance, work speed and combustion chamber pressure.

5.2.2.1 Effect of spray parameters on decarburization of WC-Co17 coating

The main objective of this part of the study was to measure the carbon loss of WC-Co17 coating during spraying. F/O ratio, work distance and work speed were used as spray parameters. Chamber pressure and F/O ratio were used as spray parameters with the HV-2000 gun in order to see the carbon loss during spraying. The WC-Co17 coating was deposited with a Jet-Kote HVOF gun (Figure 21) and a Miller HV 2000 HVOF gun (Figure 23). The effects of F/O ratio are presented in Figure 21. The spray gun used was a Jet-Kote and the spray parameter details can be seen in Table 7. The figures show a decrease in carbon content, when the F/O ratio was adjusted from 1.25 to 3.75. Other spray parameters were held constant: the work speed was 3 m/s and the work distance, 300 mm.

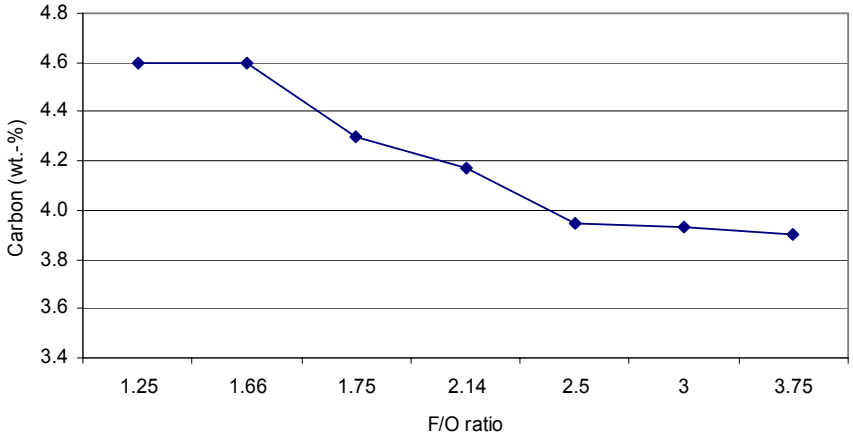

Figure 21. *Carbon depletion in WC-Co17 coating as a function of F/O ratio. Work speed 3 m/s and spray distance 300 mm. Carbon content of WC-Co17 coating decreases when F/O ratio becomes richer.*

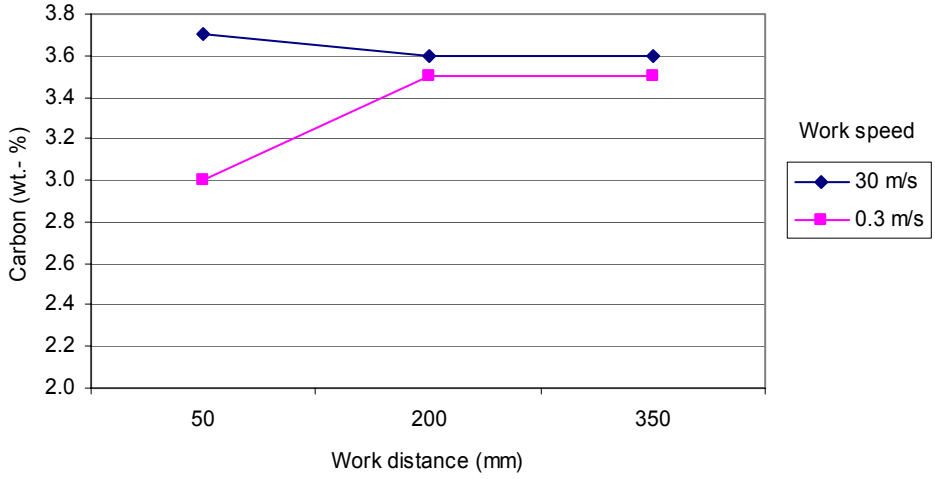

Figure 22. *Carbon depletion in WC-Co17 coating as a function of the work distance and the work speed. F/O ratio was held constant.*

There are two other spray parameters of interest in decarburization. The effect of the work distance and the work speed is shown in Figure 22. The results show that decarburization is independent of the work distance, if the work speed is high (30 m/s). The degree of decarburization increases by 22 %, if work speed is decreased to 0.3 m/s at short work distance (50 mm) and reaches the same level at the high work distance (200-350 mm).

5.2.2.2 Effect of spray parameters on the microstructural changes and decarburization of carbide coatings

The microstructures were examined with OM and SEM with SE and BE mode. Most of the findings were already well known from the literature, but the effect of the F/O ratio was not identified on these features on the microstructure. The coatings were sprayed with the HV-2000 and Jet-Kote spray guns, Table 7. Table 10 shows the F/O parameters and degree of decarburization of the WC-Co17 coating.

The effects of the spray parameters on the decarburization of WC-Co17 powder were studied in coating microstructures, by using different HVOF gas velocities (chamber pressures 2 and 3.5 bar) 1100/1600 m/s, and a variety of F/O ratios. The coatings were sprayed with a Miller Thermal HV-2000 HVOF spray gun using hydrogen and oxygen as combusting gases, Table 8.

Figure 23 (a-h) and Figure 24 (a-g) show the results of the degree of decarburization of the WC-Co17 coating. Under each microstructure picture, the F/O ratio is given and on the right side, the respective X-ray diffraction pattern. The results were obtained with microstructural studies and XRD-analyses. Microstructure was studied by etching the coatings with Murakami's reagent, in order to highlight the decarburized areas of the coatings. The degree of decarburization was seen as an increase of the black area in the WC-Co17 coating microstructures (16). XRD-patterns show also the degree of decarburization in WC-Co17 coatings. The degree of decarburization can be seen as an increase of the height of the curve in 2θ angle (~40°), called "amorphous hill hump". The area of "amorphous hill hump" is indicated in the XRD-spectrum with an arrow, ↓.The WC-Co17 coating results were achieved using a HVOF gun with F/O ratios of 2.0-4.13, chamber pressures of 2 and 3.5 bar, and gas velocities of 1100 m/s and 1560 m/s respectively. The lower gas velocity was obtained with a barrel nozzle (chamber pressure 2.0 bar) and the higher gas velocity was obtained with a de Laval nozzle (chamber pressure 3.5 bar). The coating experiments showed that the F/O ratio (flame temperature) had a strong effect on the rate of decarburization of the coating. A hotter stoichiometric flame (F/O ratio = 2.0) seemed to produce the maximal decarburization. Increasing the chamber pressure vs. gas velocity decreased the degree of decarburization. A low HVOF gas velocity (1100 m/s) produced a high degree of decarburization, i.e. multiple black areas in the coating microstructure. In Figure 23 (a) non-decarburized sintered WC-Co17 powder and its respective XRD-patterns can be seen in Figure 23 and Figure 24, the effect of decarburization can be seen. Decarburization proceeds from the surface to the core of the spray particles. The light lamellar spray particles transform black. The most heavily decarburized surface of the spray particles was etched away. The degree of decarburization increased when the F/O ratio was adjusted from 4.13 to a stoichiometric ratio of 2.0. When round particles impacted on the substrate, they deformed to flat lamellas. High combustion chamber pressure decreases the degree of decarburization compared to a high flame speed. XRD-patterns and microstructures show semi-qualitative results of the coating degree of decarburization. Etching makes the boundaries of the deformed spray particles visible.

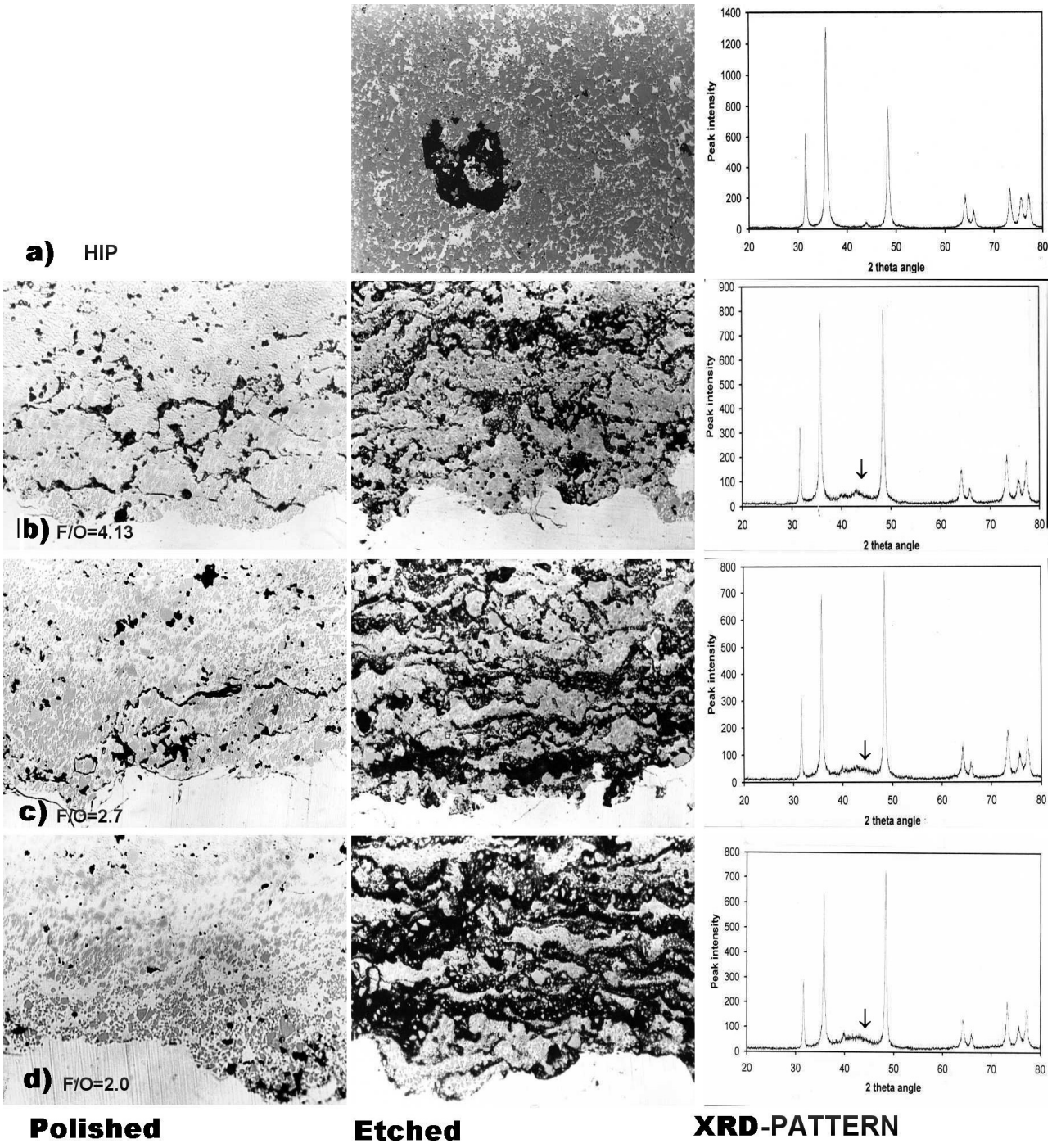

Figure 23. *Rows (b-d). Effect of F/O ratio on degree of decarburisation of WC-Co17 coating. Combustion pressure 3.5 bar with a 19 mm de Laval nozzle. Polished and etched microstructures, and XRD patterns of the coatings. On the row a) microstructure and XRD pattern of HIP sintered spray powder WC-Co17 are shown. Magnification 500x.*

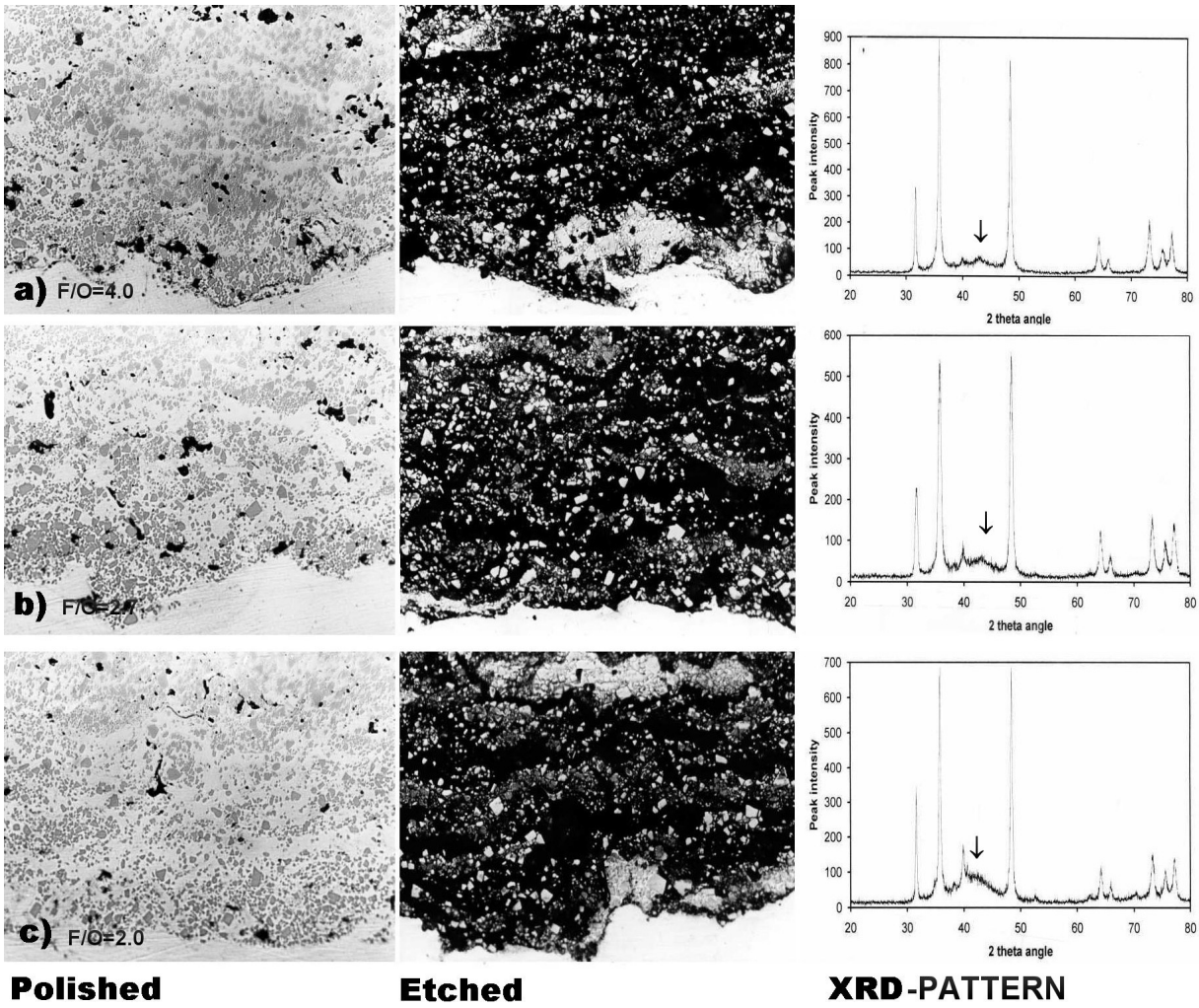

Figure 24. *Rows (a-c). Effect of F/O ratio on the microstructure and degree of decarburization of WC-Co17. Combustion pressure 2.0 bar with a 19 mm barrel nozzle. Comparison of polished and etched microstructures. Respective XRD images are shown on the right. Magnification 500x.*

The effects of decarburization on WC-Co17 coating were tested using an HV-2000 HVOF gun. The aim of the experiments was either to show, or to propose, an explanation for the traces of oxidation/decarburization in the microstructure of the coating. The original non-decarburized WC-Co17 structure is dense and contains no W_2C or nanophase, as can be seen in Figure 23(a). The following structures were found by SEM-BEI image using a high magnification (>5000x), as shown in Figure 25: angular and prismatic non-decarburized WC grains, 0.5-5 μm in diameter, are embedded in the Co matrix. Angular WC grains are decarburized "round" to WC/W_2C carbides. Some of the round decarburized WC grains are surrounded by a round white shell, which is expected to be a decarburized layer of W_2C or W-rich dendrites around the original WC grains. Round black or elliptical holes (<1 μm in diameter) of the gas bubbles can be seen, and these are expected to form due to the degassing-off of $2WC + ½O_2(g) = W_2C + CO(g)$ in the decarburization process. The grey phases are regarded as a matrix for the W_2C and WC grains, their shape being flat and wavy, and also surrounding the spray particles. The dark grey Co phase contains no decarburized sharp prismatic WC grains. The very white small details are thought to be precipitates of W, the black gas bubble around is expected to be CO(g) from $W_2C + ½O_2(g) = 2W + CO(g)$ reaction.

The following details have been observed in the microstructure:

1. Grey angular and prismatic shapes were recognised as WC grains,
2. White and grey round shapes are W_2C + WC grains,
3. Round and elliptical shapes are gas bubbles, assumedly CO
4. Dark black binder phase is Co,
5. Grey phase is nano crystal phase WCCo(l),
6. A lamella interface between two spray particles,
7. White image in the black gas bubble is metallic W.

In the BEI-images, the white colour indicates the heavier phase (compounds) W and WC/W_2C while the grey colour indicates the lighter phases compounds, such as WC and $Co_xC_yW_z$ or nano crystal. Dark grey indicates Co and black is a gas hole.

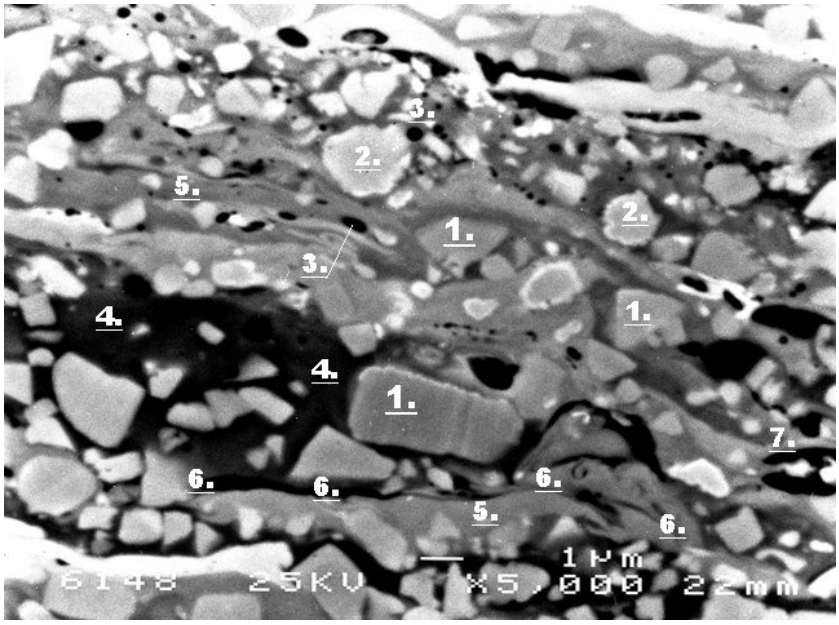

Figure 25. *SEM-BEI image of decarburized WC-Co17 coating.*

Figure 26, the effect of F/O ratio on the WC-Co17 coating microstructure is shown. The stoichiometric (F/O = 2.0) flame is hot, which results in hot spray particles. The sprayed coatings were examined simultaneously with the OM and SEM. The spray parameters and degree of decarburization can be seen in Table 10.

Table 10. *Effect of F/O ratio on the degree of decarburisation of WC-Co17 and related coating microstructures.*

Sample	A	B	C	D
Carbon content wt.-%	4.5	4.4	3.8	3.7
F/O ratio	4.0	3.2	2.7	2.0

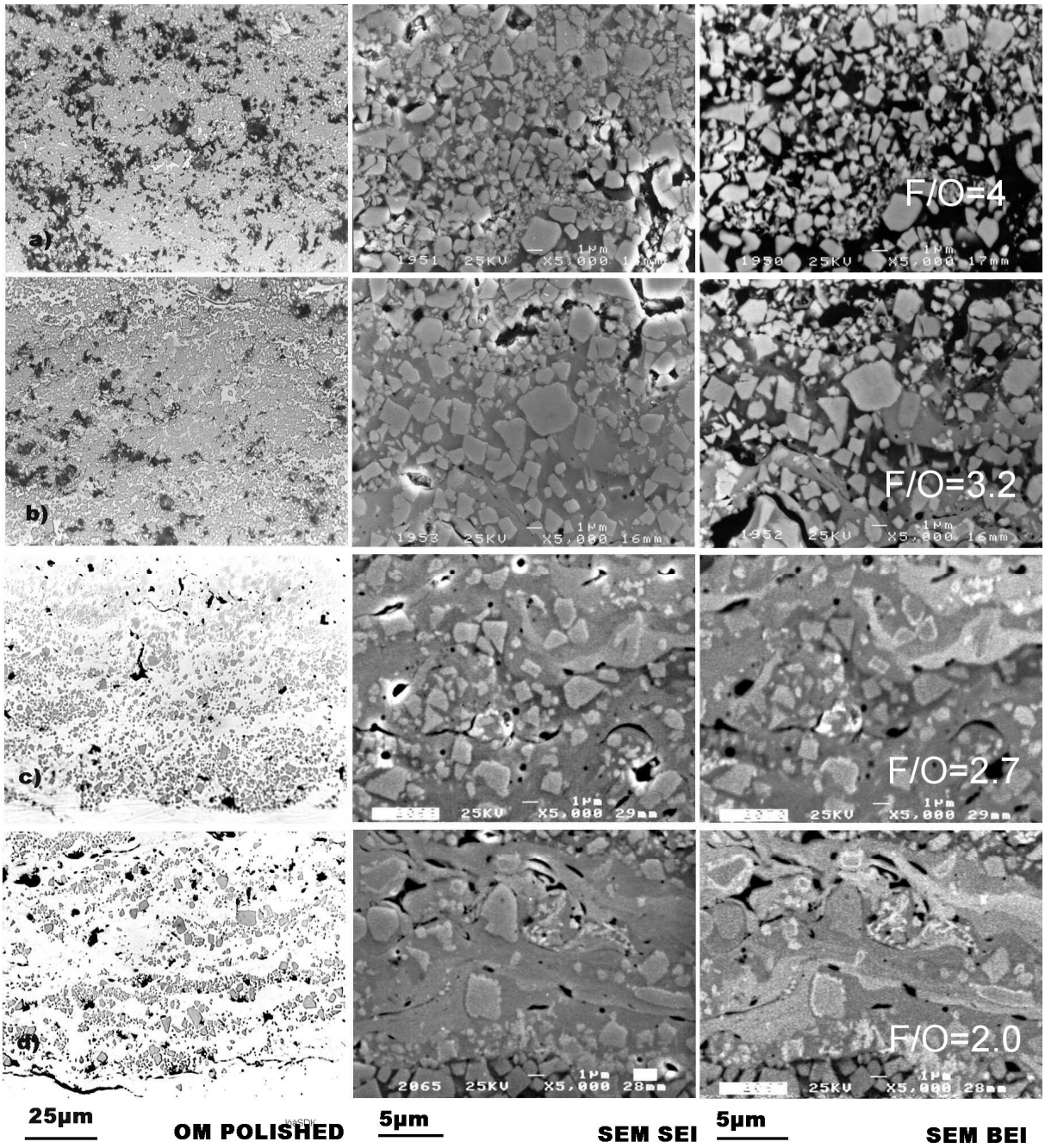

***Figure 26**. Effect of F/O ratio on WC-Co17 coating microstructure sprayed by Jet-Kote HVOF gun: OM, SEM-SEI, SEM-BEI images. F/O ratio is 4, 3.2, 2.7 and 2.0 (stoichiometric) from the top to the bottom.*

The following features were found with OM in the microstructures of WC-Co17 coating, when the F/O ratio was changed from 4 to stoichiometric. The area of WC carbides decreases, "Co-lakes" increase (lake = Co binder phase), lamellar structure appears, no oxide layer can be found around the spray particles and the porosity decreases. The results are shown in Figure 26 on the right side of the figure in the section of "OM polished". Etching of the coating with Murakami reagent reveals the structure of the splats, as shown in Figure 23. A spray particle that deforms upon impact on the substrate, is called a splat. It consists of the decarburized core (black area) and the non decarburized nucleus (grey/white area). The round spray particle has deformed into the flat splat. The coating consists of layers of splats. The cross-section of the coating is lamellar, varying between black decarburized areas, and white

and grey non-decarburized areas. When the F/O ratio is adjusted to stoichiometric, the decarburized black area is increased. Stoichiometric flame is hot (F/O = 2.0), producing the hot spray particles and remarkably decarburized microstructure (Figure 26. SEM-SEI and SEM-BEI)**.** With stoichiometric combustion the spray particles adjusted hot, the quantity of WC carbides is decreased, Co-lakes and lamellar white/grey structures appear, while porosity is decreased. Round CO gas bubbles can be found as black holes (<1 μm) between the lamellas. Small elliptical, and flattened bigger, gas bubbles are produced by stoichiometric combustion (hot flame). Increased oxidation of WC grains is seen as a "white rim" around the WC particles and as nucleation of W or W_2C on the WC grains. Bigger prismatic and angular WC particles are transformed to round ones. The corners of WC grains are dissolved to cobalt or liquid $W_xC_yCo_z$(l) phase. Small WC particles are dissolved into liquid $W_xC_yCo_z$(l) matrix. The dissolution of tungsten and carbon can be seen as white and grey shades in Co-lakes and around the boundaries of the splats. The white tungsten inclusions can be found in the splat boundaries and in the gas pores. SEM pictures clearly show the effect of F/O ratio on the microstructure. The WC grains disappear or dissolve into the matrix, when the temperature of the particles is increased. The wavy structure of the matrix $W_xC_yCo_z$ is increased.

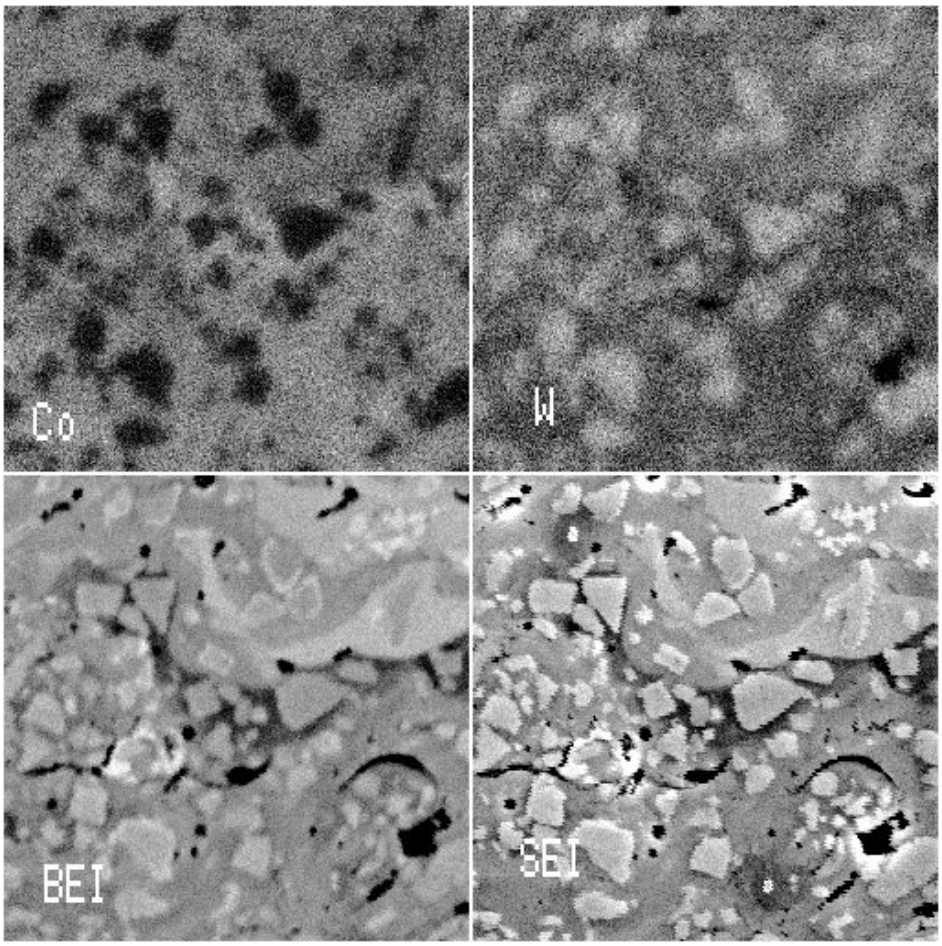

Figure 27*. Element mapping of WC-Co17 coating for Co and W (top) and corresponding BEI and SEI images (bottom).*

The aim of the experiment was to show how the elements diffuse in the liquid spray particles. The sample was taken from the WC-Co17 coating, which was sprayed with a Jet-Kote spray gun. The results can be seen in Figure 27. SEM-SEI and -BEI figures were prepared of the WC-Co17 sample. Element mapping of W and Co are seen in the corresponding area. In the (Co and W) figures, WC grains can be seen as dark angular blocks surrounded by Co matrix.

W appears to be diffuse and dissolved evenly around the whole structure of the Co matrix. On the other hand, the solubility of Co in the tungsten-rich phase cannot be detected, due to the very high melting point of WC. Dissolution of carbon cannot be seen in Figure 25 and Figure 26, but it is assumed that carbon is also dissolved into the matrix, similar to W.

5.2.2.3 Oxidation of NiCr80/20 coating

In this section, the oxidation phenomenon of NiCr80/20 coating at the HVOF spray process area is examined. Three types of spray parameters were tested: work distance, work speed and F/O ratio, Table 7. The coatings were sprayed with a Jet-Kote HVOF gun and the powder used was gas-atomised NiCr80/20 powder. Nominal size was – 45+22 µm. The size and shape of the spray powder was shown in Figure 18. Hydrogen and oxygen were used as combustion gases.

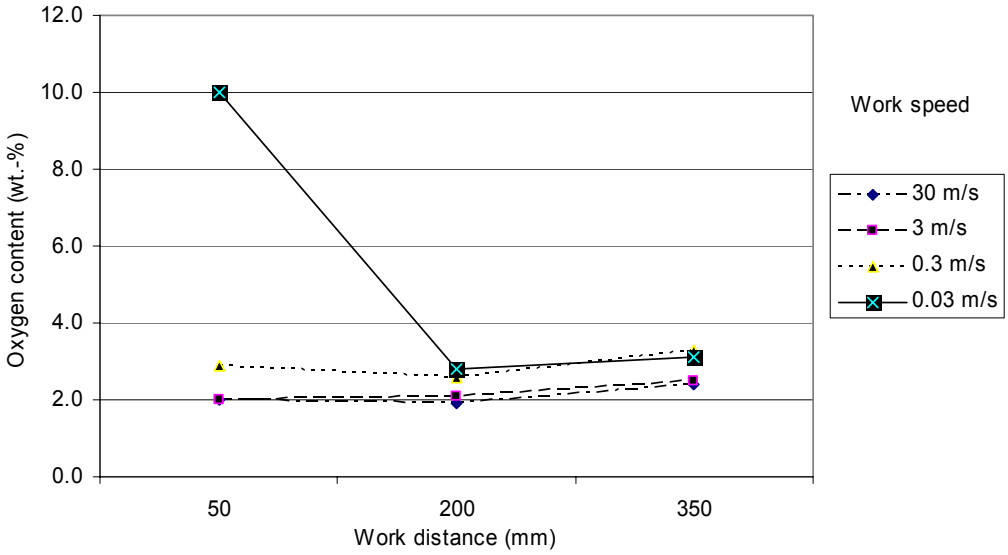

Figure 28. *The effect of work distance and work speed on the oxidation of NiCr 80/20 coating.*

In the first experiment was to tested the effect of work distance and work speed on the oxidation of the spray powder. The work distance was 50, 250 and 350 mm while the work speed was 30, 3, 0.3 and 0.03 m/s respectively. The F/O ratio was kept constant at F/O = 2.7. Figure 28 presents the results of the degree of oxidation. It can be seen that the work distance and the work speed have little effect on the degree of oxidation. The most oxidised sample (10 wt %) was sprayed using a low work speed and a short work distance (0.03 m/s and 50 mm). Oxygen level varied from 2.0 to 3 wt % in the other samples. The samples were cross-sectioned and the microstructures are shown in Figure 30 and Figure 31.

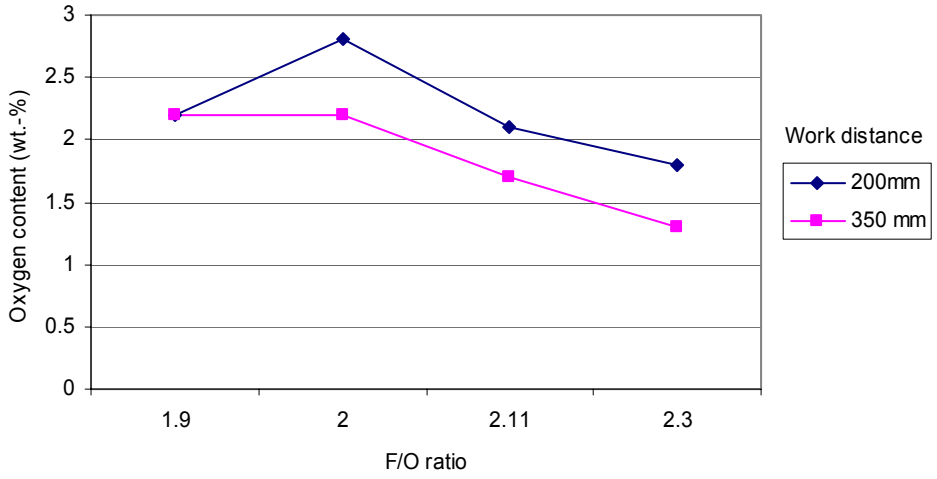

***Figure 29**. The effect of F/O ratio and work distance on oxygen content of NiCr 80/20 coating.*

Figure 29 shows the results of the experiments with varied F/O ratio and the effect of the work distance. The results showed that increasing the F/O ratio from 1.9 to 2.3 (colder flame) decreases the degree of oxidation, while increasing the work distance from 200 to 350 mm decreases the oxygen content of NiCr80/20 coating. The work speed was 3 m/s. The level of the oxygen content varied from 2.8 to 1.3 wt %.

5.2.2.4 Microstructural changes of NiCr80/20 coating

In this section, the eventual effects of the microstructure of NiCr80/20 coating are discussed. The aim of the work was to observe changes in the microstructure, when oxygen content and degree of deformation in NiCr80/20 coatings were changed by varying the substrate work speed and work distances. HVOF gun combustion gas parameters, F/O ratio and gas flow rate were held constant, Table 7.

In NiCr80/20 coating, the work speeds of the substrate were 0.003, 0.3, 3 and 30 m/s while the work distances were 50, 200 and 350 mm. Both spray parameters affect the quenching rate of the spray particle and flight dwell time. During each experiment, the flow rate of the combustion gas, i.e. the gas temperature and velocity were held constant. This was expected to result in a constant temperature and velocity of the spray particles. Detailed parameters for these experiments were given in Table 7. Cross sections of microstructures of NiCr80/20 coatings can be seen in Figure 30, (a-f) and Figure 31, (a-f). In the microstructures, oxide formation is seen as thin, black and grey layers, surrounding the spray particles. Around the deformed spray particles, the oxide forms a wavy shape. The original round form of the oxidised spray particles disappears when it impacts on the substrate. Figure 18 shows the SEM picture of the original round NiCr80/20 powder. The degree of deformation of the spray particles were not the highest obtainable in the HVOF spray process, due to the relatively low temperature of the spray particles.

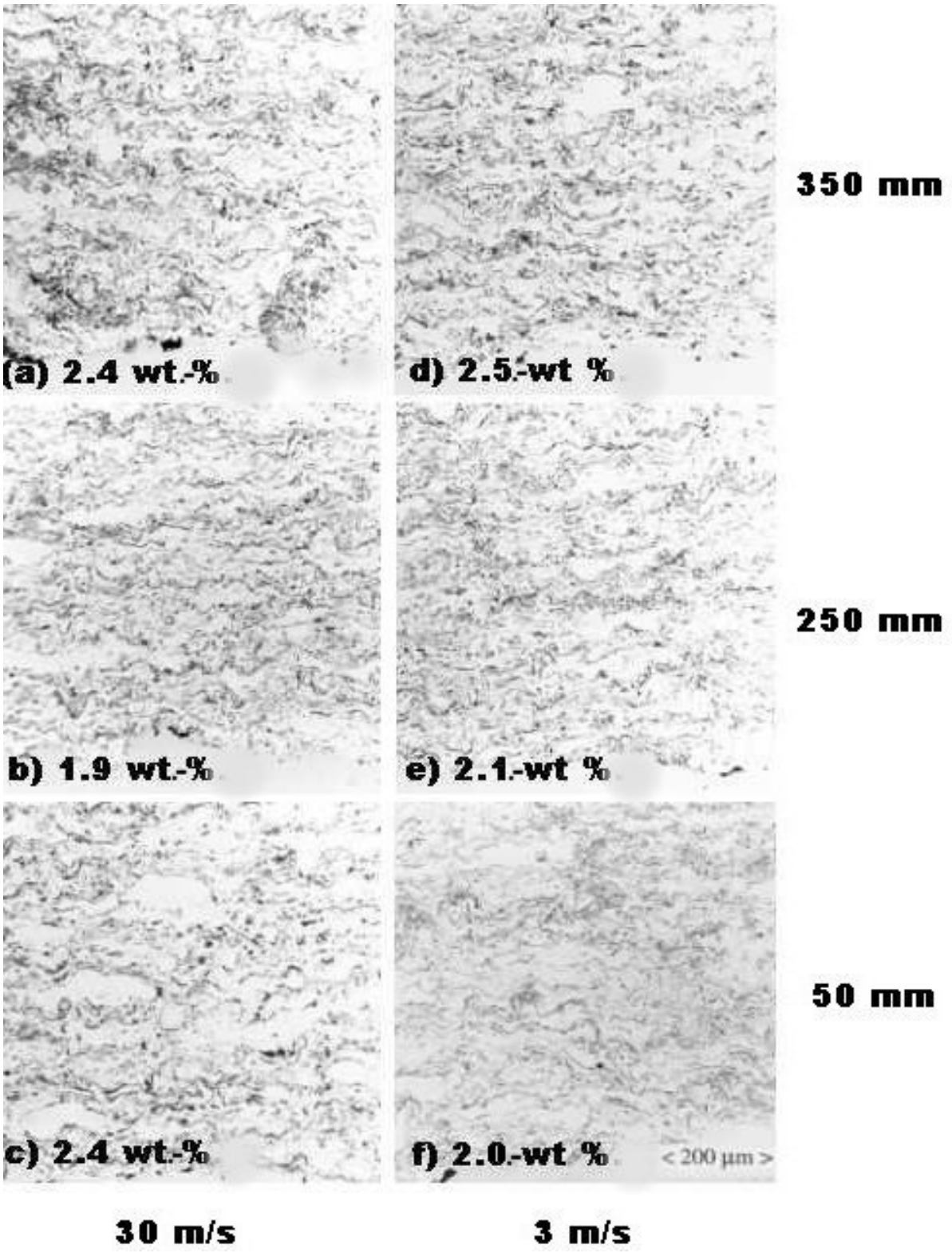

***Figure 30**. The effect of work speed (m/s) and work distance (mm) on the microstructures and oxygen concentration in wt% of NiCr80/20 coatings. Work speed was held high from 3 to 30 m/s.*

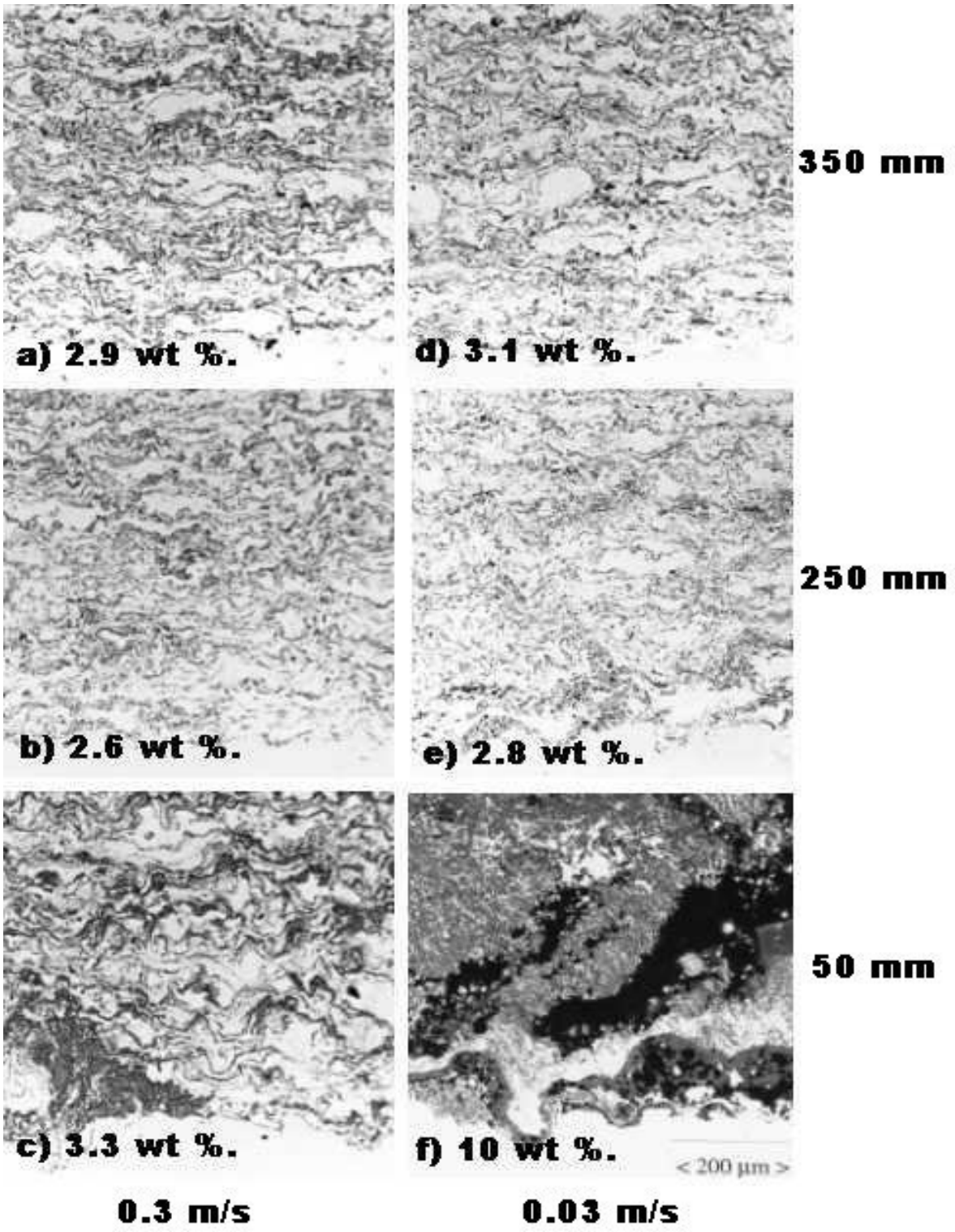

***Figure 31**. The effect of work speed (m/s) and spray distance (mm) on the microstructures and oxygen concentration (wt%) of NiCr80/20 coatings. Work speed was held low from 0.3 to 0.03 m/s.*

When the substrate work speed was held high, 3 or 30 m/s, the oxygen content increased by only a small amount, from 2.0 to 2.4 wt % while the work distance was increased from 50 to 350 mm, as shown in Figure 30, (a-f). The oxygen content remained almost constant due to the very low heat input on the surface to be coated. It was not possible to observe any changes in the microstructure of the coating. The degree of deformation of the spray particles

remained constant over the whole range of the work distance, and no significant differences in the coating microstructure could be observed.

When the work speed of the substrate was held slow, 0.3 and 0.03 m/s, at a low work distance of 50 mm, the quantity of oxides and melting of the spray particles increased significantly, as shown in Figure 31, (c) and (f). Oxygen contents of the coatings in wt % are shown in Figure 28. Oxygen content increases with a slow work speed (0.03 m/s) and short work distance (50 mm).

5.3 Summary of experiments

Summary of the spraying experiments, materials, variables, oxidation results, main test methods and corresponding references to Figures are shown in Table 11.

***Table 11**. Summary of spraying experiments: materials/variables/results/method of analyses.*

Spray material and figure	**Spray parameters**	**Results/method**
WC-Co17, Figure 21	F/O ratio	C wt% loss/Leco
WC-Co17 Figure 22	Work distance and the work speed.	C wt% loss/Leco
WC-Co17 Figure 23 and 24	Gas velocity/ and F/O ratio	Microstructure/phases/OM/XRF
WC-Co17 Figure 25	Constant	Microstructure/SEM
WC-Co17 Figure 26	F/O ratio	Microstructure comparison OM, SEM SEI and BEI
WC-Co17 Figure 27	Constant spray parameter	Element mapping/ SEM SEI and BEI
NiCr 80/20 Figure 28	Work distance and work speed	Oxygen content wt%/Leco
NiCr 80/20 Figure 29	Work distance and F/O ratio	Oxygen content wt%/Leco
NiCr 80/20 Figure 30 and 31	The effect of F/O ratio and work distance	Microstructure, Oxygen content OM/Leco
Cr_3C_2-NiCr 75/25 Table 9. Table *9*	Constant	Elements changes/SEM EDS

6. DISCUSSION

In this chapter, the experimental findings of the work are discussed and compared to previously published studies. The oxidation phenomena and the degree of decarburization and microstructural changes are the main interest. Thermodynamic calculations are also performed and a model for decarburization process of WC-Co17 coating is presented.

6.1 Thermodynamic examination of oxidation in flame

The thermodynamic basis of oxidation of different metals and other compounds, in the HVOF combustion process are examined. Two questions were studied in particular. Firstly, the manner in which different powders are oxidised in the combustion process, and secondly, whether in the HVOF combustion process, the prevailing partial pressure of oxygen is too high to avoid oxidation of metal. Calculation ranges were selected according to typical spray conditions as shown in Table 2 and Table 3. The calculations were made for two areas:

- combustion chamber, nozzle and flame area,
- plume and substrate.

It is generally known that oxygen partial pressure is low, $p_{O2} < 10^{-10}$ bar, in the combustion chamber, in the nozzle and in the flame. Oxygen partial pressure is high, $p_{O2} > 1$ vol %, in the plume and on the substrate. The fuels which were compared, were hydrogen H_2 and kerosene $C_{10}H_{20}$. The combustion chemistry used was stoichiometric combustion and rich flame combustion with 50% excess fuel. The most stable oxides between 900-2000°C for Cr, Ni and Co were chosen to be Cr_2O_3(s), NiO(s) and CoO(s, l), respectively. Calculations were carried out with HSC Chemistry for Windows + Solgasmix routine (57) and according to the Ellingham diagram, Figure 3. The results are presented as equilibrium diagrams for Cr-, Ni- and Co-oxide systems and stability regions with different hydrogen, kerosene and oxygen gas compositions. The conditions used in the calculations are shown in Table 12.

Table 12. *Components and variables of calculation of metal/oxide equilibria.*

Metal materials and oxides	Cr, Ni, Co, Cr_2O_3, NiO, CoO
Fuel gases	Hydrogen and kerosene
Fuel oxygen ratio F/O	Stoichiometric: $H_2 + ½O_2 = cH_2O + dO_2 + eO + fOH$ $C_{10}H_{20} + 15O_2 = cH_2O + dCO + eCO_2 + fO_2 + gO + hOH$ 50% stoichiometric (fuel rich) $1.5H_2 + ½O_2 = cH_2O + dO_2 + eO + fOH$ $C_{10}H_{20} + 10O_2 = cH_2O + dCO + eCO_2 + fO_2 + gO + hOH$
Temperature range	900-2000°C
Oxygen partial pressure, p_{O2} , bar	$10^{-6}…10^{-16}$

Figure 32 and Figure 33 show the values of the equilibrium partial pressures for Cr, Ni and Co and their respective oxides, in the temperature range of 900 to 2000°C. Furthermore, the equilibrium p_{O2} values were calculated for the combustion gas with stoichiometric and rich F/O ratios for hydrogen and kerosene, respectively. Calculations showed that the partial pressure of oxygen was fairly high at the stoichiometric F/O ratio, ranging from p_{O2} 10^{-6} to 10^{-2} bar, but much lower p_{O2} 10^{-5} to 10^{-16} bar for fuel-rich combustion, depending on the temperature. The HSC PC-program calculations also showed that the combustion gas primarily contains H_2O, CO_2 and CO (57). The subsequent calculations showed that differences in the oxidation potential p_{O2} of hydrogen and kerosene combustion gases were not significant. In combustion gas, the concentration of oxygen p_{O2}, water p_{H2O} and carbon dioxide p_{CO2} are controlled by the F/O ratio. Lean fuels (F/O below the stoichiometric ratio) produce high p_{O2}, p_{H2O} and p_{CO2} concentrations, while reducing components p_{H2} and p_{CO} remain at a low level. Rich fuels (F/O above the stoichiometric ratio) produce low p_{O2}, p_{H2O} and p_{CO2}, while reducing components p_{H2} and p_{CO} remain at a high level. The calculations show that chromium tends to oxidise in the conditions of HVOF spraying, while it is possible to avoid oxidation with cobalt and nickel. The typical p_{O2} partial pressure limits for metal oxidation for Ni, Co and Fe are, at 1200°C, 10^{-3}, 10^{-6} and 10^{-7} bar, respectively. For Cr, Ti and Al, the partial pressure p_{O2} limits at temperatures of 1200°C, are much lower, being 10^{-17}, 10^{-20} and 10^{-27} bar, respectively (57, 41).

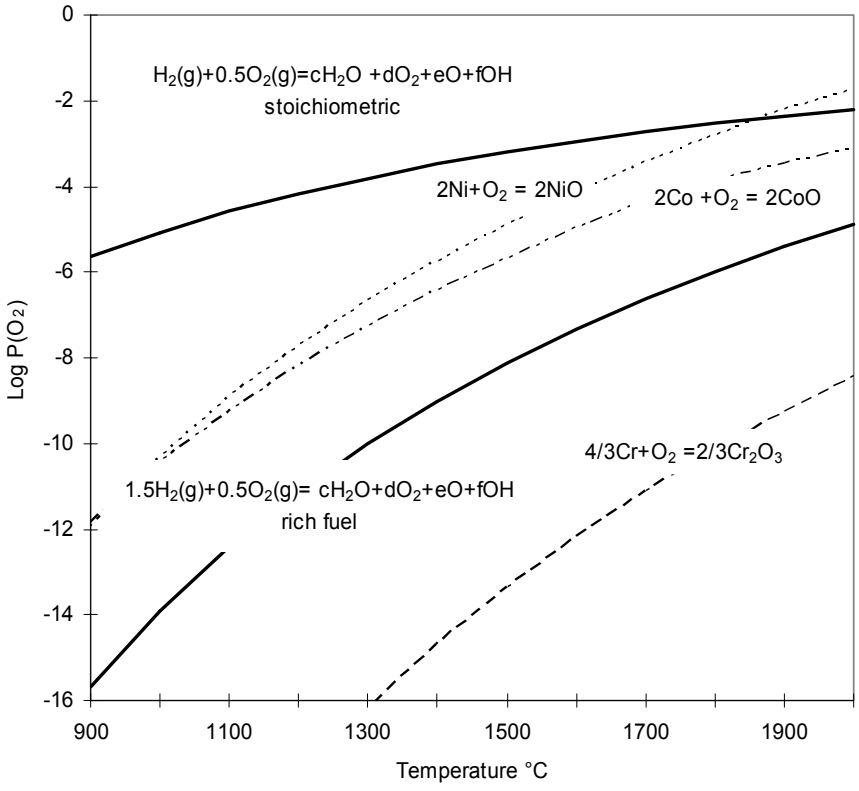

***Figure 32**. Metal / oxide equilibria for Cr, Ni and Co, as well as equilibria with different hydrogen and oxygen ratios in the combustion. Oxygen pressure expressed in bars.*

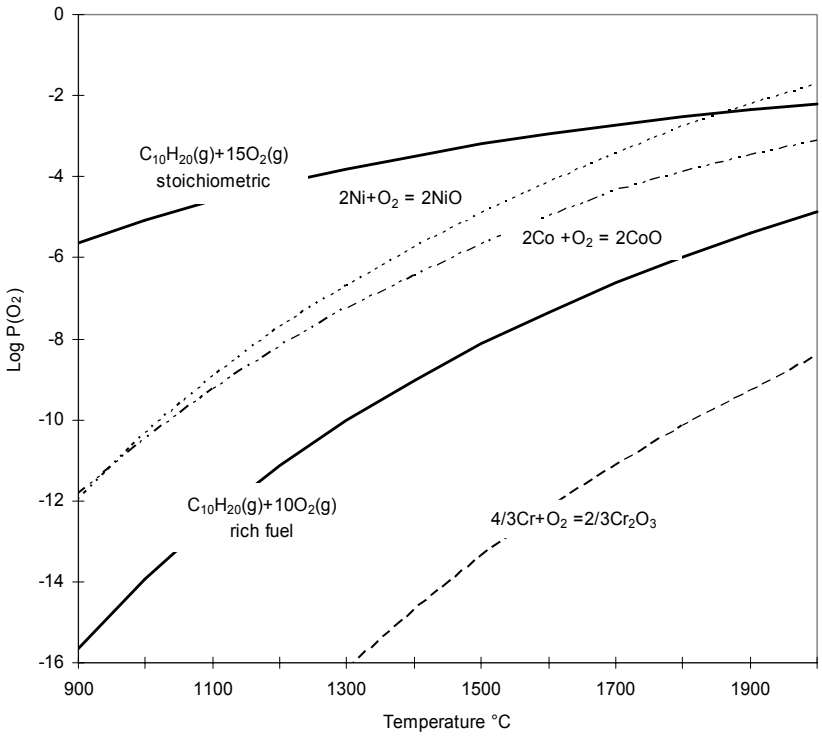

***Figure 33**. Metal / oxide equilibria for Cr, Ni and Co, as well as equilibria with different kerosene $C_{10}H_{20}$ and oxygen ratios in the combustion. Oxygen pressure expressed in bars.*

6.1.1 Plume and substrate

In these zones, the oxygen partial pressure can be quite high and the temperature of the flame can be low. Oxidation of metals and alloys is evident, in near-atmospheric conditions (p_{O2} >1 vol. %) and where the temperature of substrate metal, T = 100-200°C. According to HSC calculation and the Ellingham diagram shown in Figure 3, all metals and alloys discussed here, are oxidized in such conditions, more or less, as shown in Figure 3. It is clear that atmospheric conditions (in the plume of HVOF gun) in stoichiometric combustion of gas H_2(g) or liquid $C_{10}H_{20}$(l) fuel, will not prevent metal oxidation. Thermodynamic theory describes the tendency of metals to oxidise, although does not describe the rate of oxidation. In such low temperature and high oxygen partial pressure, the oxidation rate is very low! Practically, the oxidation rate is negligible at low temperature compared to high temperature (> 1000°C).

The calculations in Figure 32 and Figure 33 were performed for chemical equilibria at the flame conditions. However, in practical spraying conditions, combustion is seldom completed, the p_{O2} level is higher than calculated, and chemical equilibrium is not reached. The verification of the calculated partial pressures of oxygen appears to be impossible because of the difficulty of measuring p_{O2} at high gas temperatures (>2000°C) in the small nozzle (diameter <10 mm).

The combustion conditions p_{O2} are almost such, that most metals and alloys should readily oxidise. Calculation showed that oxidation starts in the nozzle and at the end of the shock diamonds, which is a low p_{O2} concentration region. The main reason for oxidation is the high affinity of metals for oxygen. As shown in the calculations and Ellingham diagram, oxidation

of metals starts at low p_{O2} values. The calculations also indicated that it is not possible to produce an oxide-free coating with a shrouded HVOF spray gun. Oxidation starts in a nozzle of a spray gun, therefore shrouding does not protect metal to be oxidised. How much oxidation actually takes place is more a question of oxidation kinetics. Thermodynamic calculation results in Figure 32 and Figure 33 with HSC also showed that some metals such as Co, Cu, Fe, W and Ni can be sprayed without oxidation taking place in the HVOF combustion chamber or in the nozzle. However, they do oxidise in the plume. Metals such as Cr, Ti, Mn and Al, which have a high affinity for oxygen, will always oxidise to some extent.

The third result was the different tendency of elements to oxidise. This means in practise that elements in alloys oxidise selectively in differing order, some elements oxidising faster than others. This is shown clearly in the case of WC-Co spray powder, where carbon oxidises before other elements, tungsten and cobalt. Thermodynamic calculations do not show the real oxidation situation because in the actual spray process, neither the spray particles nor the combustion gas are at a uniform temperature. Both the particles and the gas are in a non-isothermal situation and the gas is hotter than the spray particles. This means that the p_{O2} concentration in the flame will be higher than calculated, which makes the oxidation of metals more probable. The question, "Why did we not choose a higher gas temperature?" must be asked. The reason for not doing so, was (1) that the partial pressure p_{O2} for metal/alloy oxidation is nearly always achieved, and (2) because oxidation kinetics play a more important part in the oxidation process than the calculated p_{O2} level. Limitation of thermodynamic calculations is that they do not take into account the kinetics of oxidation. They are only able to describe whether oxide formation is possible or not, under certain conditions of temperature and oxygen partial pressure.

6.2 Thermodynamic examination of oxidation reactions in the coatings

The strength of thermodynamics is the power to explain and predict the result of the experiments. Thermodynamics suggests that the reaction order is related to the change in Gibbs free energy (ΔG) of the compounds and the elements. The element which has the highest negative value of ΔG, oxidises first. In the oxidation process, we do not expect that all alloying elements will react at the same oxidation rate. The spraying experiments of the WC-Co17, Cr_3C_2-NiCr and NiCr80/20 coatings, showed that oxidation is a very complex process, where several mechanisms could be stated. Different components have different affinity for oxygen, which leads in selective oxidation.

Formation of volatile oxides such as CO(g), CrO_3(g) and WO_3(g) are also possible. The analyses done from the nano-powders are not the most accurate, due to the small number of experiments. However, they do demonstrate the main phenomena in oxidation processes.

A possible phenomenon affecting both the thermodynamic and kinetic characteristics of oxidation is the formation of liquid solution, when particles melt and react at high temperatures in the plume. The activities of dissolved species (if solution is not saturated) differ from unity and oxidation rate of individual species might be dependent on their diffusivities in the solution. When the solution is cooling down and solidifying, oxides precipitate from the solution. In this respect carbon and metallic constituents are in different position as carbon forms gaseous oxidation product (CO).

In the Cr_3C_2-NiCr75/25 experiment, the small, spray dust size (<1 μm) indicates that nanometer-scale particles have come from the molten surface of the spray particles. No such fine powder fraction exists in the original spray powder, with a particle size of +15 - 45 μm. The change in the ratio of Cr/Ni elements indicates that the nano-size dust suffers Ni depletion, Δ = -2.4 wt %. On the other hand, chromium concentrates on spray dust, Δ = +4.6 wt %. C loss was estimated as –2 wt %, according to Zimmerman (97).

It was expected that enrichment of chromium on the surface of the spray powder occurred via diffusion from the NiCr alloy and Cr_3C_2 carbides. The driving force for Cr diffusion is the greater negative Gibbs energy of Cr_3C_2-compared to NiO (Table 13). Formation of gaseous CrO_3(g) was also considered possible (50), as shown by Equation (33). Formation of CrO_3(g) would cause chromium depletion in the composition of NiCr alloy. Zimmerman (97) showed that decarburising occurs (2-3 wt %) in Cr_3C_2-NiCr spray powder. Carbon in chromium carbide reacts with oxygen according to Equation (32), and escapes as carbon monoxide. The results show that Cr_3C_2-NiCr forms solid oxides, Cr_2O_3 and NiO, and gaseous oxide, CO(g). Selective oxidation also occurs, causing enrichment of Cr_2O_3 on the surface of spray particles, according to Equation (34).

. $$Cr_3C_2+3.25\ O_2(g) = 1.5\ Cr_2O_3 + 2CO(g) \quad (32)$$

$$Cr + 3/2O_2(g) = CrO_3(g) \quad (33)$$

$$2Cr + 3/2O_2(g) = Cr_2O_3 \quad (34)$$

$$Ni + 1/2\ O_2(g) = NiO \quad (35)$$

Zimmerman (97) has shown that Cr_2O_3 can be found in the XRD spectrum of HVOF-sprayed Cr_3C_2-NiCr75/25 coatings.

Table 13. *Gibbs energies for formation $\Delta_R G°$ (kJ/mol) of Cr_2O_3, CrO_3, NiO and for various possible oxides in WC-Co system at 1800℃*

Cr_2O_3 -602	CrO_3(g) -182	NiO -106
CO(g) -583	WO_3(g) -231	CoO -172

WC-Co17 coating suffered carbon loss, but the W to Co ratio remained unchanged. The following mechanism has been proposed for the carbon oxidation reaction is shown in Equation (36) (16):

$$2WC + 1/2O_2(g) = W_2C + CO(g) \quad (36)$$

This is related to the higher affinity of C for oxygen, over WO_3(g) formation. Furthermore, no visible black or grey oxide layer was observed when examining the microstructures of the WC-Co17 coatings. We propose that in the WC-Co17 coating, C is first oxidised to CO(g) gas. No solid oxides of CoO or WO_3 are formed, and therefore no black splat boundaries are seen. Solid oxides (NiO, Cr_2O_3, etc.) result in a corresponding black oxide layer around the splats in the microstructure of alloy coatings (NiCr, Inconel, Cr_3C_2-NiCr, etc). No black oxide layer can be seen in the microstructure of the WC-Co17 coating. Due to CO gas evaporation, only very low oxygen concentrations were detected in the WC-Co17 coatings, which indicates selective oxidation of elements and volatile carbon mono-oxide (16). In the WC-Co17 coating, elements are able to form oxides of CO(g), WO_3(g) and CoO. Table 13 shows

calculated ΔG values for these oxides at 1800°C (57). Thermodynamics suggest that carbon should be oxidised first (41, 50), tungsten (W) next and cobalt last, since carbon has the highest negative ΔG value, as shown in Table 13. The analyses of the sprayed particles shown in Table 9.

Table 9 indicates that only carbon is oxidised to CO(g), resulting in 0.8 wt % C loss, and that the W/Co ratio remains constant. Thermodynamics suggests that the ratio of W to Co will remain constant as long as carbon is being consumed. The formation of WO_3(g) and CoO is prevented because the formation of CO is more probable, due to CO(g) possessing the highest negative ΔG. The following reactions Equation(37-39) are proposed for the oxidation of solid WC-Co17:

$$2WC + 1/2\ O_2(g) = W_2C + CO(g) \quad (37)$$

$$W_2C + 1/2\ O_2(g) = 2W + CO(g) \quad (38)$$

$$W + 3/2\ O_2(g) = WO_3(g) \quad (39)$$

These reactions suggest that at least two steps occur before WO_3(g) is formed. CoO formation is also prevented because the formation of CO(g) is more probable, as C is the reducing element in the coating i.e. oxygen consuming element. The oxidation of the WC-Co17 system has been widely studied and only reduction of C is reported. In the earlier works the oxygen content of the coatings analysed has been very low (<0.2 wt %) and the content of WO_3 was not reported in the XRD studies (13, 16) WO_3(g) is volatile at temperatures above 700°C. Therefore WO_3(g) does not exist in the coatings and no change in the W to Co ratio could be find. The reported results support our experiments, but the studies have not discussed selective oxidation. This topic is discussed in details in section 6.3

In the experiments of NiCr80/20 coating, chromium increased with Δ = + 2.7 wt % to 26.6 wt %, while Ni decreased with Δ = -2.5 wt %. The oxides should be solid NiO and Cr_2O_3. Ellingham diagram (Figure 3) shows that formation of Cr_2O_3 should be more probable than formation of NiO. The oxide layer of NiCr80/20 coating should therefore contain more Cr_2O_3 than NiO. The results suggest selective oxidation resulting in chromium enrichment on the surface of the spray particles and formation of solid oxides.

6.2.1 Factors affecting the degree of decarburization in WC- Co17 coating

The oxidation of carbon from coatings was shown in Figure 21 and Figure 22. The F/O ratio controls the degree of decarburization most effectively. Adjustment of the F/O ratio controls the temperature of the flame, as shown in Figure 5. The temperature of the particles was shown in Figure 17. Hanson et al (98) obtained similar results when spraying with AISI 316 steel powder. Figure 34 shows the relationship of the gas temperature effects on the temperature of the spray particles. Adjusting the F/O ratio to stoichiometric causes the temperature of the flame to become hotter, resulting in a rise in temperature of the spray particles. Hydrogen and oxygen were used as combustion gases. The calculation was performed with HSC software. Spray particle temperature was measured with the SprayWatch on-line temperature and particle velocity measurement instrument (99).

The control of the temperature of the flame influences the particle temperature very

effectively as shown in Figure 34. The high particle temperature increases the degree of decarburization of WC-Co17 coating. The Arrhenius Equation (18) also suggests that the degree of decarburization of the spray particles is more sensitive to temperature changes than other factors.

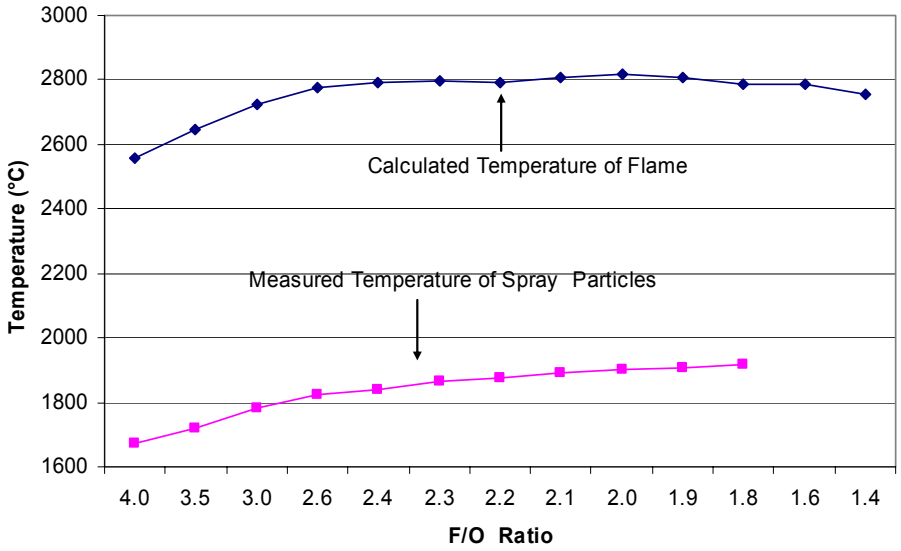

***Figure 34**. Measured temperatures of spray particles (93) and calculated temperatures of the combustion gas as a function of F/O ratio.*

There are also other factors, which affect the oxidation/decarburization rate, such as time, oxygen partial pressure and the surface area of the powder. The high oxygen partial pressure (in the plume) has been expected to be the main factor causing the high oxidation rate. The measurements (Figure 12) and calculations (Table 4) show that oxygen partial pressure varies from a low value to high ambient values. The F/O ratio and the work distance (Figure 13) control the oxygen partial pressure.

The effect of work distance can be seen in Figure 22. The degree of decarburization is already high (2.2 wt %) at the exit of the nozzle, at the work distance of 50 mm. The degree of decarburization of the coating increases only by 0.2 wt % at the work distance of 350 mm. The plume area from the nozzle to the substrate (50 to 350 mm) has a high oxygen partial pressure (Figure 13).

An explanation for the relatively low decarburizing rate in the plume and on the substrate needs to be sought. In the plume, the particles still have a high temperature whereas the plume surroundings have a much lower temperature (<1000°C) but a high oxygen partial pressure. Due to the quite short flight time (about 1 ms), the degree of decarburization is low.
The effect of work speed could be seen in Figure 22. Work speed does not influence the degree of decarburization of the coating. Only a very low work speed affects the decarburization rate at a low work distance. An explanation for this is that this occurs as the result of high temperature of the spray sample (300-400°C). High temperature of the spray sample does not allow the coating to “freeze”, while the high temperature flame heats and oxidises the coating. Decarburization of WC-Co17 did not occur at high work speed (30 m/s), because of the cooling effect of the air and substrate. The flame power distribution on the substrate was also very low compared that at the low work speed. Power is defined as the heat

flux per surface area to be coated per time unit.

Example: Slow work speed (0.03 m/s) heats the item to be coated to 200-400°C. At high work speed (>10 m/s) the item to be coated is heated up to below 100°C. The excess heat accumulated in the item to be coated, must be removed with external cooling, air blowing, water-cooling, etc.

The combustion chamber pressures of HVOF guns, and the F/O ratio are also factors that control the temperature and velocity of the spray particle. If the F/O ratio is adjusted to stoichiometric, the combustion temperature and the gas velocity increase, as was shown in Figure 10 and Figure 5. As a result of the increase in gas velocity and temperature, the velocity of the spray particle and temperature also increase. The result of the F/O ratio on the temperature and velocity of the spray particle can be seen in Figure 17. If the combustion chamber pressure is increased with the de Laval nozzle, particle and gas velocity are increased. This causes shorter flying time for the spray particle. Hanson et al (98) calculated the particle residence time to be about 2 ms. If the shorter flight time of the spray particles is shortened further, decarburization will stop. The flight time can thus become a controlling factor for the degree of oxidation. Adjusting the F/O ratio controls the degree of decarburization of the spray particles and the temperature of the flame. The higher the temperature of the flame and spray particles, the greater the degree of decarburization.

The decarburization process in spray particles behaves as oxidation kinetics suggests, i.e. as the F/O ratio is adjusted to stoichiometric, the temperature of flame and particle increased, and the rate of decarburization and particle oxidation also increased. In addition, when using a lower HVOF gas velocity (1100 m/s), the degree of decarburization increased. A lower gas velocity (1100 m/s) resulted in higher particle temperatures than a high gas velocity (1560 m/s) because of the longer dwell time in the nozzle in the presence of hot combustion gas (2200-2800°C). The temperature of the spray particle is a more important factor in the decarburization process than the residence time in the HVOF process.

Fincke and Bartuli (75, 100) studied the effect of spray parameters on WC-Co decarburization. They found that the main influence on decarburization rate was the length of the nozzle. The F/O ratio had a lesser effect on the degree of decarburization. Barttuli´s results can be explained as follows. The JP-5000 HVOF gun operates with a lower F/O ratio compared to the HV-2000 or the Jet-Kote. The main operating parameters of the JP-5000 are the chamber pressure and nozzle length. Therefore, their results are not comparable to our result of decarburization. The general results of the coating are similar, with longer residence time in the nozzle increasing the degree of decarburization. The simulated and measured temperatures of the spray particles were also lower (1500°C) as compared to those of the HV-2000 and the DJ-Hybrid (1800°C) guns, are shown in Figure 17 (75, 100). The higher temperature of the spray particle explains the stronger effect of the F/O ratio on the degree of oxidation.

6.2.2 Microstructural changes of WC-Co17

A straightforward comparison of WC-Co17 microstructures with the literature is not possible, as the results reported by other authors have been obtained with combinations of different spray parameters, powders, fuels and spray guns. Nevertheless, some common features can be

found, i.e. reduced amount of WC carbide and increase of the binder phase, when the spray particles become hot. However, the effect of the F/O ratio has not been clearly shown.

Etching with Murakami´s reagent showed the occurrence of WC decarburizing. Decarburizing takes place from the surface to the centre of the spray particle. The etching shows the progress of decarburization in the spray particle, when temperature increases (Figure 21). The results confirm the model presented by Vernon (101). The modification of the microstructures is supported by carbon analysis. When the quantity of carbides decreases in the microstructure of the coating, the carbon content also decreases.

6.3 Mechanism of decomposition of WC-Co17

In this study, the eventual reactions are discussed and their probabilities are presented based on Gibbs energy. A model of oxidation is also presented for liquid-gas and liquid-liquid reactions, in molten WC-Co17 spray particles. Many chemical reactions can occur when hot spray particles fly in a nozzle and in a plume. The process surroundings vary along the path of the spray particles, e.g. temperature first rises and then falls. The chemical composition of the gas varies considerably in the process atmosphere. The most significant gases for oxidation of WC-Co17, from a chemical point of view, are oxygen, carbon dioxide and water vapour. Carbon monoxide is considered to be a reducing agent. It has been claimed that there are two processes for tungsten carbide decomposition (75, 24):

- thermal decomposition
- chemical decomposition

The decomposition of WC-Co17 can occur simultaneously as a combination of these two. Thermal decomposition occurs according to the phase diagram, at a temperature of 2785°C. At this temperature, tungsten carbide decomposes to liquid tungsten and solid graphite (gr) according to the reaction (40):

$$WC(s) = W(l) + C(gr) \quad (40)$$

The direct decomposition of tungsten carbide is possible only in plasma spraying, where the flame temperature is sufficiently high. Several authors have found WC-Co17 coating to decompose via oxidation or thermal decomposition (24). Therefore, thermal decomposition of WC-Co17 is not associated with HVOF spraying. Chemical decomposition has been associated with the entrance of air to the flame of the plasma or HVOF gun, or “free oxygen” in a HVOF gun.

6.3.1 Low temperature oxidation of WC-Co17 in air

Oxidation of WC-Co17 commences at 500°C, when heated up in air. The solid oxidation reaction can continue up to 1000°C. Decomposition times of WC-Co17 coating are from several hours to days. Oxygen reacts with carbon in tungsten carbide, forming carbon dioxide (CO_2) (102, 103). Cobalt and tungsten are also oxidised, forming solid oxides, $CoWO_4$, WO_3(s), CoO(s), and Co_3O_4. The products of low temperature oxidation are different from those of high temperature oxidation. Therefore the chemical reactions, which occur in air and at low temperature, cannot be applied to the high temperature decarburization of HVOF spraying.

6.3.2 High temperature decarburization of WC-Co17

The findings in the coating experiments, i.e. the high degree of oxidation in the nozzle and CO bubbles in the microstructure, allow us to propose the following oxidation mechanism for WC-Co17 coating. The decomposition of the coating occurs via chemical decomposition and oxidation occurs in three different ways:

- solid-gas
- liquid-gas
- liquid-liquid

At low temperatures, oxidation starts with solid-gas reactions. When the temperature of the particles increases to melting point of the material, oxidation starts with a liquid-gas reaction. Liquid-liquid reaction takes place inside or on the surface of the molten spray particle, during flight. As coating on the work piece progresses, the oxidation reaction transforms again to a solid-gas reaction.

Oxidation of WC-Co17 occurs in the barrel of the HVOF gun in two ways, either in a solid or molten state. Temperatures of the spray particles are below or above the melting point of cobalt (1493°C). In the solid state, composition of the coating is heterogeneous, consisting of WC grains and binder phase cobalt. WC and Co oxidise separately without significant interaction with each other. In the molten state, WC and W_2C dissolve to Co matrix. The oxidising agents are oxygen, water vapour and carbon dioxide. Liquid-liquid reactions occur on and in molten spray particles.

6.3.2.1 Solid-gas oxidation

Oxidation of WC and Co is expected to take place in separate phases. No significant mass transfer occurs between WC and Co. Table 14 shows the possible oxidation reactions and equivalent negative or positive Gibbs energies. In the solid state, several reactions can take place simultaneously. Reaction rates can vary for kinetic reasons, and is dependent on temperature, mass transfer in the reaction zone, oxygen partial pressure, etc. In general, it can be concluded that solid-state oxidation is less important compared to the oxidation reaction in the liquid state, due to kinetic constraints.

In reaction equations for oxidation reactions and their respective Gibbs energies are shown. The high reaction rate requires solid-gas or liquid-gas reactions. Solid-solid reactions are too slow for the HVOF spraying process, as the spray particles are in reaction conditions less than 2 ms. Thus, only the most probable reactions occur. The reactions are divided in two categories; reactions with pure oxygen, and reactions with carbon dioxide and water vapour. These are the main combustion products of HVOF spraying and are effective gases in the plume.

Table 14. *Reaction equations system concerning reactions of WC-Co with oxygen and combustion gases. Respective Gibbs energies for reactions at temperatures 1000°C and 1800°C.*

Reaction	$\Delta_R G°$1000°C/ kJmol^{-1}	$\Delta_R G°$1800°C/ kJmol^{-1}
Reactions with oxygen		
$4WC + O_2(g) = 2W_2C + 2CO(g)$	-362	-543
$2WC + O_2(g) = W_2C + CO_2(g)$	-352	-375
$2WC + O_2(g) = 2W + 2CO(g)$	-378	-517
$WC + O_2(g) = W + CO_2(g)$	-360	-362
$WC + O_2(g) = WO(g) + CO(g)$	102	- 43
$2/3WC + O_2(g) = 2/3WO_2 + 2/3CO(g)$	-366	-324
$2/3WC + O_{2(}g) = 2/3WO_2(g) + 2/3CO(g)$	-111	-176
$1/2WC + O_2(g) = 1/4W_2O_6(g) + 1/2CO(g)$	-306	-295
$1/2WC + O_2(g) = 1/6W_3O_9(g) + 1/2CO(g)$	-327	-300
$2W_2C + O_2(g) = 4W + 2CO(g)$	-393	-490
$W_2C + O_2(g) = 2W + CO_2(g)$	-338	-349
$2W + O_2(g) = 2WO(g)$	-583	-429
$2/3W + O_2(g) = 2/3WO_3$	-346	-231
$2\ Co + O_2(g) = 2CoO$	-289	-172
$2C + O_2\ (g) = 2CO\ (g)$	-448	-583
$2H_2(g) + O_2\ (g) = 2H_2O\ (g)$	-354	-262
Reactions with H_2O and CO_2		
$C + H_2O\ (g) = CO(g) + H_2(g)$	-46	-160
$2WC + CO_2(g) = W_2C + 2CO(g)$	-9.2	-168
$2WC + H_2O(g) = W_2C + CO(g) + H_2(g)$	-3.7	-140
$W_2C + H_2O(g) = 2W + CO(g) + H2(g)$	-19.2	-113
$W_2C + CO_2(g) = 2W + 2CO(g)$	-24	-141
$Co + H_2O(g) = CoO + H_2(g)$	**+32**	**+45**
$Co + CO_2(g) = CoO + CO(g)$	**+27**	**+17**
Other reactions		
$2WC + CoO = W_2C + Co + CO(g)$	-66	-185
$WO_3(g) + 3WC(s) = 4W + 3CO(g)$	-344	-599

6.3.2.1.1 Decarburization of WC-Co17 by oxygen

In the WC-Co17 system at solid state, the main reaction is decarburization of tungsten carbide. WC decarburizes according to the reaction shown in Equation 41:

$$4WC + O_2(g) = 2W_2C + 2CO(g) \qquad (41)$$

The decarburization reaction has a high value, $\Delta_R G° = -423$ kJ/mol at 1200°C, which means that the decomposition of WC is highly probable via this reaction, providing oxygen is available. Further oxidation of W_2C is possible as well:

$$2W_2C + O_2 = 4W + 2CO \quad (42)$$

There are also other possible decomposing reactions, which are presented in Table 14. WC-Co17 coating has cobalt as a binder phase. Carbides are embedded in cobalt, which has a tendency to oxidise. Cobalt can oxidise according to the following reaction:

$$2Co + O_2 = 2CoO \quad (43)$$

The reaction has a high negative Gibbs energy, $\Delta_R G° = -290$ kJ/mol 1000°C. Cobalt therefore has a tendency to oxidise. However, the formation of CoO is only possible in the plume, a high p_{O2} area of the combustion gas

6.3.2.1.2 Decarburization of WC-Co17 by CO_2 and H_2O

The combustion process produces CO_2 and H_2O. The CO_2 and H_2O concentration are high in combustion process as shown in Table 2. The CO_2 reaction with tungsten carbide is:

$$2WC + CO_2(g) = W_2C + 2CO(g) \quad (44)$$

The value of $\Delta_R G°$ is –9.2 kJ/mol at 1000°C, and –160 kJ/mol at 1800°C. The reaction with water, $H_2O(g)$, also has to be considered:

$$2WC + H_2O(g) = W_2C + CO(g) + H_2(g) \quad (45)$$

The value of $\Delta_R G°$ is –3.7 kJ/mol at 1000°C and –140 kJ/mol at 1800°C. Oxidation tendency is very low at 1000°C, but increases at the higher temperature of 1800°C. Water vapour and carbon dioxide are protective below 1000°C, but change oxidising at higher temperatures.

Cobalt does not oxidise by the to reaction with Equation (46), in the nozzle of the HVOF gun. The value of $\Delta_R G°$ is positive (+32 kJ/mol) at a temperature of 1000°C. The positive value shows the tendency of cobalt oxide to decompose into metallic cobalt:

$$Co + H_2O\ (g) = CoO + H_2(g) \quad (46)$$

Additionally there is a solid-solid reaction:

$$2WC + CoO = W_2C + Co + CO(g) \quad (47)$$

The value of $\Delta_R G°$ is –66.8 kJ/mol at 1000°C. The reaction looks probable, but the formation of CoO in the nozzle and in the flame is prevented, according to Equation (46), and there is too little time for a solid-solid reaction (41) to occur in the plume or on the substrate. Possible reactions in the HVOF spraying process were listed in Table 14. Most of the reactions produce carbon monoxide, which burns to carbon dioxide and forms heat, as in Equation (48).

$$2CO(g) + O_2(g) = 2CO_2(g) \quad (48)$$

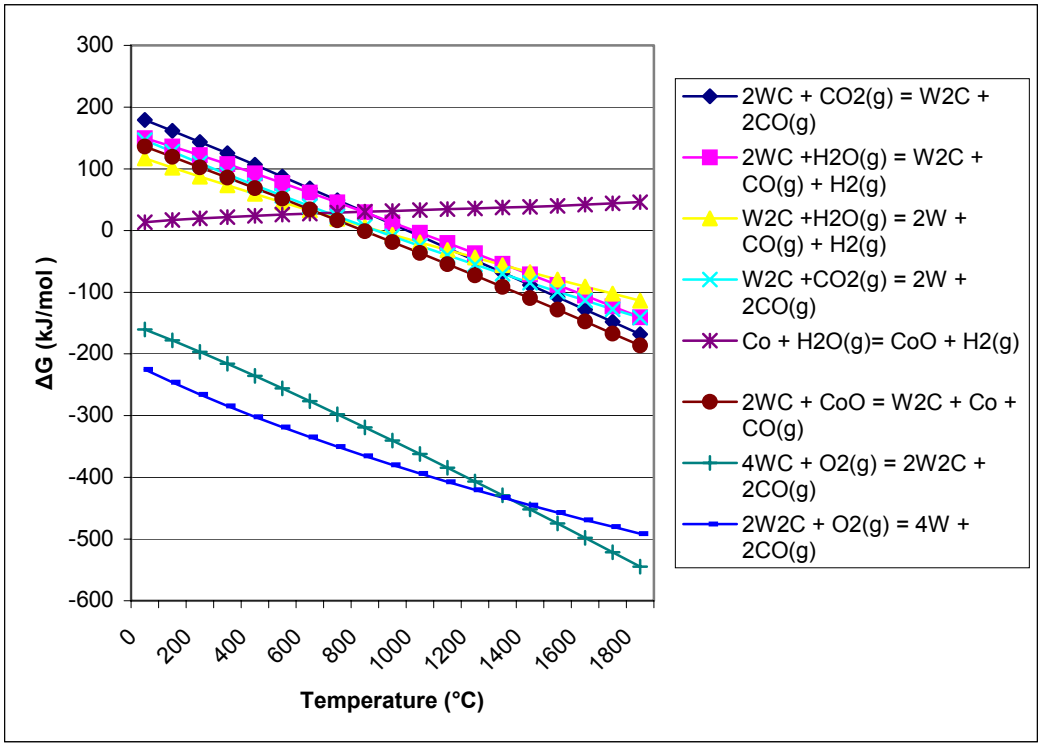

***Figure 35**. Gibbs energy as a function of temperature for some important reactions of WC-Co with H_2O, CO_2 and O_2.*

6.3.3 Liquid-gas oxidation

Liquid-gas oxidation is expected to be the main mechanism of WC-Co oxidation. The high rate of oxidation is expected to result from the high temperature and the existence of liquid phase in the WC-Co system. Models forming a solid oxide layer (parabolic, linear model) on the surface, do work at higher temperatures in corresponding cases (44, 50). These models are based on a solid protective solid oxide layer on the surface. In the molten state, spray particles do not have a solid oxide layer.

There are few models for oxidation or decarburization of liquid alloys, at very high temperatures (over 1500°C) and in liquid states. The most useful model of the process, to apply to the decarburization of WC-Co17, is the refining of steel, which aims at the decarburization of liquid hot metal from about 4 wt % to very low carbon content in the final steel. The metal refining process is based on differing affinity of various elements for oxygen. However, it also depends on the chemical activities of elements dissolved in the metallic phase.

Decarburization of molten WC-Co17 is a comparable process to the refining of steel. Carbon is oxidized from steel by oxygen (54). In decarburizing ("refining") of WC- Co17, carbon is oxidized from molten WC-Co17 by oxygen, H_2O and CO_2.In the decarburizing process of WC-Co spray powder, WC dissolves in Co during spraying, when the temperature of the particle rises above 1500°C. WC-Co forms a ternary alloy of $W_xC_yCo_z$, The constitution of the alloy varies from place to place. The melt also consists of solid particles of WC, shown in Figure 25, and therefore is heterogeneous. The higher the spray particle temperature has been, the lower the quantity of WC carbides it has. Because the temperature of the melt is high, the rate of the oxidation reaction is also high.

Many different reactions take place on and in the spray particle, including mass and heat transfer, chemical reactions, melting, and evolution of gases and formation of heat. Decarburization of the WC-Co coating can be expected to take place in several stages:

- warming up
- decarburization in solid state by oxidation of carbides (WC)
- melting of Co and dissolving of WC
- formation of W_2C and $W_xC_yCo_z(l)$
- carbon diffusion to the surface of a spray particle
- internal and surface oxidation of carbon
- reduction of CoO and WO_3
- nucleation of CO, formation of CO bubbles and their release
- solidification
- phase changes, solid solution reactions, precipitation of W, M_6C and $M_{12}C$, carbides.

6.3.3.1 W-C-Co system at high temperatures

Decarburization consumes carbon in the WC-Co coating. The balance of W and Co remains constant. The behavior of the WC-Co system can be examined with the ternary diagram, W-Co-C. This diagram shows the possible phases of WC-Co in chemical equilibrium. The direction of the carbon consuming process is shown by the arrow in Figure 36. The arrow indicates the composition changes of the W-C-Co system during the spray process, which transforms W-Co-Co to Co-W alloy when all carbon is consumed. The following phases can

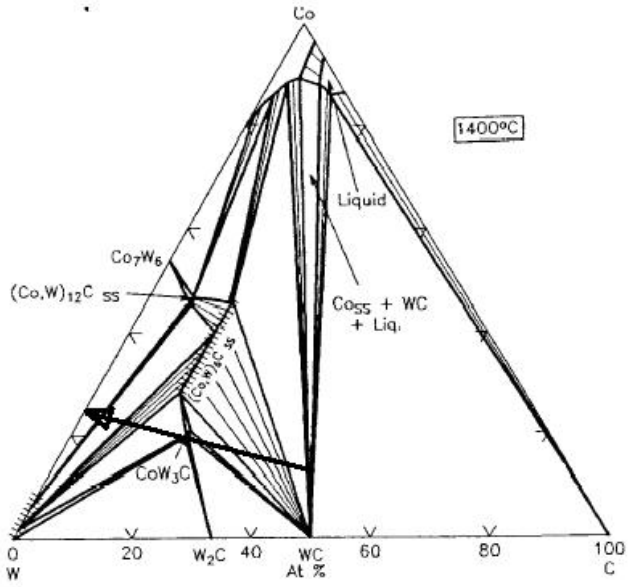

***Figure 36**. W-Co-C isothermal section at 1400°C (104). Location of WC-Co17 is at Co/W at 40/60 wt/at %. The arrow indicates the direction of decarburizing process.*

be found; M_6C, $M_{12}C$, W_2C, W, Co_3W and Co_7W_6. M is the sum of Co and W. The ternary phase diagram of W-Co-C is presented in Figure 36 (104). The arrow shows the composition change of WC-Co17 spray powder during the spray process. All carbon can be consumed locally on the surface of spray particle, while it is in nominal composition inside the spray particle.

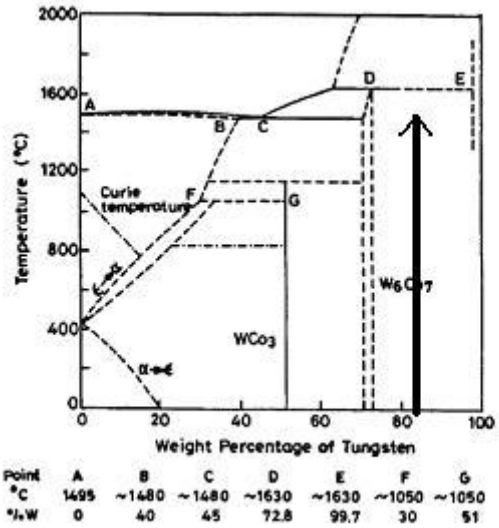

Figure 37*. Binary phase diagram of Co-W (105). The arrow indicates the composition of the carbon-free W–Co alloy corresponding to the initial composition of WC-Co17.*

Some areas of the spray particles can suffer from lack of carbon as a result of the high degree of local decarburization. Such areas are typically on the outer shell of the spray particles. The high decarburization forms tungsten-rich cobalt solution/melt with a constitution of Co/W 17/83 wt % and 40/60 at%, respectively. The equilibrium diagram of W-Co is presented in Figure 37. Such W-rich solid solution forms of W and Co_3W, occur at low temperatures.

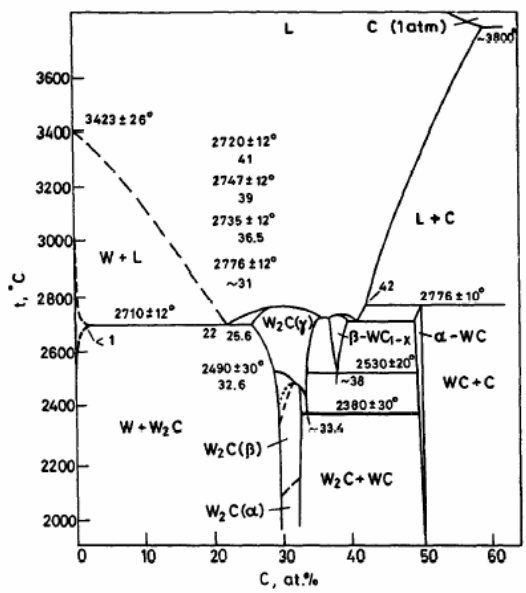

Figure 38*. Binary phase diagram of W-C (105).*

In the W-C system, two carbides are mainly found, WC and W_2C. Even a small amount of decarburization can cause formation of W_2C from WC. Higher degrees of decarburization cause formation of W and W_2C. The W-C system is presented in Figure 38.

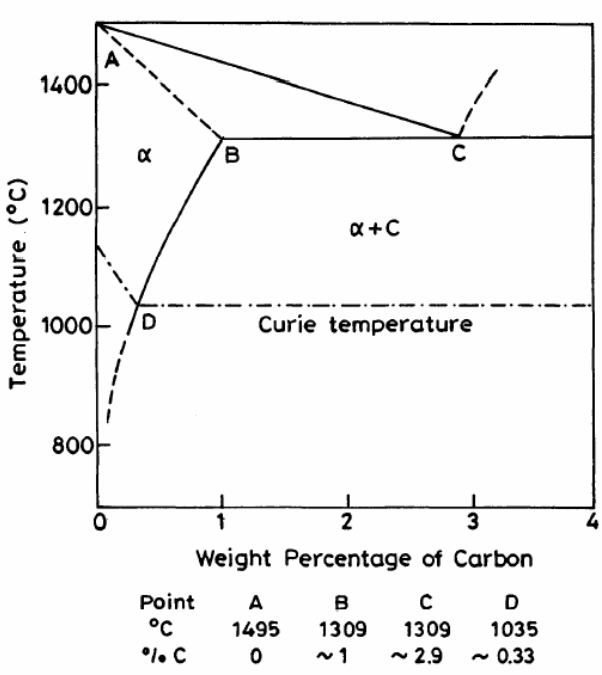

***Figure 39**. Binary phase diagram of Co-C (105).*

Liquid cobalt dissolves about 3/13 wt/at % of carbon at the eutectic melting point, 1309°C. The ability of liquid cobalt to dissolve carbon is the key issue in the dissolution of WC in Co. The equilibrium diagram of Co-C is shown in Figure 39. Liquid cobalt acts as sink for carbon in the WC-Co system. In the solid state, carbon is nearly insoluble in cobalt, and will precipitate as graphite in the cobalt matrix.

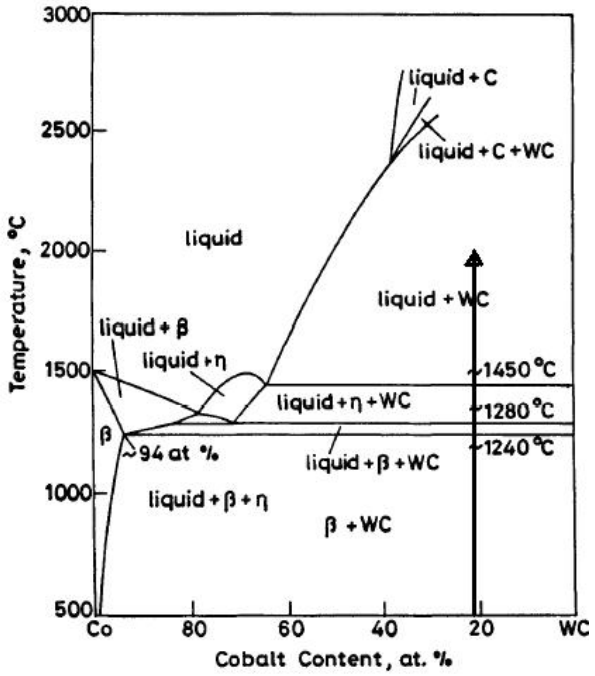

***Figure 40**. Vertical section between stoichiometric WC and Co in W-Co-C phase diagram (105). The arrow indicates composition of WC-Co17.*

Figure 40 shows the vertical section between stoichiometric WC and Co in the W-Co-C phase diagram. In such conditions, where no decarburization occurs, WC and Co are stable at

temperatures over 1450°C. In spray particles, the inner part of the particle can be in a stable condition. The arrow indicates phase stability and composition of WC-Co17, and phase formed if no decarburization occurs. At high temperatures, WC dissolves in Co and during slow cooling, W and C precipitate again into WC crystals.

6.3.3.2 Phases formed during the spraying process

In spraying, WC-Co powder undergoes decarburization and phase transformations. The original WC-Co structure of the powder changes to metastable phases, such as W_2C and amorphous binder phase.. The degree of the phase changes related to degree of decarburization, is presented in Figure 41. The metastable phase can transform to stable phases by annealing the coatings in temperatures above the recrystallization temperature (> 850°C) (7, 106). However, the phases formed during annealing are not the same as the equilibrium phases of the W-C-Co system. The phases found in the WC-Co system are presented in Table 15. The non-equilibrium states of phases after annealing are caused by the heterogeneity of the coating. There are many local variations in the composition of the coating and spray droplets (107). The inner part of the coating can be non-decarburized while the core of the droplet can be heavily decarburized. Local heterogeneity in a coating allows observation of non-equilibrium states in the XRD spectrum. Phase changes after annealing are presented in Figure 42.

***Table 15**. Phase structures of the WC-Co system in different process conditions; powder, coating, annealed coating, and equilibrium phases.*

State	Phases	Comments
Powder	WC, Co, M_6C $M_{12}C$	M_6C and $M_{12}C$ seldom
Coating	WC, WC_{1-x}, W_2C, W, amorphous, M_6C, $M_{12}C$	Co disappeared, no CoO or WO_3
Annealed coating	WC, W, M_6C, $M_{12}C$	Amorphous phase and W_2C disappear
Equilibrium in W-C-Co	WC, W, M_6C, $M_{12}C$, Co	C=0, then Co_3W and W

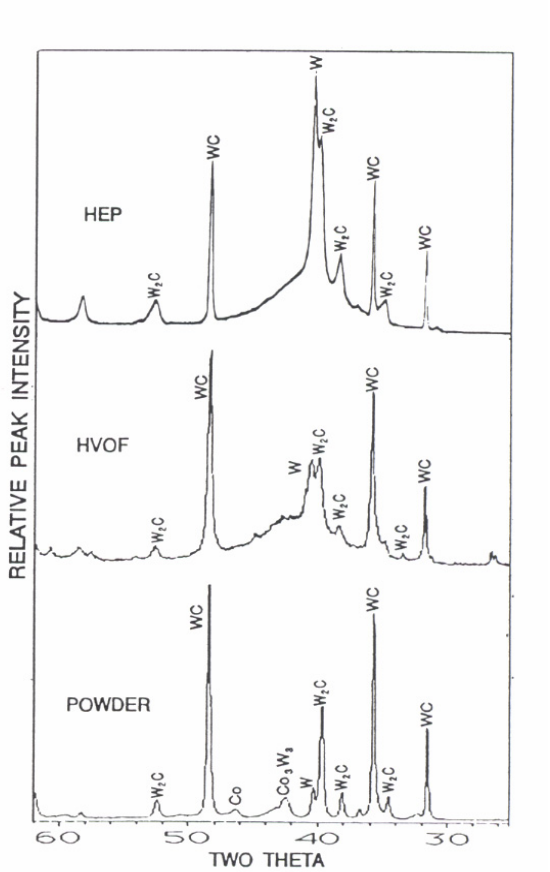

Figure 41. *XRF patterns of phase changes in WC-Co12 during HVOF and plasma (HEP = APS) spraying (7). Powder is feed stock material, HVOF and HEP are sprayed coatings.*

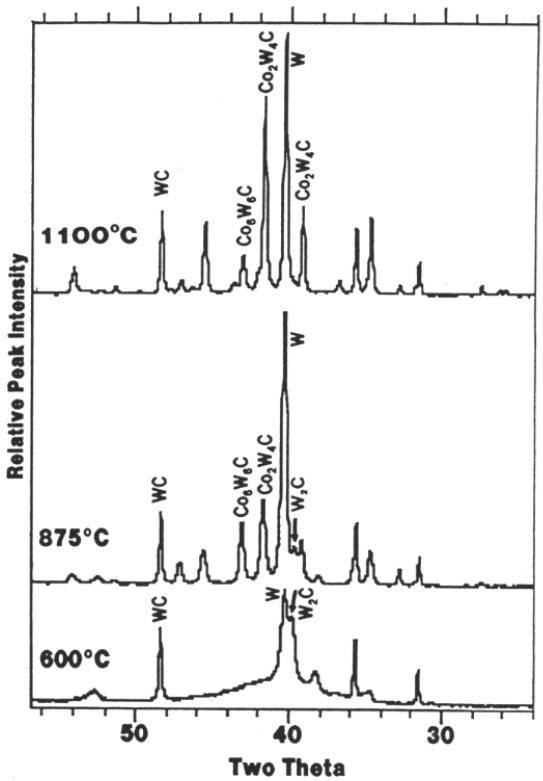

Figure 42. *XRF patterns of phase changes during heat treatment of sprayed coatings. The heat treatment shifts the composition of the coating to thermodynamic equilibrium phases (7).*

6.3.3.3 Formation of W_2C and WxCyCoz(l)

Numerous temperature measurements of spray particles and microstructures of coatings, have verified the molten state of spray particles. Binder phase Co melts at 1450°C and temperatures of spray particles above 1900°C have been measured. Microstructures of the coatings have also shown structures characteristic of molten spray particles.

Decarburization of WC-Co is based on dissolving WC in the Co melt. It is well known in hard metal production and in thermal spraying, that Co dissolves WC at temperatures above 1450°C, in spite of the high melting point of WC (2770°C). Co and WC form $W_xC_yCo_z$ melt, with carbon diffusing to the surface of the droplet where it oxidizes to carbon monoxide. Only a small quantity of carbide oxidizes internally. The reaction of oxygen with WC particles in the melt can be considered a minor effect. XRD, TEM and SEM observations suggest that dissolution of WC in Co occurs in two steps (7, 101, 107). In XRD spectrums, it has been noticed that WC-Co first forms W_2C and then an amorphous structure. In TEM observations it has been found that WC grains transform to a WC/W_2C structure, as presented in Figure 43. There is a thin layer of W_2C on the WC crystals (<0.1µm). Numbers of SEM observations have noted disappearance and rounding of WC crystals in the Co matrix indicating dissolution of WC in the Co matrix. The findings lead to the suggestion that the following reactions occur in the Co melt; dissolution of WC in two steps, and during cooling, $W_xC_yCo_z$(l) solidifies on WC/W_2C crystals as W_2C. Dissolution of WC in Co is shown in Equations (49-52):

$$2WC = W_2C+[C]_{Co} \quad (49)$$

$$W_2C = 2[W]_{Co} + [C]_{Co} \quad (50)$$

or dissolves directly in the Co melt

$$WC = [W]_{Co} + [C]_{Co} \quad (51)$$

where $[W]_{Co}$ and $[C]_{Co}$ denote elements dissolved in the Co melt. Here, W_2C denotes forming of a W_2C layer by diffusion on a WC grain, as presented in Figure 43. WC and Co form a heterogeneous melt:

$$W_xC_y + zCo(l) = W_xC_yCo_z(l) \quad (52)$$

Here $_{x,y,z}$ denote different numbers of atoms. The melt is heterogeneous, consisting of molten and solid WC crystals. The constitution of the melt has been reported to vary between the W/Co ratios 16/84-66/34 wt % (107). Theoretically, the homogenous composition of the WC-Co17 melt can be found at W/Co 60/40 wt %.

Most of decarburizing takes place on the surface of the spray particle, and therefore the carbon has to move to the surface of the spray particle. Dissolved carbon is homogenously distributed in the spray particle. Carbon mass transfer to the surface can take place via solid WC particles or molten $W_xC_yCo_z$(l). Mass transfer favors the molten phase, because diffusion is 100 to 1000 times faster in the molten phase than in the solid phase (108). The melt acts as a diffusion path for carbon to the surface of the droplet.

In equilibrium, the W-C-Co system forms WC-Co and M_6C and $M_{12}C$ phases. However, the melt solidifies in rapid cooling, as amorphous phase W, WC and W_2C , which can find be found in TEM and XRD observations (101, 107).

Formation of WC/W_2C seems natural during the dissolving process, because cobalt dissolves carbon 3/13 wt/at % at the melting point of Co. The free energy change associated with the transformation of WC to W_2C is low, approximately –7 kJ/mol at 1800°C. Dissolving WC in Co requires energy. WC is not a very stable compound, with a Gibbs free energy of, $\Delta_R G°$ = -33.328 kJ/mol at 1800°C. The structure of a dissolving WC/W_2C grain is presented in Figure 43 (101).

White fringes have been found around large WC crystals in the microstructures, as presented in Figure 25 and Figure 26. These fringes can be attributed to a solidification process of liquid $W_xC_yCo_z(l)$. W_2C dendrites, fringes, and nucleate form homogenously from the melt on the surface of the WC/W_2C crystals are shown in Equation (53). EDS analysis suggests these fringes are W_2C. This process is presented in Figure 46.

$$W_xC_yCo_z(l) \Rightarrow W_2C_{(WC/W2C)} + \text{nanocrystal matrix} \qquad (53)$$

Vernon and Guilemany (101, 107) have also reported epitaxial growth of W_2C on the WC crystal as shown in Figure 43.

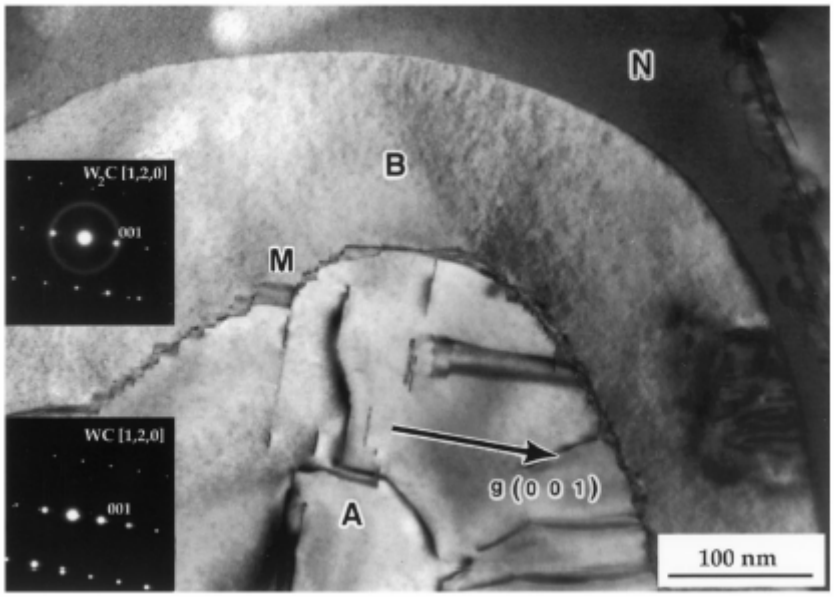

***Figure 43**. TEM image of the WC/W_2C structure. A is WC, B is W_2C and N indicates amorphous nanophase (solidified WxCyCoz). The structure indicates growth of W_2C on the WC by diffusion of carbon onto Co (101).*

6.3.3.4 Internal and surface decarburization

Carbon can oxidize either on the surface, or inside a spray droplet. However, oxidation of carbon occurs mainly on the surface of the spray droplet, forming carbon monoxide gas which escapes into the atmosphere. Traces of oxidation can also be observed as small gas bubbles in the coating. W and Co remain metallic, but if they do oxidize, they are reduced back to the metallic form, by carbon. For this reason, no oxides can be found in the WC-Co coatings.

Chemical reactions inside and on the melt are presented in Equations 54-61. Carbon moves to the surface of the molten particle by diffusion, and is oxidized on the surface of the droplet by combustion gases, O_2, H_2O or CO_2. The temperature of the combustion gas is approximately 2000-2200°C. Reactions with water vapor and carbon dioxide are expected to be important because the availability of oxygen is limited and there is little time for oxidation. Inside the droplet, oxidation takes place with oxygen dissolved in the melt according to Reactions 55 and 57. For the reaction of carbon with oxygen in liquid cobalt (without W) $\Delta_R G°$= -75 kJ/mol at 1800°C was given (109):

$$1/2O_2 = [O]_{WCCo} \quad (54)$$

$$[O]_{WCCo} + [C]_{WCCo} = CO\ (g) \quad (55)$$

$$2[C]_{WCCo} + O_2(g) = 2CO(g) \quad (56)$$

$$[C]_{WCCo} + 2[O]_{WCCo} = CO_2 \quad (57)$$

$$[C]_{WCCo} + CO_2(g) = 2CO(g) \quad (58)$$

$$[C]_{WCCo} + H_2O(g) = H_2(g) + CO(g) \quad (59)$$

$$CoO + [C]_{WCCo} = Co + CO(g) \quad (60)$$

$$\Delta_R G = \Delta_R G° + RT\ln[p_{CO}/(a_C * a_O)] \quad (61)$$

Figure 44 shows the data of Kulikov for equilibria of carbon and oxygen in liquid cobalt (109). The maximum solubility of oxygen in cobalt is about 0.23 wt% at the melting point of cobalt 1451°C (91). When carbon is added reaction (Equation 55) takes place with equilibrium reaction shown by curves 1 in Figure 44. At high carbon and low oxygen content the dominant reaction is production of CO, Equation 55, but with decreasing carbon and increasing oxygen contents more CO_2 is formed (Equation 57). The interaction effect of tungsten (W) on carbon and oxygen in cobalt is not known. Carbon monoxide nucleates as bubbles in the supersaturated melt, forming small round bubbles <1 µm, as shown in Figure 45, but it was observed that oxygen content in WC-Co17 coating was approximately 0.1 wt % and the cobalt content 17 wt %.

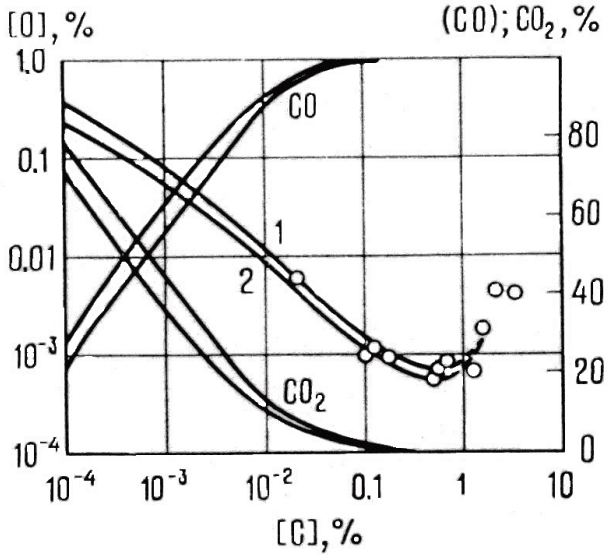

Figure 44. *Oxygen - carbon equilibria in liquid cobalt at 1873K (1) and 1768K (2) and partial pressures of carbon monoxide and carbon dioxide in the gas phase, respectively. Dots in the plot are experimental data (109).*

6.3.3.5 Gas evolution

Evolution of carbon monoxide is significant in decarburization of WC-Co. Even a small amount of decarburization can produce much carbon monoxide, e.g. 0.25 wt % loss of carbon produces 60 times more gas than the volume of the coating itself. Carbon loss of 2.5 wt % can produce 600 times of the volume of the coating itself. Such a large quantity of gas evolution is possible only if oxidation takes place mainly on the surface of the droplet, otherwise the coating would be full of CO bubbles. Thus, only a small portion of a coating oxidizes internally.

The formed CO nucleates in liquid $W_xC_yCo_z$(l) as gas bubbles, the size of which is from 0.1 to 5 μm as shown in Figure 25 and 26. They become deformed to elliptic shapes vertical to the spray direction. Bigger bubbles (> 5μm), which have collapsed, are seen as thin black lines in many SEM micrographs of WC-Co17. CO dissolves in the melt and forms an equilibrium concentration. Continuous chemical reactions and solidification make the melt supersaturated with [C] and [O] and there will be a tendency to form a new phase. In the supersaturated melt, gas bubbles can be produced by two ways. Carbon and oxygen reach the surface either by diffusion or convection, and react there, forming CO molecules. Gas bubbles may also form in the liquid metal. In the latter case, a new interface is formed even at a great distance from the outside surface. Gas bubbles can exist only if the equilibrium pressure p_e of a gas bubble is greater than the total external pressure p_{ex} (1 atm) and sum of capillary pressure $p\sigma = 2\sigma/r$, as shown in Equation 62 (110, 111). The surface energy of the metal is σ (mJ/m) while r is the radius of the bubble. Typical σ values for metal such as Fe and Ni, are 1950 and 2280 mJ/m^2, respectively (111).

$$p_e = 2\sigma/ r + p_{ex} \qquad (62)$$

Formation of gas bubbles depends on the presence of bubble nuclei, which must be able to grow. The expansion of the gas bubble requires a certain amount of work. Therefore, critical bubble radius r, or pressure p_e, must be exceeded, if the bubble is to remain stable and to

obtain equilibrium pressure. The internal pressure of a 0.01 µm gas bubble can be 7000 bar, in steel. For homogenous nucleation of nitrogen in stainless steel is difficult. Critical pressures have been reported, such as 70000 bar in pure iron (112).

Nucleation of small gas bubbles (>0.01µm) inside the liquid metal is thus, practically impossible. Therefore, the heterogeneous nucleation of gas bubbles occurs more easily. This decreases the energy and pressure required for the nucleation of gas bubbles. Here, heterogeneous nucleation is denoted as the formation of a new phase (bubble) with the aid of a third phase (solid or gas). The melt contains many small particles and cavities as nucleation sites for heterogeneous nucleation of gas bubbles. The solid interface of WC-Co, WC and W_2C particles may be considered as a source/nucleation site of bubbles in WCCo(l). Bubbles are seen to form at the boundary of solidifying metal, eg. on WC grains, are shown in Figure 25. The critical radius for heterogeneous nucleation in the WC-Co 35 system has been found to be 0.016 µm and the equilibrium pressure for a bubble has been found to be around 1200 bar (113). For homogenous nucleation, a pressure approximation can be calculated for a bubble of the same size to be about 4000 bar in WCCo(l). Liquid WCCo has a surface energy of approximately 1700 mJm^{-2}. Approximated equilibrium pressure of CO bubbles found in the WCCo (l) is at least 700 bar, in bubbles of 0.1 µm. Mass transfer (bubble growing) between a bubble and liquid phase occurs via diffusion.

The high pressure in the bubbles also explains why in thermal spraying, bubbles do not collapse and walls of the bubbles do not weld together during impact. Bubbles behave like an elastic ball during the impact moment, as shown in Figure 25. Gas bubbles in a coating and in a spray droplet are shown in Figure 45 and Figure 46. Bubbles are black round dots in the micrographs. Gas bubbles favor heterogeneous nucleation on the splat borders or on the W_2C dendrites.

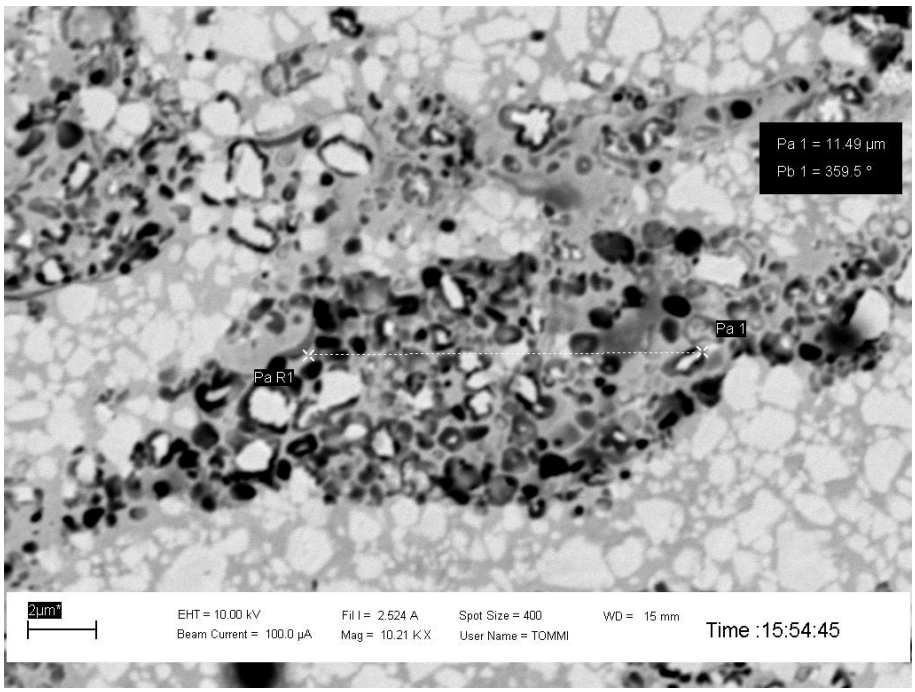

***Figure 45**. Gas porosity along splat boundaries. Black holes are gas bubbles and white/grey areas are the centre of the splat.*

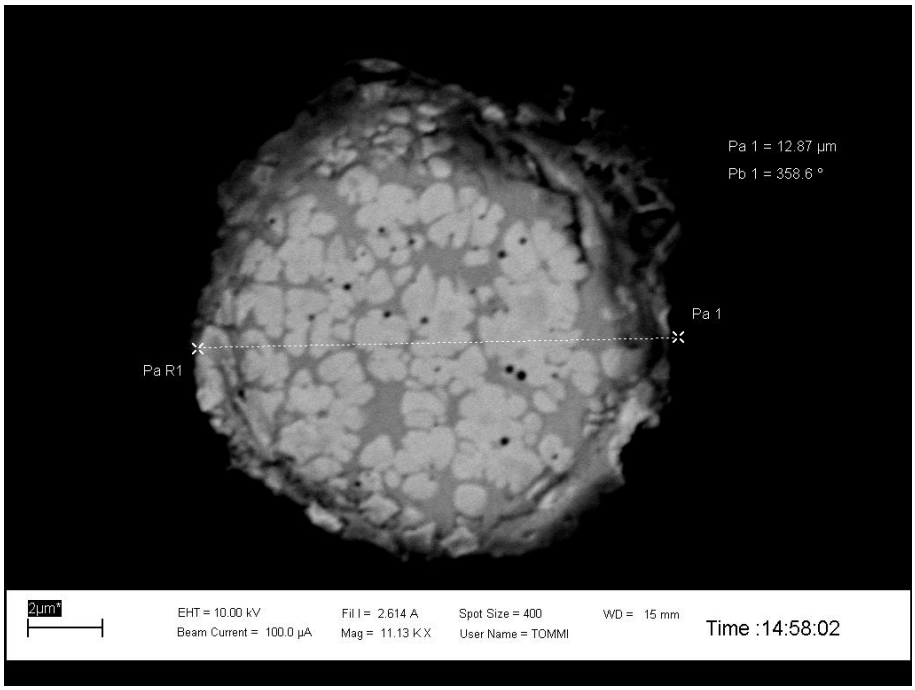

***Figure 46**. Cross-section of WC-CoCr spray particle after HVOF spraying. White areas are dendrites (W_2C) and grey areas are matrix around the WC grain. Black small holes are CO gas bubbles.*

6.3.3.6 Behavior of tungsten and cobalt

Spray particles undergo melting and solidification during flight. When the temperature of the spray particle lowers, solidification and precipitation occurs in the particle. In the XRD studies, tungsten has been found. The amount of tungsten increases as a function of an increasing degree of decarburization. Tungsten is not an equilibrium product of W-C-Co system and can still be found in the WC-Co structure after annealing of coating. Due to the decarburization, tungsten, cobalt and carbon should form M_6C and $M_{12}C$ carbides in equilibrium, in the W-C-Co system.

Tungsten can be formed in two ways in a coating; direct oxidation of solid WC, or precipitation/solidification of W from a melt of WCo. Direct oxidation of WC can occur on the surface of a spray particle when there is contact with combustion gases. The "open" surface of the WC-Co particle is presented in Figure 47. WC grains are seen on the surface of the WC-Co powder. Tungsten carbide can decompose via reaction of WC->W_2C->W, as presented in Table 14.

Solidification and precipitation is an alternative way of forming tungsten in the WC-Co system. Both Vernon (101) and we have found small W particles on the boundaries of two splats. Hot combustion gases decarburize the surface of the molten spray particle. The molten WCCo(l) transforms to carbon free WCo(l) melt. The melt consists of 60/40 wt/at % to 15/85 wt/at % of Co/W, and is supersaturated with W. The melt solidifies to amorphous phase and solid tungsten during the impact and cooling on the substrate. Small W precipitates (0.1 µm) can be found on the boundaries of two splats. Tungsten precipitate is shown in Figure 48 (101).

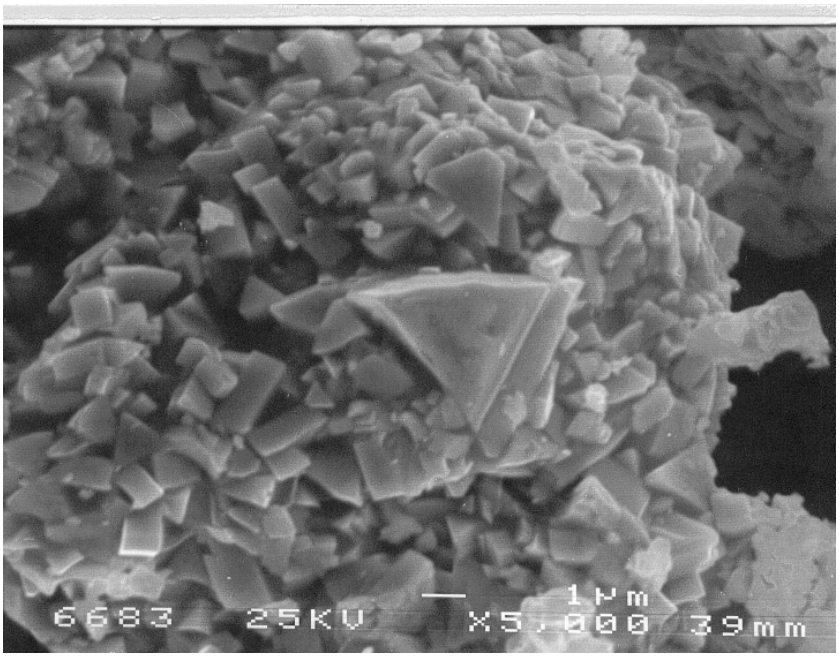

***Figure 47**. Surface of a WC-Co17 spray particle. Direct oxidation of WC can take place on a surface of a spray particle. Prismatic WC grains are embedded in the Co matrix.*

Carbon has a strong affinity for oxygen, and therefore reactions of oxygen with Co and W are not remarkable. Carbon reaction with WO_3, inside or on the melt of $W_xC_yCo_z(l)$, is not considered possible, because WO_3 is volatile above 700°C. $WO_3(g)$ is formed on the surface of the spray particle, and evaporates immediately on the surface of $W_xC_yCo_z(l)$ or WC. Therefore, WO_3 does not dissolve in liquid $W_xC_yCo_z(l)$ and cannot react with dissolved carbon [C]. In the plasma coating process, WC-Co17 emission of tungsten can be seen in the plume of a plasma gun. The emission of tungsten $WO_3(g)$ shows that volatile oxide of tungsten has formed (114). Emission of tungsten is not possible from pure tungsten, because the boiling point of tungsten is 5500°C.

Cobalt oxidizes in atmospheric O_2, but as was shown earlier, Co does not oxidize with CO_2 or H_2O. However, the formation of CoO is possible with the aid of oxygen on the surface of the spray particle. It is possible that CoO can be mixed into the melt by aerodynamic steering and is reduced by carbon. CoO dissolves into the melt of $W_xC_yCo_z(l)$, above the melting point of CoO (1810°C). Carbon, however, reduces CoO back to metallic Co. This is called liquid-liquid reaction during flight of the spray particle. Oxidation of tungsten is possible with O_2, but not H_2O and CO_2. As shown earlier, WO_3 is volatile and therefore cannot be found in the coatings. Furthermore, carbon can reduce WO_3 to metallic W. Non-oxidation of cobalt is considered be important for the mechanical properties of WC-Co coating. Cobalt does not make oxide layers between two splats or lamellas. The nonoxidised surfaces of splats are believed to improve the internal strength of the coating.

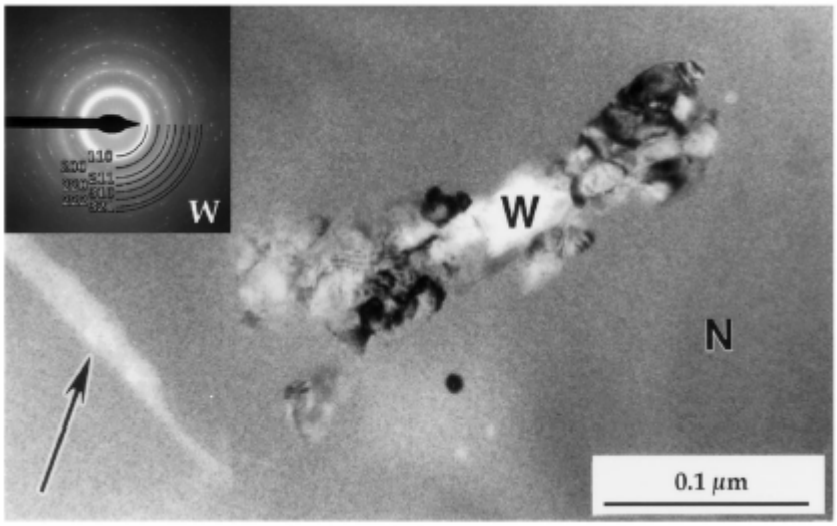

***Figure 48**. TEM micrograph of W precipitate in a coating. N indicates nano-crystalline WCCo binder phase (101).*

6.3.3.7 Structural changes in in-flight spray particles

Thermal spraying decarburizes 10-60% of carbon in WC-Co coatings. The balance of Co and W remains constant. Experimentally it has been observed that the reaction rate of carbon is controlled by the temperature of the spray particles. High temperature of spray particles leads to a high degree of decarburization. Therefore spraying of WC-Co coatings has changed to using colder spray processes; plasma APS, to HVOF and HVAF (High Velocity Air Fuel) spraying. Spray particle temperature controls the carbon diffusion rate to the surface of the spray particle. The reaction rate is controlled by the diffusion of carbon to the surface of the spray particle. Oxidizing gases are $O_2/H_2O/CO_2$.

The degree of decarburization can be analyzed by several methods: LECO analysis gives carbon loss in wt % and XRF shows phase changes. However, the features examined in this section need microstructural visualization. Visualizing in-flight oxidation can be done by spraying particles into water. The microstructure of cross-sectioned and polished particles was examined by SEM. The particles were sprayed into water to prevent the destruction of in-flight microstructure during impact on the substrate. Examples of the investigated in-flight structures of WC-CoCr spray particles are presented in Figure 49 - 52.

The SEM micrographs of the spray droplets show the evolution of WC particles in the WCCo melt. During spraying, small WC grains dissolve, while large grains become round. Finally, all grains dissolve into the melt. During cooling, W-C rich dendrites grow on the surface of the remaining WC crystals, forming W_2C. When decarburization proceeds, oxygen dissolves in the melt, forming carbon monoxide bubbles. The surface tension makes the surface of the spray particle smooth and round. Grain size of carbides seems to increase during the spray process.

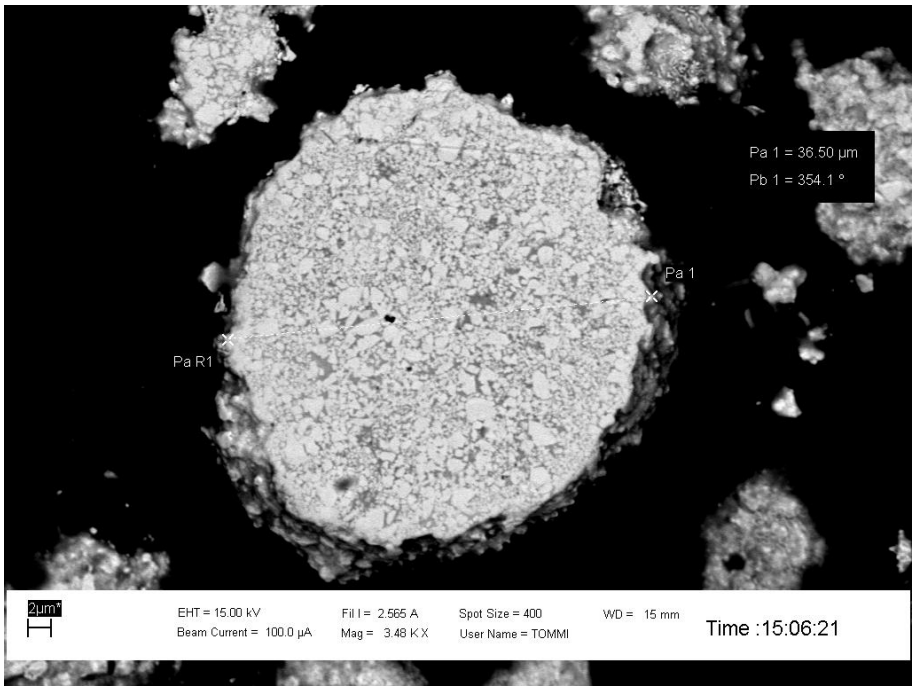

Figure 49. *Cross-section of an initial WC-CoCr particle before spraying. Particle contains many sharp small WC grains and a low concentration of CrCo matrix.*

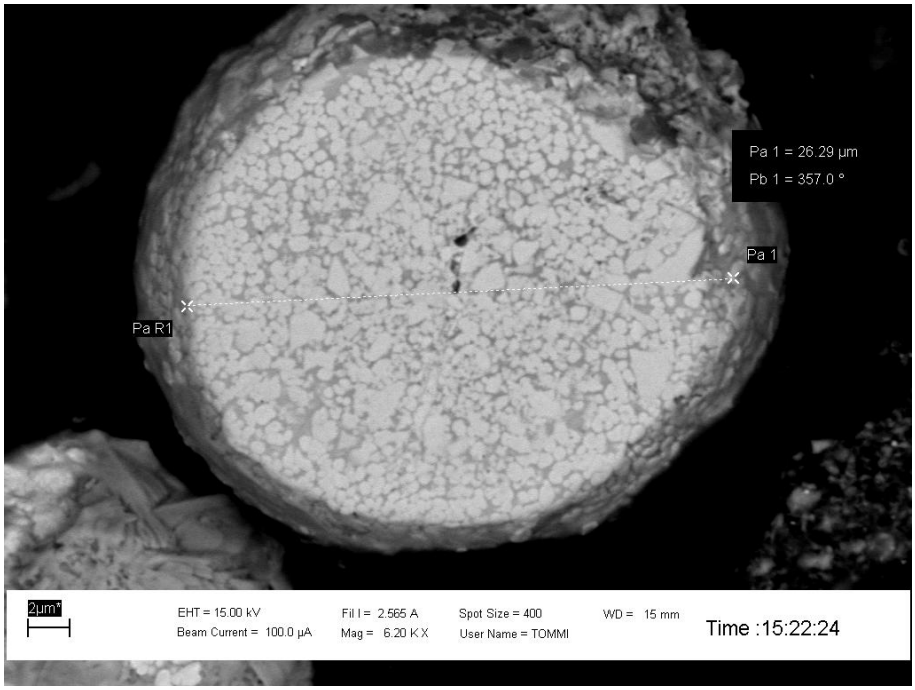

Figure 50. *Cross-section of an in-flight WC-CoCr particle. Low F/O ratio in spraying, low particle temperature. Melting has started, WC grains have decreased, and grey matrix has increased.*

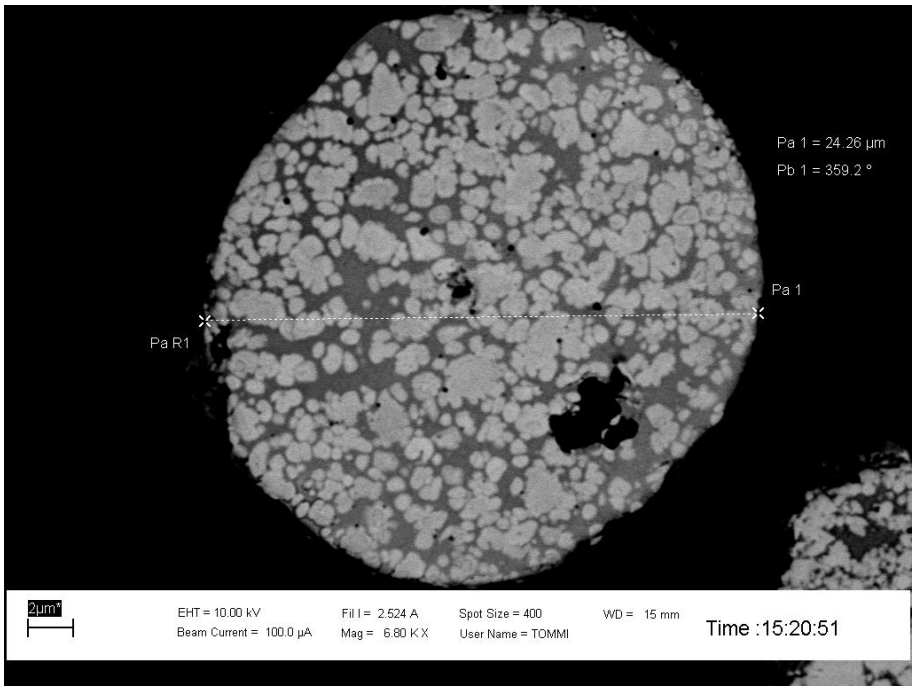

Figure 51. *Cross-section of in-flight WC-CoCr particle. Higher F/O ratio and particle temperature than in Fig. 50. WC grains have decreased and dendrite structure has developed around the remaining WC grains.*

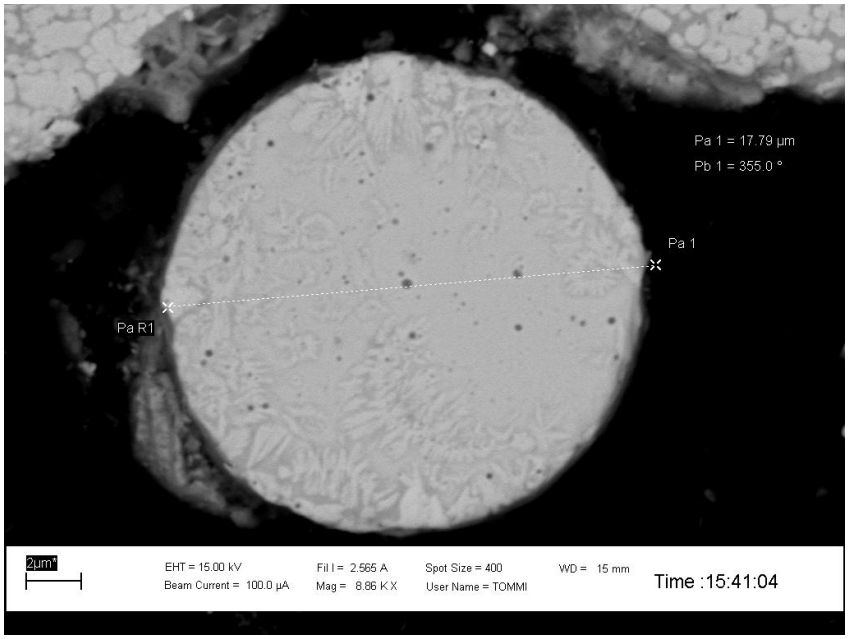

Figure 52. *Cross-section of in-flight WC-CoCr particle. The highest F/O ratio and particle temperature. WC grains have completely dissolved in the matrix and CO bubbles appear in the structure.*

6.3.3.8 Adiabatic heating of spray particles

Combustion of carbon forms carbon monoxide and heat. Carbon loss of 2 wt % liberates heat (220 J/kg) in the WC-Co17 coating. The carbon content of WC-Co17 is 5.2 wt %. The heat released during decarburization raises the adiabatic temperature, ΔT^{ad}, of the coating to approximately

1000°C. The coating also releases the combustion gas (CO) at 40 l/kg. Most of heat and gas formed is liberated in the HVOF process. All the heat which has been released, cannot be used to raise the temperature of the spray particles. The high heat and gas liberation is typical for WC-Co particles.

6.4 Oxidation of NiCr80/20 coating

The NiCr80/20 experiments showed that a high quenching rate of the coating has a strong effect on the microstructure of the coating and the degree of oxidation. The results are shown in Figure 30 and 31. High quenching rates can be obtained with long work distances (200 to 350 mm). High coating quenching rates can also be obtained by using high work speeds, which is a new finding. This experiment showed why the typical HVOF work distance is always recommended to be from 200 to 350 mm. Varying the work speed range from 0.03 to 30 m/s, made it possible to vary the HVOF gun flame power (≅100 kW/area/time) energy density to the substrate, in a ratio of 1:1000. The high oxygen content found, indicates that a high quenching rate is important in obtaining low oxygen content. If the intense heat of the hot plume contacts the substrate, high quenching rates of the spray particles are impossible. The coating begins to oxidise more on the substrate than in either the gun nozzle or the plume. This result can be clearly seen in the microstructure of the coating, as the substrate oxidation phenomenon, Figure 31 (g) and Figure 53. As evidenced by the oxide layers observed around the spray particles, the degree of deformation remained constant at all work distances and work speeds. The constant degree of deformation observed, indicates that no significant heating or cooling of spray particles takes place at work distances between 50 and 300 mm. This finding indicates that spray particles were already heated and oxidised in the HVOF gun nozzle. The spray particles in-flight temperature measurements, have also shown that the spray particles have a nearly constant temperature, from the HVOF gun nozzle to the work distance of 400 mm (90). The low flame heat input on the substrate was the result of the high HVOF jet work speed. This produced the low coating and spray coupon surface temperature. High work speed avoided burning of the coating by the hot flame and allowed the spray particles to cool quickly.

The result of oxygen content (50 mm work distance) showed that NiCr80/20 spray particles already oxidise in the nozzle. The increase in the degree of oxidation is relatively small during the flight in the plume to the substrate, some 0.5 wt %. The coating on the first coupon (at 50 mm work distance) showed that 70% of the oxidation of the NiCr80/20 coatings occurred in the nozzle. Additional oxidation in the plume and on the coupons at work distances of 100 to 350 mm, were relatively low, only 30% of the total amount of oxidation. These results of oxidation of coatings were supported by the thermodynamic calculations, which showed that oxidation is possible, both in the nozzle and in the combustion chamber.

Both measured and calculated (HSC) values of p_{O2} showed that the values of p_{O2} are always too high to avoid Cr oxidation in the HVOF gun nozzle and in the plume. The oxygen partial pressure in the combustion chamber and in the nozzle is very low, with typical values for p_{O2} being $<10^{-6}$ bar. This low concentration level of p_{O2}, suggests that hardly any metal oxidation occurs in a HVOF gun. It was expected that the oxidation rate would be slow in the combustion chamber and nozzle, compared to the rate in the plume. It was for this reason that the coating material was expected to largely oxidise, in the plume or on the substrate, as Hackett has proposed (14). The mixing of air with the plume of the jet always causes the prevailing gas atmosphere to become highly oxidising for all metals and alloys, p_{O2} rising to

over 0.1 bar (81, 82). On the substrate, the measured p_{O2} levels are always too high to avoid metal oxidation.

Calculations with HSC showed that there is also a high concentration of H_2O in the nozzle, when combusting hydrogen and oxygen. If the fuel is a hydrocarbon, the oxidising compound, CO_2, is also present in the nozzle. In the nozzle, the H_2O concentration can be over 50% depending on the F/O ratio and flame temperature (Tables 1 and 2). If we compare the ratio of free oxygen, O_2, to H_2O, we see that the concentration of H_2O is several orders of magnitude higher than that of O_2. The low calculated and measured values for p_{O2} level, raise the question of whether any other oxidation reactions then direct oxidation by pure oxygen, is present. The results suggest the following reations for oxidation in the nozzle:

$$H_2O(g) + Me = MeO + H_2(g) \quad (63)$$

and

$$CO_2(g) + Me = MeO + CO(g) \quad (64)$$

where Me is a metal or an alloy. As Equations 63 and 64 show that oxidation of metals or alloys is also possible with the aid of H_2O and CO_2, we consider that the main cause of metal oxidation is the high concentration of H_2O and CO_2 in the nozzle rather than "free oxygen", i.e. O_2. When the hot spray powder travels inside the plume, from a 50 mm work distance to one of 350 mm, the increase of oxygen content in the NiCr80/20 coating is relatively small, ≈ 0.5 wt %. Although the p_{O2} level in the plume atmosphere (see Figure 12), is ten thousand times higher than the p_{O2} level in the flame at the HVOF gun nozzle, the coating oxidises less in the plume than in the nozzle. Measurements and calculations have shown that the dominant oxidising compound in the plume is pure oxygen rather than H_2O or CO_2, as a result of air mixing with the jet, (Figure 12 and Figure 13). Calculations showed that oxidation of NiCr alloy is possible with the aid of H_2O and CO_2 (Table 16). The reactions are shown at 1000°C and 1800°C. The reaction of Ni with H_2O is not possible because of the high positive Gibbs energy.

Table 16. *Reaction equations of Ni and Cr with oxygen and combustion gases. Gibbs energies for chemical reactions at temperatures of 1000°C and 1800°C.*

Reaction	$\Delta_R G°1000°C$ kJ/mol^{-1}	$\Delta_R G°1800°C$ kJ/mol^{-1}
$4/3Cr+O_2(g) = 2/3Cr_2O_3$	-602.199	-401.614
$2Ni+O_{2(g)}=2NiO$	-249.952	-249.952
$2Cr +3H_2O(g) = Cr_2O_3+3H_2(g)$	-262.574	-207.238
$Ni+H_2O(g)=NiO+H_2(g)$	52.527	78.248
$2Cr + 3CO_2(g) = Cr_2O_3+3CO(g)$	-287.260	-290.037
$2/3Cr+O_2 (g)= 2/3CrO_3(g)$	-159.868	-121.517

The high degree of spray powder oxidation in the HVOF gun nozzle, is likely to be the result of the high temperature (2000-2500°C) in the nozzle. The gas temperature is much lower in the plume (1000-400°C) than in the nozzle. Oxidation kinetics suggests that gas temperature is the most powerful factor in the oxidation process. Furthermore, the oxide layer growing on the surface of the spray powder slows down the oxidation rate.
The oxygen content of the NiCr80/20 coating was found to be 2.0, 2.2 and 2.5 wt %, at work

distances of 50, 200 and 350 mm, respectively. Figure 28 shows the oxygen content of NiCr80/20 coating as a function of the work distance. The results show that the coating is already oxidised at the short work distance and oxygen content of the coating increases as the work distance increases.

A similar type of result was obtained with WC-Co17 powder, when carbon depletion in the coating was analysed instead of oxidation. The WC-Co17 coatings were sprayed at work distances of 50, 200 and 350 mm and a work speed of 3 m/s. The carbon loss in the coatings was measured and found to vary from 2.0 to 2.4 wt %. Carbon content in the WC-Co17 coating was observed to decrease with increasing work distance increases, as shown in earlier Figure 21.

The spray area, flame and a part of the plume proved to be the low p_{O2} areas of the flame. It was expected that in a real process, this position would produce relatively low oxidation of coatings, because both the measured and calculated p_{O2} levels would be low in the flame. The work speed was set high in order to keep heat input from the flame to the surface to be coated, at a low level. Rapid quenching was expected to stop the oxidation process, immediately after the spray particles impact on the substrate (115).

Finally, we can observe the microstructural changes caused by internal surface oxidation. Surface oxidation occurs on the spray coupon. Oxidation occurs during each pass of the spray gun. The hot substrate or low work speed can cause internal surface oxidation as shown in Figure 53. The black vertical oxidation patterns represent each HVOF gun pass over the substrate. Six spray passes can be identified in the cross section of the coating. The main cause of the surface oxidation is low cooling speed of the spray particles. If the molten particles do not solidify quickly, hot combustion gases oxidise the spray particles. Low working speed allows the hot combustion gases to heat the coating. Therefore it is necessary to use a high work speed during the spray process, as presented in Figure 31. The temperature of the substrate can easily rise from 100 to 400°C, if low work speed is used. In the case of Figure 53, internal surface oxidation can be avoided by increasing the work speed. The increased work speed reduces the local surface temperature, allowing the spray particles to cool below oxidation temperature.

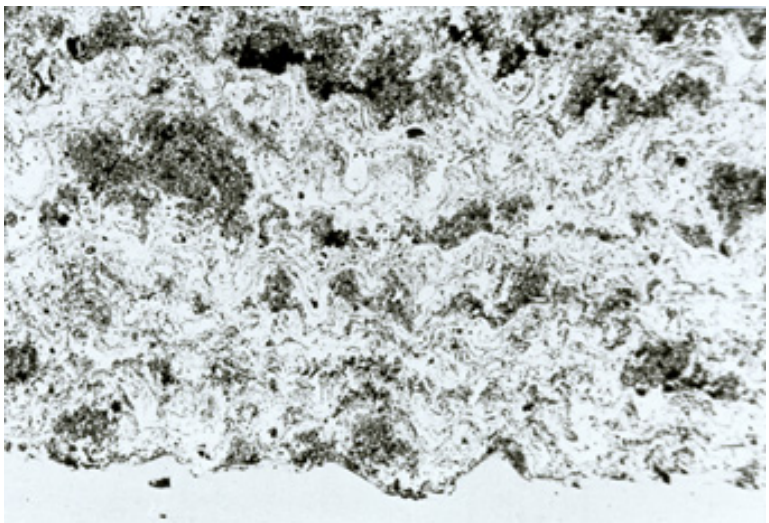

Figure 53. *Microstructure showing internal surface oxidation. Effect of low quenching rate of the spray particles on the microstructure of the coating. Cross-section of oxidised Inconel 625 coating.*

6.5 Overall discussion of oxidation in HVOF spraying

In the next section the main features of oxidation processes in HVOF spraying are summarised. Model of decarburization of WC-Co spray particle is presented.

6.5.1 Oxidation environment in HVOF spraying

As a conclusion of the thermodynamic calculations and the spraying experiments, two schematic figures of the oxidation process in the HVOF gun, can be drawn. The first one presents locations of the starting points of element oxidation in HVOF spraying and the second one which presents effect of HVOF process variables on the oxidation and decarburizing degree of WC-Co and NiCr coatings.

Different elements, alloys and compounds start to oxidize in different locations in HVOF spraying. Figure 54 shows the starting point of oxidation for Ni, Co, WC and Cr. The starting point is related to the element affinity for oxygen, the temperature and the partial pressure of oxygen in the gas. Figure 54 shows that the partial pressure of oxygen depends on the F/O ratio and the ambient temperature as shown earlier in Figure 32 and Figure 33. The upper curve is for the stoichiometric F/O ratio, 2/1 and the lower curve is for F/O ratio, 4/1. The results are combined with oxygen partial pressure measurements (72) and equilibrium calculations for the hydrogen-oxygen flame (57). The air entrance in the plume increases oxygen partial pressure, but do not effect on the starting point of oxidation of elements. The elements start to oxidise in the nozzle and in the beginning of the plume. The oxidation of elements continues in the end of the plume and stops on the substrate.

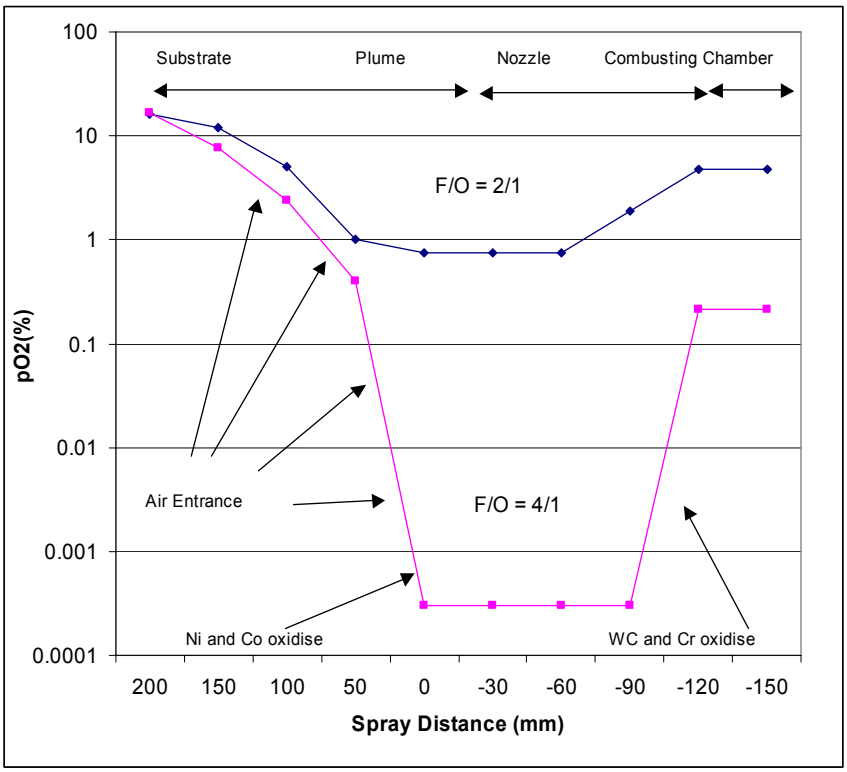

Figure 54. *Locations of the starting points of element oxidation in HVOF spraying. Oxygen partial pressures were calculated for hydrogen combustion with oxygen in HVOF spraying process.*

Oxygen partial pressure is quite high in the combustion chamber (0.2-4.7 mol %) for the hydrogen-oxygen flame. It is high because the high temperature (2750°C) shifts the chemical equilibrium to the direction of the reactants. The combustion chamber is the place where Cr and WC start to oxidise, while Co and Ni remain unoxidised.

The partial pressure of oxygen decreases in the nozzle due to a temperature drop of the flame to 2000°C, caused by heat transfer to the environment and partial conversion of the flame heat energy to gas velocity. The chemical equilibrium shifts towards the product side of the reactions (Equations 22 and 26). The flame remains protective for some metals, i.e. Co, Ni and Fe. The entrance of air increases the oxygen partial pressure of the flame/plume and Ni, Co, Fe and other metals start to oxidize.

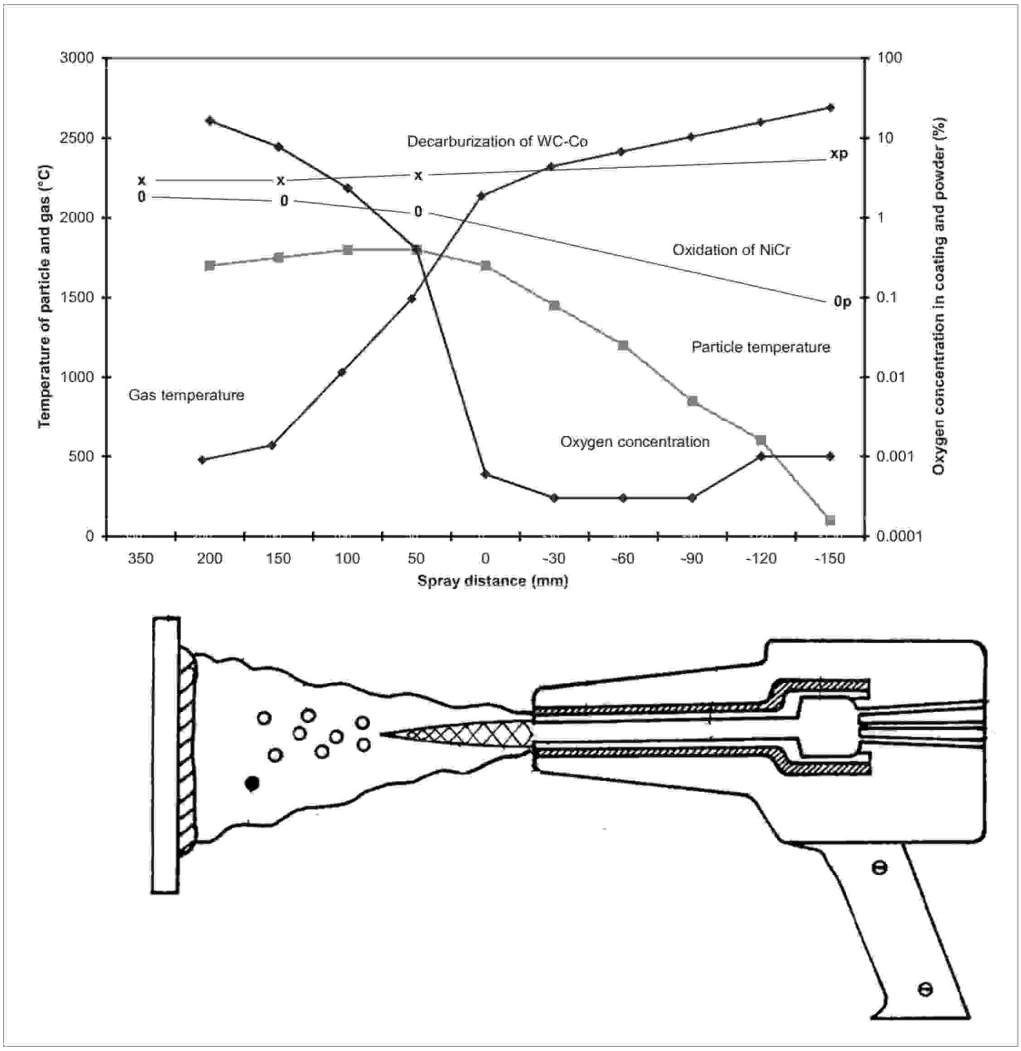

Figure 55. *Schematic presentation of the decarburizing and oxidation process in HVOF spraying: the oxidation degree of coatings (WC-Co and NiCr) is shown as a function of location (spray distance) and gas and particle temperatures and oxygen partial pressures. The lines marked with xp and 0p represent initial carbon and oxygen contents in the spray powders, respectively. Below a schematic cross section of a HVOF gun presented in Fig 1 and fitted in the scale of spraying schema.*

The oxidation and decarburization degrees are related to the place and temperature in the flame. The oxidation and decarburization process is presented schematically in Figure 55. The figure shows the oxidation or decarburization degree of lines marked with WC-Co(**x**) and

NiCr (**0**) as a function of spray distance, as presented in Figure 22 and Figure 28. The lines marked with **xp** and **0p** represent the starting content of carbon and oxygen in the corresponding spray powders. The oxidation and decarburization did not increase significantly in the plume. Most of oxidation and decarburization of the spray particles already occurred in the hot nozzle of HVOF gun. Temperature of the flame drops in the plume while the temperature of the particles has only minor changes. Oxygen content rises up to 100 – 1000 times higher level in the plume than in the nozzle. From the Figure 55 one can make a conclusion that the flame temperature has a stronger effect on the oxidation degree than the oxygen partial pressure. To minimize oxidation a short spraying distance (50 mm) should be favored. Unfortunately, a short spray distance causes overheating of spray items and, therefore, in practical spraying a compromise must be found between these different factors.

Figure 55 was constructed based on the measured gas temperatures and oxygen partial pressures and the thermodynamic calculations carried out. The spray particle temperature was obtained by measurements. The results of oxidation of NiCr and WC-Co were measured in this work.

6.5.2 Proposed mechanism for decarburization of WC-Co

The following model is proposed for decarburization of WC-Co particles and coating in HVOF spraying, is shown in Figure 56. The main reasons for decarburization of WC-Co are the high particle (1800°C) and gas temperature (2200°C) in the HVOF nozzle, even though the oxygen partial pressure is very low both in the nozzle and in the combustion chamber. The other spray parameters, the work speed, the chamber pressure and the work distance control the degree of oxidation and decarburization less than expected.

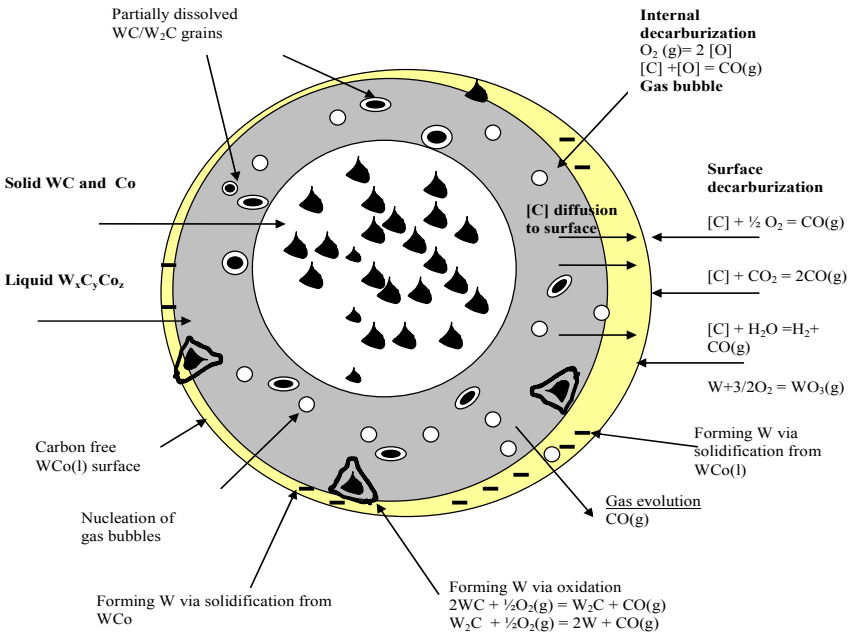

Figure 56. *Decarburization process of WC-Co particle during flight. Spray particle temperature is above the melting point of cobalt, > 1451°C, and in a HVOF combustion atmosphere at gas temperature above 2000°C.*

The main oxidation mechanism for WC-Co decarburization is liquid oxidation, taking place

above >1500°C. Liquid oxidation is based on dissolving WC in the Co matrix. WC and Co form the liquid phase of $W_xC_yCo_z$, which acts as a diffusion path for carbon. Carbon diffuses to the surface of a spray particle, where most of oxidation occurs. Carbon oxidizes to carbon monoxide with the aid of combustion gases and air. Evolution of gas is a significant phenomenon; the volume of gas can be 500 times more than the volume of the coating itself. Cobalt and tungsten do not oxidize due to the high affinity of carbon for oxygen. Carbon reduces the other oxides.

During the melting and solidification processes, metastable phases are formed in the ternary W-C-Co system. Such phases do not exist in the feed stock powder and normal hard metal production. The metastable products of rapid melting and solidification are W_2C, W and a nano-phase .

The results were obtained with sintered and crushed WC-Co17 spray powder. It is expected that these results can be generalised to other types of WC-Co powders, both agglomerated and sintered, with higher or lower Co content in the WC-Co powder too. These results can also be applied to bigger and smaller particle sizes of a spray powder.

7. SUMMARY

The aim of thesis was to study oxidation phenomena in the HVOF spraying process. The experimental and theoretical work performed, led to the following main conclusions:

1. Oxidation always occurs in HVOF spraying. Thermodynamic calculations show that oxidation cannot be avoided by altering the fuel or the metal composition.

2. Due to the short dwell time of the process, oxidation of alloys and metals proceed only to a certain degree. Oxidation took place in three distinct steps which were confirmed by thermodynamic calculations:

- in the HVOF gun nozzle,
- in the HVOF gun plume,
- on the substrate.

3. In this study, for the first time, it was clearly shown that spray powder oxidises primarily in the HVOF gun nozzle, only to a small extent in the plume, and to quite a small degree at the surface to be coated, if the surface is cold and the work speed is sufficiently high.

4. The thermodynamic calculations, examination of reaction kinetics, and experimental studies, showed that the spray powder oxidation is a complex phenomenon involving the following processes:

- selective oxidation, with some elements oxidising more rapidly than others,
- oxides formed in the spray process, can be in some cases gaseous or volatile oxides, or they can be solid or liquid oxides depending on the compound and the ambient temperature,
- oxidation rate is strongly related to gas and particle temperatures and the surface area of the spray powders being employed,
- in addition to pure oxygen, CO_2 and H_2O can also act as oxidizing gases,
- the flame can be non-oxidizing for some elements, such as Co and Ni, but it is always highly oxidising for other elements such as Cr, W and C. However, all elements are are in an oxidised state, more or less, in the plume depending on the spray conditions.

5. Thermodynamic and kinetic estimations, supported by experimental observations, showed that the oxidation process in the HVOF spray cannot be completely prevented, but can be controlled by the following means:

- reduction of the flame temperature, i.e. lowering the spray particle temperature,
- reduction of the spray particle surface area, i.e. using a larger particle size,
- use of a higher gas velocity, higher gas density and a longer nozzle, i.e. lowering the particle dwell time in the spray process and lowering the spray particle temperature, and,
- employment of effective substrate cooling, an adequate work distance and a sufficiently rapid work speed.

All these findings can be applied in the normal thermal spray production.

Some remarks on the coating microstructure can also be made:

- Examination of the coating microstructure is an excellent way to study the coating oxidation morphology but does not provide a quantitative estimation of the degree of coating oxidation.
- In WC-Co coating, no oxides were found in the microstructure or by chemical analysis. In this case, the primary oxidising component was carbon (from WC) which forms CO gas. Gas bubbles were found in the microstructure.
- Oxidation of WC-Co coatings occurs mainly in the liquid state by carbon diffusion to the surface of a spray particle and further formation of CO(g).
- On NiCr80/20 and Cr_3C_2-NiCr75/25 coating, solid oxide (Cr_2O_3), was found, both by examining the coating microstructure, and by chemical analysis.

References

[1] Tommi, V., Rajamäki, E., Korpiola, K., Mechanical properties of thermal spray coatings, New Surfaces for a New Millennium, Proceedings of the International Thermal Spray Conference. Berndt, C., Khor, K. & Lu, E. (eds.) Lugscheider (ed.). ASM International. Materials Parks, Ohio (2001)

[2] Korpiola, K., Varis, T., Termisesti ruiskutettujen pinnoitteiden mekaaniset ominaisuudet, (Mechanical properties of thermally sprayed coatings, in Finnish) 2000. VTT Valmistustekniikka, Espoo. 39 s. VTT Tiedotteita - Meddelanden - Research Notes: 2012, ISBN 951-38-5632-1; 951-38-5633-X

[3] Taylor, M.P., Evans, H.E., Formation of diffusion cells in LPPS MCrAlY coatings, Materials at High Temperatures (UK), vol. 20, no. 4, pp. 461-465, 2003

[4]Anton, R., Birkner, J., Czech, N., Stamm, W., Degradation of advanced MCrAlY coatings by oxidation and interdiffusion, Trans. Tech. Publications Ltd., Materials Science Forum (Switzerland), vol. 369-372, Part 2, pp. 719-726, 2001

[5] Vreijling, M., Van Westing, E. P., Ferrari, G., Hofman, R., De Wit J., Corrosion protection using passivating thermal spray coatings, Norwegian University of Science and Technology (Norway), pp. 451-456, 1997

[6] Hirvonen, J-P., Mahiout, A., Likonen, J., Corrosive Wear Properties of Some HVOF-Sprayed Coatings, Deutscher Verlag fur Schweisstechnik DVS-Verlag GmbH (Germany), pp. 276-279, 1993

[7] Nerz, J.E.; Kushner B.A., Jr. Rotolico, A.J., Microstructural Evaluation of Tungsten Carbide-Cobalt Coatings, ASM International (USA), pp. 115-120, 1992.

[8] Smith, R.W., Knight, R., Thermal Spraying 1: Powder Consolidation from Coating to Forming. JOM, 1995, August, p. 32 - 39.

[9] Herman, H., Plasma Sprayed Coatings, Scientific American, Vol. 259, No. 3, 1988, s. 78 - 83.

[10] Siitonen, P., Kinos, T., Kettunen, P., Corrosion Properties of Stainless Steel Coatings Made by Different Methods of Thermal Spraying. In: Bernt, C. C. & Sampath, S. (eds.), Thermal Spray Industrial Applications. Boston, USA, 1994, ASM Intentional, Ohio, USA, 1994, p. 105 - 110.

[11] Varis T., Termisesti ruiskutetun nikkelikromipinnoitteen murtolujuuden, kimmomodulin ja Poissonin-vakion määrittäminen vetokokeella, Otaniemi, 1998, 84 p, MSc Thesis (In Finnish).

[12] Kreyer, H., Zimmermann, S., Heinrichs, S., The Role of the Fuel Gas in the HVOF Process. In: Ohimori, A., Thermal Spraying (ed.), Current Status and Future Trends. Kobe, Japan, 1995, Proceedings of ITCS 95, Kobe, Japan, 1996, p. 393 - 398.

[13] Krayer, H., Schwetzke, R., Zimmerman, S., High Velocity Oxy-Fuel Flame Spraying-Process and Coating Characteristics. In: Bernt, C. C. (ed.), Thermal Spray: Practical Solutions for Engineering Problems. Cincinnati, USA, 11 - 17 October, 1996, ASM International, Materials Park, Ohio, 1996, p. 451 - 456.

[14] Hackett, C. M., Settles, G. S., Turbulent Mixing of the HVOF Thermal Spray and Coating Oxidation, In: Bernt, C. C. & Sampath, S. (eds.), Thermal Spray Industrial Applications. Boston, USA, 1994, ASM Intentional, Ohio, USA, 1994, p. 307 - 312.

[15] Korpiola, K., Jalkanen, H., Kinos, T., Siitonen, P., Vuoristo, P., Oxygen Partial Pressure Measurements. In: Bernt, C. C. (ed.). Thermal Spray: Practical Solutions for Engineering Problems. Cincinnati. USA. 7 - 11 October. 1996. ASM International, Materials Park, Ohio, 1996, p. 471 - 488.

[16] Korpiola, K., Vuoristo, P., Effect of HVOF Gas Velocity and Fuel to Oxygen Ratio on the Wear Properties of Tungsten Carbide Coating. In: Bernt, C. C. (ed.). Thermal Spray: Practical Solutions for Engineering Problems. Cincinnati. USA. 11 - 17 October. 1996. ASM International. Materials Park. Ohio, 1996, ASM International, Ohio, 1996, p. 177 - 184.

[17] Karami, A., K., Verdon, C. H., Hydro Abrasive Wear Behaviors of High Velocity Oxy/Fuel Thermally Sprayed WC - M Coatings, Surface and Coating Technology, 1993, 62, p. 493 - 498.

[18] Kirner, K., Concerning the Metallurgy of Tungsten Carbides in Thermal Spraying, Welding and Cutting, 1989, No 11, p. 194 - 195.

[19] Mäntylä, T. A., Niemi, K. J., Vuoristo, P., Abrasion Wear Resistance of Tungsten Carbide Coatings Prepared by Various Thermal Spraying Techniques. In: Proc. 2 nd Plasma Technik Symposium. Vol. 1., Lucerne, Switzerland, June 5 - 7, 1991, Switzerland, 1991, p. 287 - 297.

[20] Tu, D., Chang, S., Chao, C., Lin, C., Tungsten Carbide Phase Transformation during the Plasma Spray Process, J. Vac. Sci. Technology, 1985, A3(6). Nov./Dec., p. 25 - 30.

[21] Chandler, P.E., Nicoll, A.R., Plasma Sprayed Tungsten-Carbide Cobalt Coatings, In: Proceedings of 2nd International Conference on Surface Engineering. Stratford-upon-Avon, England, 16 - 18 June 1987, p. 403 - 411.

[23] Ramnaht, V., Jayaraman, N., Characterizing and Wear Performance of Plasma Sprayed WC-Co Coatings, Material Science and Technology, 1989, Vol. 5, April, p.120 - 130.

[24] Vinayo, M. E., Kassabji, F., Guyonnet, J., Fauchais, P., Plasma Sprayed WC - Co Coatings: Influence of Spray Conditions (Atmospheric and Low Pressure Plasma Spraying) on the Crystal Structure, Porosity and Hardness. J. Vac. Sci. Technology, 1985, A3(6), Nov./Dec., p. 100 - 110.

[25] Niemi, K., Vuoristo, P., Mäntylä, T., Barbetzat, G., Nicoll, A. R., Abrasion Wear Resistance of Carbide Coatings Deposited by Plasma and High Velocity Combustion Process, In: Bernt, C. C. (ed.), Thermal Spray: International Advances in Coating Technology, Orlando, USA, 1992, ASM International, Materials Park, Ohio, 1992, p.685 - 690.

[26] Metals Handbook. Ninth Edition. Vol. 9. Metallography and Microstructures, American Society of Metals Park, Ohio, USA, 1992, p. 272 - 279.

[27] Wayne, S. F., Sampath, S., Structure/Property Relationship in Sintered and Thermally Sprayed WC - Co. Journal of Thermal Spray Technology, 1992, Vol. 1(4), p. 307 - 316.

[28] Kannan, R., Nicoll, A. R., Plasma Sprayed Tungsten Carbide-Cobalt Coatings, In: ASTM, National Symposium in Surface Treatment of Metals. Bombay, India, 1987, p. 15 - 25.

[29] Vuoristo, P., Niemi, K., Mäntylä, T., Berger, L-M., Nebelung, M., Comparison of Different Hardmetal- Like Coatings Sprayed by Plasma and Detonation Process, In: Berndt, C. C. & Sampath, S. (eds.), Advances in Thermal Spray Science and Technology. Houston, Texas, USA, 1995, ASM International, Ohio, 1995, p. 7 - 10.

[30] 1988 Annual Book of ASTM Standards, Non-ferrous Metal Products, Vol. 02.05, Standard Test Method for Metallographic Determination of Microstructures in Cemented Carbides, p. 434 - 438.

[31] Brookes, K. J. A., Hard Metals and Other Hard Materials, EMPA, UK 1992, p. 200.

[32] Swank, W. D., Fincke, J. R., Haggard, D. C., HVOF Gas Flow Field Characteristics, In: Bernt, C. C. & Sampath, S. (eds.), Thermal Spray Industrial Applications. Boston, USA, 1994, ASM International, Ohio, USA, 1994, p. 313 - 318.

[33] Sobolev, V. V., Guilemany, J. M., Calero, J. A., Formation of Structure of WC - Co Coatings on Aluminum Alloy Substrate During High Velocity-Oxygen Fuel (HVOF) Spraying. Journal of Thermal Spray Technology, 1995, Vol. 4, No. 4, p. 401 - 407.

[34] Thorpe, M. L., Richter, H. J., Pragmatic Analysis and Comparison of HVOF Process. Journal of Thermal Spray Technology, 1992, Vol. 1, No. 2, p. 161 - 170.

[35] Fantassi, S., Vardelle, M., Vardelle, A., Fauchais, P., Influence of the Velocity of Plasma-Sprayed Particles on Splat Formation. Journal of Thermal Spray Technology, 1993, Vol. 2, No. 4, p. 379 - 384.

[36] Chang, C. H., More, R. L., Numerical Simulation of Gas Particle Flow in a High Velocity Oxygen Fuel (HVOF) Torch. Journal of Thermal Spray Technology, 1995, Vol. 4, No 4, p. 358 - 366.

[37] Shaphiro, A. H., The Dynamics and Thermodynamics of Compressible Fluid Flow. Ronald Press, New York, 1953, 510 p.

[38] Anderson, J. D. Jr., Hypersonic and High Temperature Gas Dynamics. McGraw-Hill International Editions, New York, 1989, p. 468 - 530.

[39] Sutton, G. R., Ross, D. M., Rocket Propulsion Elements, John Willey-Sons, New York, 1976, p. 173 - 279.

[40] Hodge, B. K., Koenig, K., Compressible Fluid Dynamics, Prentice-Hall, New Jersey, USA, 610 p.

[41] Gaskell, D., Introduction Metallurgical Thermodynamics. Mc-Graw-Hill, Tokyo, 1973, p. 210 - 490.

[42] Magome, D., Ogawa, K. S., Computer Application on Anti-Corrosive Properties of Ni-Cr Plasma Coatings, In: Berndt, C. C & Sampath S. (eds.), Thermal Spray Coatings: Properties, Processes and Applications. Pittsburgh, USA, 1991, ASM International, Ohio, USA, 1991, p. 457 - 463.

[43] Lall, C., Fundamental of High Temperature Sintering: Application to Stainless Steels and Soft Magnetic Alloys. The International Journal of Powder Metallurgy, 1996, Vol. 27, No 4, p. 315 - 329.

[44] Brinks, N., Meier, G. H., Introduction to High Temperature Oxidation of Metals, Edward-Arnold, London, 1983, 187 p.

[45] Jokilaakso, A., Virtaustekniikan lämmönsiiron ja aineensiirron perusteet. No. 496 Otakustantamo, Karisto, Hameenlinna, 1988, 191 p.

[46] Themelis, N. J., Transport and Chemical Rate Phenomena, Gordon and Breach Publisher, Basel, 1995, 370 p.

[47] Tunturi, P. J. (ed.), Korroosiokäsikirja, Corrosion Handbook, Suomen Korroosioyhdistys, SKY Hangon kirjapaino, 1988, 952 p. In Finnish,

[48] Kubaschewski, O., Evans, E. L., Alcock, C. B., Metallurgical Thermo Chemistry, 4 Th.(ed.), Pergamon Press, New York, 1967, 330 p.

[49] Magome, M., Kavarada, K., Ogawa, S., Computer Application on Anti-Corrosive Properties of NiCr Plasma Coatings, In: Bernecki, T. F. (ed.), Thermal Spray Coatings: Properties Processes and Applications. Pittsburgh, 1991, ASM International, Ohio, USA, 1991, p. 457 - 463.

[50] Kofstad, P., High Temperature Corrosion. Elsevier Applied Science, London, 1988, p. 556.

[51] Sims, C.T., Stoloff, N. S., Hagel, W. C., Super Alloys 2. John - Willey and Sons, New York, 1987, p. 612.

[52] Fontana, M., Greene, N., Corrosion Engineering, McGraw-Hill, Tokyo, 1983, p. 345 - 376.

[53] Meier, G. H., Research on Oxidation and Embrittlement of Intermetallic Compounds in the U.S. Materials and Corrosion, 1996, Vol. 47, p. 596 - 618.

[54] Rosenquist, T., Principles of Extractive Metallurgy, McGraw-Hill, London, 1988, 506 p.

[55] Smallman, R. E., Modern Physical Metallurgy. Third Edition, Butterworths, London, 1980, 534 p.

[56] Fristrom, R. M., Flame Structures and Processes. Oxford University Press, New York, 1995, 510 p.

[57] HSC Thermodynamic Calculation Program 4.0., Outokumpu Research Oyj, Pori, 2001

[58] Yang, Y. M., Liao, H., Codet, C., Numerical Modeling of combustion Flow Characteristic in HVOF System with Chemical Equilibrium Approach. In: Ohimori, A. (ed.), Thermal Spraying Current Status and the Trends. Kobe, Japan, May, 1995, Proceedings of ITSC 95, Kobe, Japan, 1995, p. 399 - 404.

[59] Gordon, S., McBridge, B. J., Computational Program for Calculation of Complex Chemical Equilibrium Compositions Rocket Performance Incident and Reflected Shocks and Chapman-Jauguet Detonations, NASA SP - 273, 1971.

[60] Krayer, H., Schwechtzke, R., Zimmermann, S., Influence of the Fuel Gas on Microstructure and Properties of HVOF Coatings. In: Lugscheider E. (ed.), Conference Proceeding TS 96, Essen, Germany, 1996, German Welding Society, Essen, Germany, 1996, p. 95 - 98.

[61] Heinrich, P., Meinass, H., Penszior Ch.,: Gases for thermal spray technology Proc. 5th HVOF Colloquium, 16.-17.11.2000, Erding, Germany. p. 65-77 Publisher GTS E.V.

[62] Sturgeon, A. J., Harvey, M. D. F., Blunt, F., Dunkerton, S. B., The Influence of Fuel Gas on the Microstructure and Wear Performance of Alumina Coatings. In: Ohmori, A., (ed.), Thermal Spraying Current Status and the Trends. Kobe, Japan, May 1995, Proceedings of ITSC 95, Kobe, Japan, 1995, p. 669 - 673.

[63] Gu, S., Eastwick, C.N., Simmons, K. A, Computational fluid dynamic Modeling of Gas Flow Characteristics in a High-Velocity-Oxy-Fuel Thermal Spray System, Journal of Thermal Spray Technology, 2001, Vol. 10, No 3, p. 461 - 469.

[64] Korpiola, K., Jokinen, P., Termisen ruiskutuksen in situ diognostiikka. COST 515 Thermal Spraying in Situ Diagnostic, VTT Project Report, 1th of January, 1996, p. 25.

[65] OSY Castorp-Rauxel, Bulletin of HVOF Gun Carbide Jet System, 1996.

[66] Metco Technical Bulletin, Metco DJ-Hybrid High Velocity Oxygen Fuel Process, 1997, 27 p.

[67] Mathaus, G., Personal Communication, OSY Castorp-Rauxel, 1996.

[68] Korpiola, K., Hirvonen, J. P., Laas, L., Rossi, F., The Influence of Nozzle Design on HVOF Exit Gas Velocity and Coating Microstructure, Journal of Thermal Spray Technology, 1997, Vol. 6, No 4, p. 469 - 474.

[69] Dvorak, M., Browning, J. A, Extended limit of HVOF, Thermal Spraying - Current Status and Future Trends, Proceedings, 14th International Thermal Spray Conference, Kobe, Japan, Vol.1; 22-26 May 1995. pp. 405-409. 1995

[70] Korpiola, K., Private Communication from OSY Ghb, Matthaus, G., 1997.

[71] Browning, J.A., Matus, R. J., Richter, H. J., A New HVOF Thermal Spray Concept, In: Berndt, C. C. & Sampath, S. (eds.), Advances in Thermal Spray Science and Technology. Houston, Texas, 1995, ASM International, Ohio, USA, 1995, p. 7 - 10.

[72] Korpiola, K., Jokinen, P., Termisen ruiskutuksen in situ diagnostiikka. COST 515 Thermal Spraying in Situ Diagnostic. VTT Project Report, January 18, 1996, Otaniemi, p. 12.

[73] Pawlowski, L., The Science and Engineering of Thermal Spray Coatings. John Willey and Sons, New York, 1995, 412 p.

[74] Dvorak, M., Browning, J. A., Extended Limits of HVOF, In: Ohimori, A. (ed.), Thermal Spraying Current Status and the Trends. Proceedings of ITSC 95, Kobe, Japan, May, 1995, ITSC, Kobe, Japan, 1995, p. 405 - 409.

[75] Fincke, J. R., Comparison of the Characteristic of HVOF and Plasma Thermal Spray. In: Berndt, C. C. & Sampath, S. (eds.), Thermal Spray Industrial Applications. Boston, 1994, ASM International, Ohio, USA, 1994, p. 325 - 330.

[76] Hackett, G. S., Settles, J. D., Miller, S., On The Gas Dynamics of HVOF Thermal Sprays. Journal of Thermal Spray Technology, 1994, Vol. 3, No 3, p. 299 - 304.

[77] Oberkamf, W. L., Talpillinkar, M., Analysis of a High Velocity Oxygen-Fuel (HVOF) Thermal Spray Torch, Part 1. Numerical Formulation. Journal of Thermal Spray Technology, 1996, Vol. 5, No 1, p. 53 - 62.

[78] Oberkampf, W. L., Talpalinkar, M., Analysis of a High Velocity Oxygen-Fuel (HVOF) Thermal Spray Torch, Part 2. Numerical Formulation. Journal of Thermal Spray Technology, 1996, Vol. 5, No 1, p. 63 - 68.

[79] Alonso, M., Finn, E., Fundamental University Physics. Vol. 1. Addison-Wesley Publishing Company, London, 1975, 420 p.

[80] Cheng, D., Trapaga, G., McKelliget, J. W., Lavernia, E. J., Mathematic Modeling of high velocity oxy fuel thermal spraying of nanocrystalline material; an overview, Modeling and Simulation in Material Science and Engineering, 11 (2003), p 1-31

[81] Korpiola, K., Jokinen P., Termisen ruiskutuksen in situ diagnostiikka. COST 515 Thermal Spraying in Situ Diagnostic. VTT Project Report, Otaniemi, September 25, 1996.

[82] Korpiola, K., Hirvonen, J. P., Jalkanen, H., Laas, L., Rossi, F., Oxygen Partial Pressure Measurements in the HVOF Gun Tail Flame. In: Berndt, C. C. & Sampath, S. (eds.), Advances in Thermal Spray Science and Technology. Houston, USA, 1995, ASM International, Ohio, USA, 1995, p. 181 - 186.

[83] Korpiola, K., Jokinen P., COST 515 Final Report, VTT, Otaniemi, March 1998, 25 p.

[84] Knight, R., Smith, R. W., Xiao, Z., Hoffman, T. T., Particle Velocity Measurements in HVOF and APS System, In: Berndt, C. C. & Sampath, S. (eds.), Thermal Spray Industrial Applications. Boston, USA, 1994, ASM International, Ohio, USA, 1994, p. 331 - 336.

[85] Thorpe, M., Richter, H., A Pragmatic Analysis and Comparison of HVOF Processes. Bulletin: Hobart Tafa Technologies, Condor N. H., USA, 1992, 25 p.

[86] Joshi, S. V., Plasma Spraying of WC - Co Part 1 - 2: Theoretical investigation of Particle Heating and Acceleration during Spraying. Journal of Thermal Spray Technology, 1993, Vol. 2(2), June, p. 127 - 136.

[87] Das, S., Suri, V. K., Chadra, U., Sampath, K., One Dimensional Mathematical Model for Selecting Plasma Process Parameters. Journal of Thermal Spray Technology, 1995, Vol. 4(2), June, p. 153 - 162.

[88] Kadyrov E., Evdokimenko Y., Kiselv V., Worzala F., Interaction of Particles with Carrier Gas In HVOF Spraying System, Journal of Thermal Spray Technology, 1994, Vol. 3(4), p. 389 - 139.

[89] Kundas, S., Kuzmenkov, A., Lugscheider, E., Schnaut, U., Nyland, A., Ladru, F., Eritt, U., Simulation of Particle Heating and Movement During Plasma Spraying Process. In: Lugsheider, E. (ed.), Thermal Spraying Conference TS 96. Düsseldorf, 1996, German Welding Society, Düsseldorf, Germany, 1995, p. 450.

[90] Korpiola, K., Jokinen, P., COST 515 Final Report, Termisenruiskutuksen in-situ diagnostiikka, in Finnish, VTT Report, 1st of May, 1998, p. 30.

[91] Smith, R. W., Knight, R., Thermal Spraying 1: Power Consolidation- From Coating To Forming. JOM, 1995, August, p. 32 - 39.

[92] Chen, S. L., Deposition of Alumina Coatings by Atmospheric Plasma Spraying. Thesis of Tampere University of Technology, Publications No. 127, Tampere, 1993, p. 89.

[93] Korpiola, K, Particle velocity and temperature measurement of the HVOF gun, Pikoteknik Oy Raport, 2002. (Unpublished in Finnish).

[94] Praxair Thermal Inc. Spraying Parameter Tables for Spray Powders, Indianapolis, 1993.

[95] Miller Thermal inc. Thermal Spraying Parameter Tables for Spray Powders, 1993.

[96] Personal Communication from Mr. T. Kataja of Virtasen Moottori inc. 1995 - 1997.

[97] Zimmerman, S., Kreye, H., Chromium Carbide Coatings Produced with Various HVOF Spray Systems. In: Berndt C. C. (ed.), Thermal Spray: Practical Solutions for Engineering Problems. Cincinnati, 1996, ASM International, Ohio, USA, 1996, p. 147 - 152.

[98] Hansen, T. C., Hackett, T. C., and Settles G., Independent Control of HVOF Particle Velocity and Temperature,

[99] SprayWatch particle velocity and temperature sensor, Oseir Ltd, Hermiankatu 6A FIN-33720 Tampere Finland

[100] Bartuli, C., Valente, T., Cipri, F., Nano structured wear resistant WC-Co coatings deposited by HVOF, ASM International, Surface Engineering; Coatings and Heat Treatments: Proceedings of the 1st ASM International Surface Engineering and the 13th IFHTSE Congress (USA), pp. 480-487, 2003

[101] Vernon, C., Karami, A., Martin J.-L., Study of high velocity oxy-fuel thermally sprayed tungsten carbide based coatings. Part 1. Microstructures, Materials Science and Engineering A 246 (1998) 11-24

[102] Lofaj, F., Kanagovskii, YU.S. Kinetics of WC-Co oxidation accompanied by swelling, Journal of Material Science, 30 (1995), p 1811-1817.

[103] Babilus, A., Influence of Temperature on the Phase Changes of HVOF Sprayed Tungsten Carbide coatings, ISSN 1392-1320, Materials Science (medziagotyra), Vol. 30), No. 3. 2003

[104] McHal,e A., Phase Equilibrium Diagrams-Phase Diagrams for Ceramists, Vol. 10, The American Ceramic Society, Westerville, Ohio, 1994.

[105] Upadhyaya, G. S., Cemented Tungsten Carbides - Production, Properties, and Testing © 1998 William Andrew Publishing/Noyes, http://www.knovel.com/knovel2/ Toc.jsp?SpaceID = 10090&BookID=773

[106] Lim, L.C, Lim, S.C, Lai, M.O, Chong, S.F., Annealing of plasma-sprayed WC-Co coating, Surface and coatings Technology, Vol 79, (1996) 151-161 p.

[107] Guilemany, J. M., Paco, J. M., Nutting, J. ; Miguel, J. R., Characterization of the W_2C phase formed during the high velocity oxygen fuel spraying of a WC + 12%Co powder, Metallurgical and Materials Transactions A. Vol. 30A, no. 8, pp. 1913-1921. Aug. 1999

[108] Iida, T., Guthrie, R., Physical Properties of Liquid Metals, Clarendon Press, Oxford, 1988, p. 288.

[109] Kinetika i termodinamika protsessov vzaimodeistviya gazov s zidkimi metallami. Tezisi simpoziuma. Moskow, A.A.Baikov Institute of metallurgy of the Academy of Sciences of USSR, 1972, 50 p. From Kulikov I.S., Raskisleniye metallov. Moskow, "Metallurgia", 1975, 504 p.

[110] Choudhury, A., Vacuum Metallurgy, ASM International, Material Park, Ohio, 44073, USA, 1990, p.245.

[111] Jalkanen, H., Pintailmiöiden termodynaamiset perusteet, (Mak-37-135/2003), Thermo-dynamic of the surface phenomena, (in Finnish) Helsinki University of Technology, 2003, p. 27

[112] Park, Y-H., Kim, J. Kim, S-K., The Critical amount of nitrogen on the formation of nitrogen gas pores during solidification of 25Cr-7Ni duplex stainless steels, Metallurgical and Material Transactions B, Vol. 34 b, June, 2003, p. 313-319.

[113] Graf, W., The Microgravity Research Experiments (MICREX), http://mgravity.itsc.uah.edu/microgravity/micrex/exps/gra-t12.html

[114] Swank, W. D. , Fincke, J. R., Haggard, D. C. , "A Particle Temperature Sensor for Monitoring and Control of the Plasma Spray Process," Advances in Thermal Spray Science and Technology, C. Berndt and S. Sampath Eds., ASM International, 1995, pp. 111-116.

[115] Korpiola, K., Jokinen, P., Termisen ruiskutuksen In situ diagnostiikka, COST 515 Thermal Spraying In Situ Diagnostic, VTT Project Report, (in Finnish) September 25, Otaniemi, 1996, 10 p.

Appendix A.

Table 1. "Baseline" spray parameters; 88/12 WC/Co, Jet Kote® and
Fuel gas: C_3H_8
Fuel flow rate: 63.7 l/min, line pressure @ 0.55 MPa
Oxygen flow rate: 472 l/min, line pressure 0.827 MPa
Carrier gas: Ar/N_2
Carrier gas flow rate: 16.5 l/min @ 0.45 MPa
Powder size: -45+15µm
Powder feed rate: ~50 g/min (2.6 rpm)
Nozzle: Ø 7.93 x 152.4 mm l
Spray distance: 180 mm

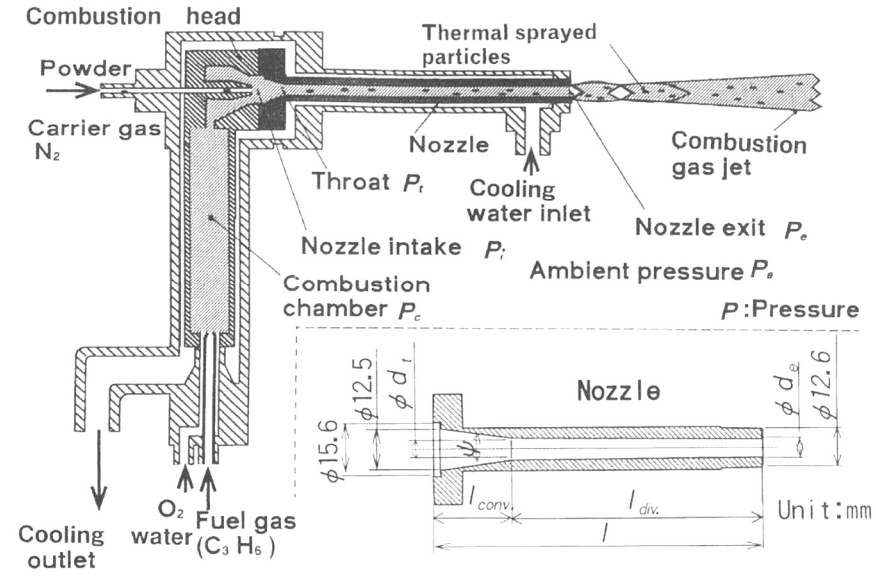

Figure 1. *Cross section diagram of Jet Kote® HVOF spray gun (1).*

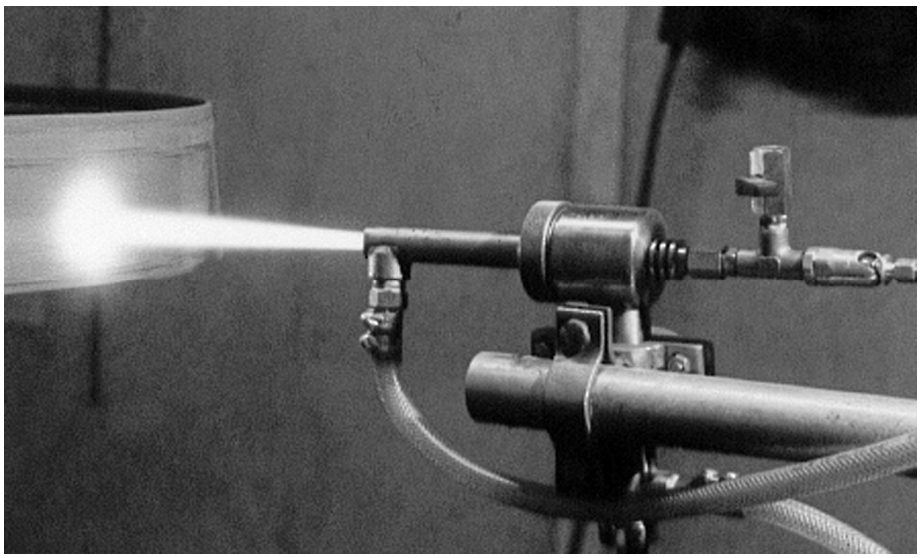

Figure 2. *Jet Kote® HVOF gun in spraying operation.*

Figure 3. *Miller Thermal HV-2000 HVOF spray gun.*

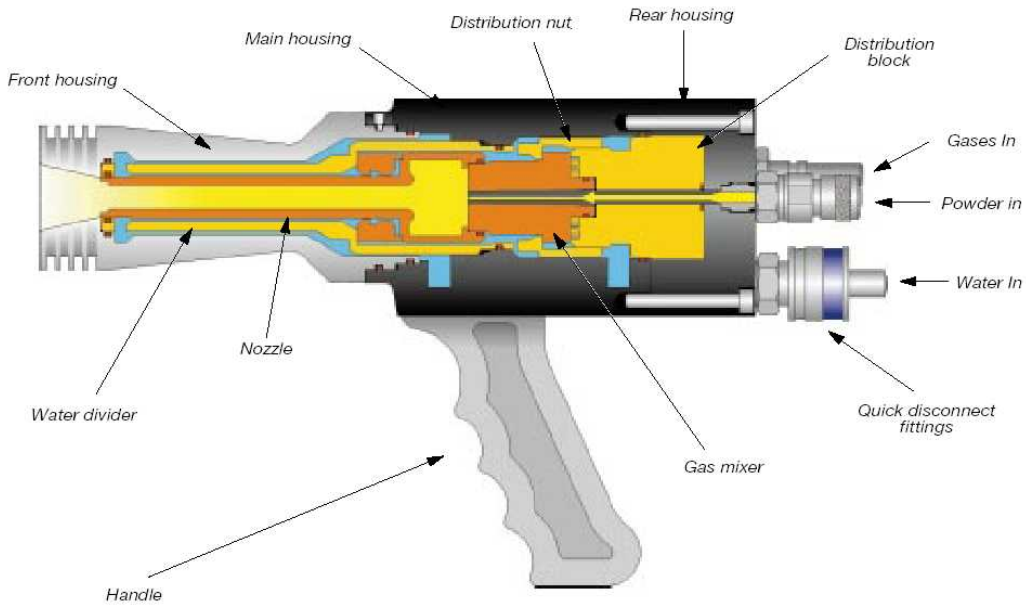

Figure 4. *Cross section diagram of Miller Thermal HV-2000 HVOF spray gun.(1)*

Table 2. "Baseline" spray parameters; 88/12 WC/Co; Miller Thermal HV-2000
Fuel gas: H_2, C_3H_8
Fuel flow rate: 550-750, 54-60 l/min
Oxygen flow rate: 200-300 l/min
Carrier gas: Ar, N_2
Carrier gas flow rate:20-30 l/min
Powder size: -45+15µm
Powder feed rate: 10-40g/min
Nozzle: Ø 8/150 mm
Spray distance: 150-250 mm

Figure 5. *Powder hopper Praxair Model 1264 (2).*

[1] Sakaki. K., Shimizy, Y., Effect of the increase in the entrance convergent section length of the gun nozzle on the high velocity fuel and cold spray process, JTS Technology, Vol. 10 No 3, September 2001, p. 487-496

[2]http://www.praxair.com/praxair.nsf/7a1106cc7ce1c54e85256a9c005accd7/6b32238a309cab8085256c7e006b662d?OpenDocument

HELSINKI UNIVERSITY OF TECHNOLOGY PUBLICATIONS IN MATERIALS SCIENCE AND METALLURGY

TKK-MK-146 Isomäki, I.,
Liuosfaasien matemaattisia malleja, osa III. 2003.

TKK-MK-147 Xia, J.,
Parametric study of flow and heat transfer in a slag cleaning furnace. 2003.

TKK-MK-148 Mäkinen, M.,
Oskilloinnin vaikutus kupariaihion pinnanlaatuun. 2003.

TKK-MK-149 Forsen, M., Holappa, L.,
Mahdollisuudet alentaa CO2-päästöjä terästeollisuudessa. 2003.

TKK-MK-150 Wang, S., Holappa,L.,
Evaluation and prospects for novel casting technologies. 2003.

TKK-MK-151 Raipala, K.,
On Hearth Phenomena and Hot Metal Carbon Content in Blast Furnace. 2003.

TKK-MK-152 Kekkonen, M. (ed.),
Seminar Course on Advanced Metallurgical Processes / 2003. Mak-37.145. 2003.

TKK-MK-153 Erola, H., Nurmi, S., Holappa, L.,
Radiosteel. 2004.

TKK-MK-154 Anttonen, K., Kaskiala, T.,
Liuosfaasien matemaattisia malleja. 2004.

TKK-MK-155 Aromaa, J. (ed.),
4th Kurt Schwabe Corrosion Symposium. Mechanisms of Corrosion and Corrosion Prevention. 2004

TKK-MK-156 Seppänen, E.,
Kallionäytekairaus. 2004.

TKK-MK-157 Oghbasilasie, H., Jalkanen, H.,
Study on Radust and Other Processes for Dust Treatment. 2004.

TKK-MK-158 Jormalainen, T., Louhenkilpi, S.,
Lämmönsiirron ja virtauksen mallintaminen senkassa ja välialtaassa valun aikana – osa 4 Loppuraraportti. 2004.

TKK-MK-159 Kekkonen, M. (ed),
Seminar Course on Advanced Metallurgical Processes / 2004 Mak-37.145. 2004.

ISBN 951-22-7312-8
ISBN 951-22-7328-4 (electronic)
ISSN 1455-2329